

**EXPERIMENTAL INVESTIGATIONS OF TRIBOLOGICAL
BEHAVIOR ON AUSTEMPERED DUCTILE IRON**

A Thesis submitted to



VISVESVARAYA TECHNOLOGICAL UNIVERSITY, BELAGAVI

for the award of the degree of

DOCTOR OF PHILOSOPHY

In

MECHANICAL ENGINEERING

Submitted by

Mr. RAJENDRA M. GALAGALI

USN: 2BL12PMN01

Under the guidance of

Dr. RAVINDRA G. TIKOTKAR



RESEARCH CENTRE

DEPARTMENT OF MECHANICAL ENGINEERING

**B.L.D.E.A'S V. P. DR. P.G. HALAKATTI
COLLEGE OF ENGINEERING & TECHNOLOGY**

VIJAYAPUR-586103

2017

**B.L.D.E.A's V. P. DR. P. G. HALAKATTI
COLLEGE OF ENGINEERING & TECHNOLOGY**

(Recognized by AICTE, Affiliated to VTU, Belagavi)

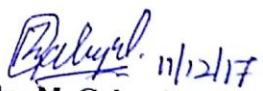
VIJAYAPUR-586103

DEPARTMENT OF MECHANICAL ENGINEERING
(Accredited by NBA, Recognized Research Centre of VTU, Belagavi)





Certificate


Certified that the thesis work entitled "**EXPERIMENTAL INVESTIGATIONS OF TRIBOLOGICAL BEHAVIOR ON AUSTEMPERED DUCTILE IRON**" is carried out by **Mr. Rajendra M. Galagali** bearing USN 2BL12PMN01, a bonafide student of **B.L.D.E.A'S V. P. DR. P. G. HALAKATTI COLLEGE OF ENGINEERING & TECHNOLOGY, VIJAYAPUR** in partial fulfillment for the award of the degree of **DOCTOR OF PHILOSOPHY** in Mechanical Engineering from Visvesvaraya Technological University, Belagavi during the year 2012-2017. The work reported in this thesis has not been submitted by me elsewhere for the award of any degree and to the best of my knowledge is not the repetition of the work carried out by others.


Rajendra M. Galagali

To the best of my knowledge the above statement made by the candidate **Mr. Rajendra M. Galagali** bearing USN 2BL12PMN01 is true.


Dr. Ravindra G. Tikotkar
Guide
Mech. Engg. Dept.
BLDEA's V.P. Dr.P.G.H. C.E.T.
BIJAPUR.


H. O. D.
HOD
Mech. Engg. Dept.
BLDEA's V.P. Dr.P.G.H. C.E.T.
BIJAPUR


Principal
B.L.D.E.A's V.P. Dr. P.G.H.
College of Engg. & Tech.
VIJAYAPUR.

Plagiarism Report



Visvesvaraya Technological University

Jnana Sangama, Belgaum – 590 018.

Prof. Satish Annigeri Ph.D
Registrar (Evaluation)

Phone: (0831) 2498136
Fax: (0831) 2405461

Ref.No / VTU / Exam / 2016-17/ 1790

Date: 15 JUL 2017

Acceptance Letter

Sir/Madam,

The soft copy of Ph.D./M.Sc. (Engineering by research) thesis of **Mr./Mrs. Rajendra M Galagali** . bearing **USN 2BL12PMN01** has been submitted for Anti-plagiarism check at the office of the undersigned through "Turn-it-in" package. The scan has been carried out and the scanned output reveals a match percentage of **08%, which is within the acceptable limit of 25%**.

To obtain the comprehensive report of the plagiarism test, research scholar can send a mail to apc@vtu.ac.in along with the USN, Name, Name of the Guide/Co-guide, Research centre and title of the thesis.

Registrar (Evaluation)

To,

Mr./Mrs Rajendra M Galagali

Research Scholar

Department of Mechanical Engineering

BLDEA's College of Engineering & Technology

Bijapur

||Shri Renuka Devi Namaha||

Dedicated to my Beloved Parents

DECLARATION

I hereby declare that the work submitted to Visvesvaraya Technological University, Belagavi, Karnataka in partial fulfillment for the award of the degree of **DOCTOR OF PHILOSOPHY** by me entitled "**EXPERIMENTAL INVESTIGATIONS OF TRIBOLOGICAL BEHAVIOR ON AUSTEMPERED DUCTILE IRON**" is in line with synopsis and topic mentioned above. The work submitted is the original work of mine and has not been submitted anywhere for the award of any other degree and to the best of my knowledge has not been carried out by anybody else and reported

Place: Vijayapur

Date: 11/12/17



Rajendra M. Galagali

Research Scholar

USN: 2BL12PMN01

ACKNOWLEDGEMENT

Attempts are never accomplished alone; there are constantly a few steady hands. This proposition is a careful aftereffect of direction of such individuals around me who have presented to me all through the way. Along these lines, I want to express gratitude toward them just for their nearness in my life throughout the work. I am to a great degree lucky to be required in a testing research work of this kind. It has advanced my life, giving me a chance to work in the territory of tribological behavior of metals. This work upgraded my reasoning capacities and understanding ability. After the finish of my work, I encountered a sentiment self-delight.

I might first want to express my profound feeling of appreciation to my guide **Dr. Ravindra G. Tikotkar** who is an exemplification of learning, consistent quality and resistance for his extraordinary course, recommendations, exceptional effort and support in the midst of my investigation work. Without his constant direction this postulation would not have been appeared. One can never wish for a superior guide and way creator in life. I might likewise want to offer my true thanks to **Prof. S. B. Koulagi**, Professor and Head of the Department of Mechanical Engineering for his consolation and lighting up criticisms amid my exploration work. I am obliged to **Dr. V. P. Huggi**, Principal whose support and help required for carrying out experimental investigations in the Organization premises along with resources and necessary infrastructure.

I whole heartedly thank **Sri. Madhwa N. Acharya**, Managing Director, Abhishek Alloys, Belagavi for helping to cast and heat treat the material as per the requirements. He has been a treasure of knowledge in my research path. I earnestly express gratitude toward **Prof. D. B. Patil** for his encouragement, cooperation and support all through the exploration work. I might extraordinarily want to express gratitude toward **Mr. Kiran Shahapurkar** for his productive remarks without which I would not have been developed as a decent analyst. Much appreciated are because of **Mr. Villson G. Madurai** for his support and help amid the specimen readiness for test work.

I express my genuine thanks and appreciation to my folks, family, instructors, companions and all other people who have been a steady wellspring of motivation and support for me through one way or the other from the very adolescence and who remained by me at all periods of my life. Finally, I say thanks to **Almighty God** for giving me a chance to work in such a domain with such great and educated individuals around.

(Rajendra M. Galagali)

ABSTRACT

This thesis reports on the research dealing with dry sliding wear behavior of two categories of Austempered Ductile Irons (ADI) at room and elevated temperature operating conditions. Currently there is a lot of enthusiasm for the wear of metals and materials all through the world. Propelled wear safe materials with low rubbing co-efficients are being researched for different applications. Metals and composites that are light in weight having suitable mechanical and tribological properties with minimal effort have appeal. This prompted the improvement of one of the high quality material known as Austempered Ductile Iron. ADIs have good fatigue resistance with favorable ductility, hardness, toughness and are wear resistant.

The first part of the thesis emphasizes on the importance of the austempering process on Ductile Iron (DI). A comparison of wear behavior of DI and ADI is made to quantify the increase in wear resistance. The development and validation of the regression model was also dealt with. A Taguchi approach was utilized in the analysis of the results. The second part deals the study of wear behavior at elevated temperature for varying speeds and loads. The behavior at elevated temperature is compared with the wear behavior at room temperature. The hardness and its profile have been studied to understand the work hardening effects. The heat flux, surface temperature and flash temperature have been calculated to understand its variation in influencing the response. Scanning Electron Microscopy analysis of worn out surfaces was additionally completed to understand the predominant wear mechanisms under the influence of load, speed and temperature. The third part throws light on the optimization of control factors with temperature as one of the influencing parameter. A regression model for the calculation of response was developed and validated. The fourth part has shown the comparative wear behavior of two categories of ADIs for varying sliding distances. The last part of the thesis dealt with the development of an optimized and well trained linear model for the prediction of wear rate for both the ADIs using Artificial Neural Networks.

The austempering heat treatment process increased wear resistance of DI to a considerable level. The developed regression model can well be utilized to estimate the wear rate of the given ADI. A considerable enhancement in the weight loss was observed at elevated temperature than at the room temperature at all operating speeds and loads.

An effort has been done to understand the shift in its behavior with the operating conditions. The weight loss reached its peak for the highest value of speed and load. The huge loss in weight renders the material's non-suitability for the elevated temperature applications. Artificial Neural Networks can well be utilized in the prediction of wear.

Keywords: Austempered Ductile Iron, Dry Sliding Wear, Coefficient of Friction, Sliding Speed, Applied Load, Elevated Temperature

CONTENTS

Chapter	Chapter title	Page
	<i>Certificate</i>	
	<i>Declaration by Candidate</i>	i
	<i>Acknowledgement</i>	ii
	<i>Abstract</i>	iii
	<i>List of Figures</i>	x
	<i>List of Tables</i>	xiv
	<i>Nomenclature</i>	xvi
Chapter 1	INTRODUCTION	1
	1.1 Background and Motivation	1
	1.2 Thesis Outline	7
Chapter 2	LITERATURE REVIEW	8
	2.1 On Ductile Iron (DI)	8
	2.1.1 History of DI	8
	2.1.2 Production of DI	9
	2.1.2.1 Raw Materials	9
	2.1.2.2 Composition Control	9
	2.1.2.3 Desulphurization	10
	2.1.2.4 Spheroidization	10
	2.1.2.5 Inoculation	11
	2.2 On Austempered Ductile Iron (ADI)	11
	2.2.1 Introduction to ADI	11
	2.2.2 Austempering Cycle	13
	2.2.3 Production of ADI	14
	2.2.4 Microstructure of ADI	15
	2.2.5 Properties of ADI	16
	2.2.6 Advantages and Disadvantages of ADI	18
	2.2.7 Applications of ADI	18
	2.3 Modes of Wear	21
	2.3.1 Adhesive Wear	22
	2.3.2 Abrasive Wear	22

2.3.3	Fatigue Wear	22
2.3.4	Corrosive Wear	23
2.4	Wear Behavior of ADI	23
2.5	Taguchi Method	28
2.6	Artificial Neural Networks	30
2.7	The knowledge Gap in Earlier Investigations	32
2.8	Objectives of the Present Work	33
	Chapter summary	
Chapter 3	MATERIALS AND METHODS	35
3.1	Introduction	35
3.2	Selection of ADI for the Present Investigation	36
3.3	Preparation of the Sample	36
3.4	Experimental Set up and Procedure	38
3.5	Estimation of the Set up Parameters for the Experimental Study	41
3.6	Measurement of Surface Temperature and Estimation of Flash Temperature	42
3.7	Heat Flux	43
3.8	Metallographic Studies on ADI	43
3.9	Wear Debris	44
3.10	Surface and Subsurface Hardness	44
3.11	Measurement of Surface Roughness	45
3.12	Taguchi Method	46
3.13	Artificial Neural Networks	47
	Chapter summary	
Chapter 4	RESULTS AND DISCUSSION – I	
	OPTIMIZATION OF WEAR CONTROL PARAMETERS AT ROOM TEMPERATURE	49
4.1	Parameters and Levels	49
4.2	Plan of Experiments	49
4.3	Influence of Parameters on Wear Rate	50
4.3.1	Experimental Results of Wear Rate	50
4.3.2	S/N Ratio Analysis	52
4.3.3	Analysis of Variance for Wear Rate	55

4.3.4	Regression Analysis	57
4.3.5	Confirmation Test	57
4.4	Influence of Parameters on Coefficient of Friction (COF)	59
4.4.1	Experimental Results of COF	59
4.4.2	S/N Ratio Analysis	59
4.4.3	Analysis of Variance of COF	63
4.4.4	Regression Model	64
4.4.5	Confirmation Test	66
Chapter 5	RESULTS AND DISCUSSION – II	
	STUDY OF WEAR BEHAVIOR	
	AT ELEVATED TEMPERATURE	66
5.1	Experimental Results and Discussion	66
5.1.1	Effect of Sliding Speed on Wear Rate	71
5.1.2	Effect of Sliding Speed on Coefficient of Friction	72
5.1.3	Effect of Sliding Speed on Surface and Flash Temperature	73
5.1.4	Effect of Sliding Speed on Hardness	74
5.1.5	Effect of Wear Rate and Specific Wear Rate for Varying Speed	74
5.1.6	Effect of Sliding Speed and Load on Heat Flux	76
5.1.7	Effect of Applied Load on Wear Rate	77
5.1.8	Effect of Applied Load on Friction	77
5.1.9	Effect of Applied Load on Surface and Flash Temperature	79
5.1.10	Effect of Applied Load on Hardness	80
5.1.11	Effect of Wear Rate and Specific Wear Rate for Varying Loads	80
5.1.12	Hardenability	81
5.1.13	Morphology of Worn Surfaces	82
5.1.14	Wear Debris Analysis	84
5.1.15	Effect of Temperature on Weight Loss and COF	93

Chapter 6	RESULTS AND DISCUSSION – III	
	OPTIMIZATION OF WEAR CONTROL	
	PARAMETERS AT ELEVATED TEMPERATURE	95
6.1	Parameters and Levels	95
6.2	Plan of Experiments	95
6.3	Influence of Parameters on Wear Rate	96
6.3.1	S/N Ratio Analysis	96
6.3.2	Analysis of Variance for Wear Rate	99
6.3.3	Regression Analysis	99
6.3.4	Confirmation Test	99
6.4	Influence of Parameters on COF	101
6.4.1	S/N Ratio Analysis	101
6.4.2	Analysis of Variance for COF	103
6.4.3	Regression Analysis	103
6.4.4	Confirmation Test	103
Chapter 7	RESULTS AND DISCUSSION – IV	
	WEAR BEHAVIOR OF ADI1 AND ADI2	105
7.1	Effect of Sliding Distance on Wear Rate	105
7.2	Effect of Sliding Distance on COF	106
7.3	Effect of Wear Rate and Specific Wear Rate	107
Chapter 8	RESULTS AND DISCUSSION – V	
	PREDICTION OF WEAR BY USING	
	ARTIFICIAL NEURAL NETWORKS	110
8.1	Prediction for ADI1	110
8.1.1	Modelling for Prediction of Weight Loss	111
8.1.2	Modelling for Prediction of COF	113
8.1.3	Comparison of Results	114
8.2	Prediction for ADI2	116
8.2.1	Modelling for Prediction of Weight Loss	116
8.2.2	Modelling for Prediction of COF	118
8.2.3	Comparison of Results	120

Chapter 9	CONCLUSIONS AND RECOMMENDATIONS	
	FOR FURTHER RESEARCH	122
9.1	Conclusions	122
9.2	Recommendation for Further Research	124
	REFERENCES	125
	APPENDICES	144
	A1. List of Publications from the Present	
	Research Work	144
	A2. Brief Bio-data of the Author	146

LIST OF FIGURES

Figure 2.1	Fe -C- Si ternary phase diagram at 2% silicon	12
Figure 2.2	Isothermal transformation diagram of a ductile iron composition	12
Figure 2.3	Schematic diagram of ADI processing steps	13
Figure 2.4	Microstructure of ausferrite	16
Figure 2.5	Photomicrographs of the ausferrite microstructure in ADI. Grade 900-650-09 ADI is shown in (a) while grade 1600-1300-01 ADI is shown in (b). The grade 900 ADI was produced by austempering at 371°C while grade 1600 ADI was produced by austempering at 260°C. Etched with 5% Nital	17
Figure 2.6	Yield strength vs. ductility for various metals	18
Figure 2.7	Constant velocity joint	19
Figure 2.8	Tow hooks	19
Figure 2.9	An ADI suspension beam that replaced a steel forging and increased durability	19
Figure 2.10	A sway bar bushing for a heavy truck axle	19
Figure 2.11	An ADI hub along with the competitive aluminium hub that it replaces	20
Figure 2.12	Seed boot	20
Figure 2.13	Plow point	20
Figure 2.14	A drive wheel for the track system	21
Figure 2.15	(a) Diesel engine timing gear, (b) Hypoid differential gears and pinions, (c) A one-piece gear and axle for a commercial lawn mower and (d) A large mill gear produced in segments and then assembled after Austempering	21
Figure 2.16	Wear modes (a) Adhesive wear (b) Abrasive wear (c) Fatigue wear (d) Corrosive wear	22
Figure 2.17	Structure of a back propagation neural network	31
Figure 3.1	Ductile iron test bar	37
Figure 3.2	Test specimen	37
Figure 3.3	Wear test pin	38
Figure 3.4	Thermocouple mounted on wear test specimen	38
Figure 3.5	Friction temperature measurement and wear track on disc	38

Figure 3.6	DUCOM pin-on-disc wear testing machine (TR-20-LE)	39
Figure 3.7	Schematic diagram of wear and friction monitor	40
Figure 3.8	Scanning electron microscope	44
Figure 3.9	Vicker's hardness tester	45
Figure 3.10	Sectioned specimen for hardenability test	45
Figure 3.11	Indentation made by the indenter on test surface	45
Figure 3.12	Surface roughness measuring instrument	46
Figure 4.1	Main effects plot of DI for S/N ratios-wear rate	53
Figure 4.2	Main effects plot of DI for means-wear rate	54
Figure 4.3	Main effects plot of ADI1 for S/N ratios-wear rate	55
Figure 4.4	Main effects plot of ADI1 for means-wear rate	55
Figure 4.5	Main effects plot of DI for S/N ratios-coefficient of friction	61
Figure 4.6	Main effects plot of DI for means-coefficient of friction	61
Figure 4.7	Main effects plot of ADI1 for S/N ratios-coefficient of friction	62
Figure 4.8	Main effects plot of ADI1 for means-coefficient of friction	62
Figure 5.1	Experimental wear rates as a function of sliding speed	71
Figure 5.2	Coefficient of friction as a function of sliding speed	72
Figure 5.3	Frictional force as function of time	72
Figure 5.4	Surface temperature as a function of sliding speed	73
Figure 5.5	Estimated flash temperature as a function of sliding speed	73
Figure 5.6	Microhardness as a function of sliding speed	74
Figure 5.7	Wear rate and specific wear rate as a function of sliding speed at RT	75
Figure 5.8	Wear rate and specific wear rate as a function of sliding speed at ET	75
Figure 5.9	Heat flux as a function of sliding speed	76
Figure 5.10	Heat flux as a function of applied load	76
Figure 5.11	Experimental wear rates as a function of applied load	77
Figure 5.12	Coefficient of friction as a function of applied load	78
Figure 5.13	Frictional force as a function of applied load	78
Figure 5.14	Frictional force as function of time	78
Figure 5.15	Surface temperature as a function of applied load	79
Figure 5.16	Estimated flash temperature as a function of applied load	79
Figure 5.17	Microhardness as a function of applied load	80
Figure 5.18	Wear rate and specific wear rate as a function of applied load at RT	81
Figure 5.19	Wear rate and specific wear rate as a function of applied load at ET	81

Figure 5.20	Microhardness profiles from worn surface for RT and ET specimens	82
Figure 5.21	SEM micrograph of DI	85
Figure 5.22	SEM micrograph of ADI1	85
Figure 5.23	SEM micrograph of ADI2	85
Figure 5.24	SEM micrograph at L=34.335N, S=6m/s, D=2000m	86
Figure 5.25	SEM micrograph at L=34.335N, S=4m/s, D=2000m	86
Figure 5.26	SEM micrograph at L=9.81N, S=3.5m/s, D=3000m	86
Figure 5.27	SEM micrograph at L=34.335N, S=2.5m/s, D=2000m	87
Figure 5.28	SEM micrograph at L=49.05N, S=3.5m/s, D=3000m	87
Figure 5.29	SEM micrograph at L=34.335N, S=1.5m/s, D=2000m	87
Figure 5.30	SEM micrograph at L=19.62N, S=3.5m/s, D=3000m	88
Figure 5.31	SEM micrograph at L=34.335N, S=2m/s, D=2000m	88
Figure 5.32	SEM micrograph at L=39.24, S=3.5m/s, D=3000m	88
Figure 5.33	SEM micrograph at L=34.335N, S=1.5m/s, D=2000m	89
Figure 5.34	SEM micrograph at L=9.81N, S=3.5m/s, D=3000m	89
Figure 5.35	SEM micrograph at L=19.62N, S=3.5m/s, D=3000m	89
Figure 5.36	SEM micrograph at L=34.335N, S=6m/s, D=2000m	90
Figure 5.37	SEM micrograph at L=49.05N, S=3.5m/s, D=3000m	90
Figure 5.38	SEM micrograph at L=34.335N, S=2m/s, D=2000m	90
Figure 5.39	SEM micrograph at L=34.335N, S=4m/s, D=2000m	91
Figure 5.40	SEM micrograph at L=39.24N, S=3.5m/s, D=3000m	91
Figure 5.41	SEM micrograph at L=34.335N, S=2.5m/s, D=2000m	91
Figure 5.42	(a), (b), (c) SEM micrographs of wear debris at L=49.05N, S=3.5m/s, D=3000m	92
Figure 5.43	Percentage weight loss as a function of sliding speed	93
Figure 5.44	Percentage variation in COF as a function of sliding speed	93
Figure 5.45	Percentage variations in weight loss as a function of load	94
Figure 5.46	Percentage variations in COF as a function of load	94
Figure 6.1	Main effects plot for means-wear rate	98
Figure 6.2	Main effects plot for S/N ratios-wear rate	98
Figure 6.3	Main effects plot for means-COF	102
Figure 6.4	Main effects plot for S/N ratios-COF	102
Figure 6.5	Variation of frictional force with time	102
Figure 7.1	Experimental wear rates as a function of sliding distance	105

Figure 7.2	Coefficient of friction as a function of sliding distance	106
Figure 7.3	Coefficient of friction as a function of time	106
Figure 7.4	Wear rate and specific wear rate of DI	107
Figure 7.5	Wear rate and specific wear rate of ADI	107
Figure 7.6	Wear rate and specific wear rate of ADI2	108
Figure 8.1	ANN model for ADI1	111
Figure 8.2	Performance plot for weight loss	112
Figure 8.3	Regression plot for weight loss	112
Figure 8.4	Normalised output results of weight loss from ANN	112
Figure 8.5	Performance plot for COF	112
Figure 8.6	Regression plot for COF	113
Figure 8.7	Normalised output results of COF from ANN	114
Figure 8.8	Comparison of experimental weight loss with the predicted loss	115
Figure 8.9	Comparison of experimental COF with predicted COF	115
Figure 8.10	ANN model for ADI2 (weight loss)	116
Figure 8.11	Performance plot for weight loss	117
Figure 8.12	Regression plot for weight loss	117
Figure 8.13	Normalised output results of weight loss from ANN	118
Figure 8.14	ANN model for ADI2 (COF)	118
Figure 8.15	Performance plot for COF	119
Figure 8.16	Regression plot for COF	119
Figure 8.17	Normalised COF output results from ANN	119
Figure 8.18	Comparison of experimental weight loss with the predicted loss	120
Figure 8.19	Comparison of experimental COF with predicted COF	121

LIST OF TABLES

Table 2.1	Grades and properties of ADI as per ASTM A897/897M-06 (reapproved 2011)	17
Table 3.1	Chemical composition of ductile iron36	
Table 3.2	Disc material chemical composition (AISI316 austenitic)	40
Table 3.3	Disc material physical and thermal properties	40
Table 3.4	Wear and friction monitor machine specifications	41
Table 4.1	Parameters and their levels	41
Table 4.2	Taguchi L ₉ orthogonal array	50
Table 4.3	Plan of experiments	50
Table 4.4	Experimental results of DI	51
Table 4.5	Experimental results of ADI1	51
Table 4.6	S/N ratio for DI	52
Table 4.7	S/N ratio for ADI1	53
Table 4.8	Response table of DI for S/N ratios - smaller is better (wear rate)	53
Table 4.9	Optimized operating conditions of DI for wear rate	54
Table 4.10	Response table of ADI1 for S/N ratios-smaller is better (wear rate)	54
Table 4.11	Optimized operating conditions of ADI1 for minimum wear rate	55
Table 4.12	Analysis of Variance for S/N ratios-wear rate (DI)	56
Table 4.13	Analysis of Variance for S/N ratios-wear rate (ADI1)	56
Table 4.14	Parameters used in the confirmation wear test	58
Table 4.15	Experimental confirmation test results	58
Table 4.16	Confirmation wear test results and their comparison with regression model	58
Table 4.17	Orthogonal array of Taguchi and experimental results of COF	59
Table 4.18	S/N ratios for DI	60
Table 4.19	S/N ratios for ADI1	60
Table 4.20	Response table of DI for S/N ratios-smaller is better (COF)	61
Table 4.21	Optimized operating conditions of DI for COF	62
Table 4.22	Response table of ADI1 for S/N ratios - smaller is better (COF)	62
Table 4.23	Optimized operating conditions of ADI1 for minimum COF	63
Table 4.24	Analysis of variance for S/N ratios - COF (DI)	63
Table 4.25	Analysis of variance for S/N ratios - COF (ADI1)	63

Table 4.26	Parameters used in the confirmation friction test	64
Table 4.27	Experimental confirmation test results	65
Table 4.28	Confirmation friction test results and comparison with regression model	65
Table 5.1	Experimental results	67
Table 5.2	Hardenability test results	69
Table 5.3	Results of surface roughness measured on worn surfaces	70
Table 6.1	Parameters and their levels	95
Table 6.2	Plan of experiments	96
Table 6.3	Experimental results of wear rate	96
Table 6.4	S/N ratio for wear rate	97
Table 6.5	Response table for S/N ratio-wear rate	97
Table 6.6	Optimum operating conditions for wear rate	98
Table 6.7	Analysis of variance for wear rate	99
Table 6.8	Parameters for confirmation test	100
Table 6.9	Experimental confirmation test results	100
Table 6.10	Confirmation wear test results and their comparison with regression model	100
Table 6.11	Experimental results of coefficient of friction	101
Table 6.12	Response table for S/N ratio-COF	101
Table 6.13	Analysis of variance for COF	103
Table 6.14	Confirmation test results	104
Table 6.15	Confirmation COF test results and their comparison with regression model	104
Table 7.1	Experimental results	109
Table 8.1	Experimental results of ADI1	110
Table 8.2	Comparison of experimental and ANN values	114
Table 8.3	Experimental results of ADI2	116
Table 8.4	Comparison of experimental and ANN values	120

NOMENCLATURE

d	Pin diameter
d_t	Track diameter
A	Contact area
S	Sliding speed
L	Normal load
D	Sliding distance
T	Temperature
F	Frictional force
μ	Coefficient of friction
K	Thermal conductivity
W_r	Wear rate
k	Specific wear rate
W_i	Initial weight
W_f	Final weight
W_o	Weight loss
C_{eq}	Equivalent of carbon
ρ	Density
N	Speed
t	Time
T_f	Flash temperature
T_s	Surface temperature
A_r	Real contact area
l	Equivalent diffusion distance
H	Hardness
q	Heat flux

Chapter 1

INTRODUCTION

1.1 Background and Motivation

Wear can be discerned as a sarcoma which deteriorates material's usefulness in application. This has been there for a long time causing incredible harm to society. Likewise it has been the focus of the study over decades yet at the same time reasons are not understood totally. Prosperity of the general population of the world can be normal if consumer goods, transportation equipment, production machinery, spare parts etc. were more solid or kept going longer. Comprehension of the wear procedure turns out to be more essential to control and expand wear life-something this work tries to further. Subsist and failure of parts, components, systems, machines etc. and their failure anticipations mainly depend on the material confiscation from surfaces in the form of wear. Few impacts of wear prompting disappointment incorporate part seizure, vibration, changed actuation time, part breakage, and changed machine exactness, spillage, changed surface harshness and changed stream rates. Further this may lead to mechanical failure or loss in mechanical performance. Understanding of wear helps in its control and elimination [1].

Intense maintenance expenditure or replacement of equipment and industrial plant signifies momentous operating cost to industry. Process plants and subsidiary processes experience greater wear issues than machine parts. Degradation in system reliability and efficiency diminution may not be so critical due to shorter life. Real exertion is required to re-establish the first condition because of wear failure. Eradication of wear effects is more pricey in terms of cost of plant, maintenance labour and machine shutdown time. Economic performance of equipment and plant measured in terms of trouble free performance and high reliability often found to be working slam to their design limits. As a system of ensuring success, high initial cost of wear parts is unacceptable. Optimization is required between maintenance effort and initial cost. Every effort goes to strike a balance between the two. It is imperative to select low cost reliable materials to realise adequate wear life. Wear is objectionable flow of material from surfaces in contact. It has to be kept within tolerable limits either by controlling energy and flows of force that appear on surface

or by absorbing energy and flow of force with proper material selection. Wear circumstances may not be considered as normal as they become brutal than desirable. Moving a condition from destructive to a permissible type practically involves the appropriate selection of a more apposite material. It is not recently enough to determine a more wear safe material sort, composition or its mechanical properties however metallographic structure must be indicated. Nowadays wear can be dealt with as a type of break in a mechanical procedure might be in sure circumstances changed by optional chemical impacts. In this manner wear resistance might be dealt with as a mechanical property. Impact of metallurgical considers on mechanical properties metals is all around explored and found out by numerous analysts. Thus a rapport exists between metallurgical structure and wear resistance. Although there are several tribologically oriented metallurgical studies, the information on hand cannot be widely applied. This has been established to cast irons to some point. But little is stated about the consequences of microstructure on wear resistance compared to mechanical properties [2-14].

Wear study can be found in any of the application fields such as automotive, aerospace, agriculture, cosmetics / personal care, coatings providers, dental implants, fabric / clothing, food processing, lubricant manufacturers, high way / transportation department, medical implants, medical diagnostics, military, shoe manufacturers, pharmaceutical, sports equipment companies, Universities / educators (Material Science and Engineering, Mechanical Engineering, Chemistry, Physics) and the list goes on. Wear witnessed in all mechanical devices used in existence has become a difficult predicament for engineers to solve. As devices got better for higher performances, wear ever more became a difficult problem to solve. Bigger forces, faster speeds, harsher conditions and higher speeds contribute to the problem of wear. Indeed, even in applications where a hard surface in contact with delicate, the hard surface destroys. This is regularly observed in continuously variable transmission using V-belts, where V-belt wears grooves in aluminium shelves [15-21].

Tribology deals with wear, friction and lubrication of intermingled surfaces in relative movement. Wear is an intricate phenomenon under tribology and has been the topic of study over a long time. Wear diminution results in considerable savings and can be achieved by enhanced friction control. Almost one third of the present world's energy is needed to beat friction in one or the other from. Lubrication is one of the ways to decrease wear by controlling friction. Wear can be defined as "It is damage to

a solid surface by dynamic loss of material between surfaces in relative movement” by American Society for Testing and Materials (ASTM). It can also be defined as “the loss of volume per unit sliding distance”. Wear by and large relies upon bearing pressure or applied load, sliding speed, material properties and geometry of the surface. Wear and friction are not inherent material properties. They rely upon working conditions and material properties. Indeed, even little changes in bearing pressure, sliding speed, frictional temperatures or material properties including microstructures results in appreciable changes in wear of contact surfaces [22].

Basically four modes of wear can be seen viz. Adhesive Wear, Abrasive Wear, Fatigue wear and Corrosive wear [23]. Two bodies in contact and relative motion experience friction. “Coefficient of friction (COF) or friction coefficient is a simple proportionality constant”. It is complicated and influenced by factors like lubricant, surface roughness, contact stress, surface chemistry, contact geometry, temperature, environment, sliding speed etc. Friction like wear is not a material property but is a system property. So COF of cast iron or COF of steel cannot be specified. Lubricant diminishes friction, wear, transports debris away from surface and provides cooling [24]. Wear investigation of metals for better life and dependability has turned into the need of the day. Highly developed wear resistant materials with stumpy friction coefficients are being investigated for various applications. Nowadays demand exists for materials with low price which are light in weight; possess better mechanical and tribological properties.

Ductile iron (DI) throughout the decades evolved as a promising material contrasted to gray cast iron with improved combination of strength and toughness. The cost of casting DI is low. In recent years, DI replaced fabricated steel components in some cases [25]. Usage of DI in crankshafts, gears, pinions created interest among the research fraternity to learn wear behavior [26, 27]. DI has exemplified by the charismatic combination of mechanical properties, manufacturing advantages and economy. It finds wide applications described by desiccated as well as lubricated sliding situations such as piston rings, disc brakes, gears and cylinder liners. Lofty strength, good resistance to fatigue and fracture toughness in DI are recounted to the presence of nodular graphite microstructure and hence gaining amplified attention over the decades [28]. The conversion of DI microstructure through an austempering heat treatment process additionally improves the properties [29, 30]. The resulting material is known as Austempered Ductile Iron (ADI) with ausferrite microstructure

which is a combination of ferrite and austenite. The microstructure in austempered steel is known as bainite that consists of ferrite and carbide. A wide variety of microstructures can be developed by changing the austempering heat treatment parameters such as austenitising temperature and time, austempering temperature and time. Austempering ADI below 300°C turns into fine ferrite platelets detached by thin slivers of stabilised austenite. Soaring strength and low ductility are the characteristic features of this microstructure. On the other hand, austempering ADI above 350°C results in coarse ferrite separated by blocky austenite. This microstructure results in meagre strength and high ductility. Quite a few investigators have reported the influence of heat treatment constraints on microstructures and impact of microstructure on mechanical properties [31-42]. During the past decade ADI materialized as a promising engineering material particularly in automotive industry [43]. High strength levels extending from 800-1600 N/mm² and elongation from 1-14% can be accomplished in ADI effectively. Replacement of steel components such as gears, cams and crankshafts by ADI resulted in significant cost benefits. It parades excellent abrasive wear resistance. However, published work on the unlubricated sliding wear is meagre [44]. ADI is picking up significance in the production of machine parts and automotive components such as camshafts, bearings and timing gears which are subjected to ruthless service conditions [45-48]. ADI is also used in the manufacture of jaw crusher components, impact plates, excavator teeth, hammers, rolls and drills [49].

Meta-stable microstructure ausferrite is acquired by austempering in bainitic region. This is an ideal structure. However, extended austempering results in the dissolution of ausferrite into a typical bainitic structure [50]. Subsequently, there is extensive penalty in terms of reduced ductility and toughness. Therefore, it needs to be evaded. Suitable selection of austempering time and temperatures, results in ADI with a wide range of mechanical properties. Mechanical properties of ADI have been investigated by quite a few authors by varying these parameters [50-57]. ADI in the temperature range of 325-400°C is gaining considerable attention. This family of ADIs exhibit high wear resistance, tensile strengths and toughness. These properties of ADI are empowering for use in ground engaging tools akin to ripper tips. Acicular to feathery ferrite microstructures within a matrix of retained austenite are characteristic attributes of this family of ADIs. Retained austenite plays a key role to determine the improvement in wear resistance. This has been the subject of much

speculation. Wear resistance is developed as retained austenite strain hardens and perhaps gets transformed into martensite. This has been proposed by many researchers [58, 59].

Tribological behavior of ADI was compared with abrasion resistant quenched and tempered steel used in earth moving applications. It performs well under different wear conditions like adhesion, abrasion and rolling contact fatigue. Some metallurgists incorporated alloy carbides in the matrix and converted into Carbide Austempered Ductile Iron (CADI). Role of Chromium in ADI was also investigated by few researchers [60, 61]. Tanaka et al. [62] reported that conversion of austenite into ferrite is more in DI austenitised at lower temperatures. DI austenitised at lower temperatures have iron carbides in matrix along with ausferrite. DI austenitised at 900°C had evenly distributed carbides in the matrix of ausferrite [63-66].

Numerous examinations in the past have been done on the alloyed assortments of ADI. It has been explained that wear resistance is 2.5 times higher to pearlitic grey cast iron [67-70]. Spheroidal graphite present proffers excellent lubricity and hence improves wear resistance [71, 72]. As ADI castings propose excellent design flexibility with relative ease of manufacturing combined with unique combination of high strength and toughness, they are pleased to be better replacement for forged steel components in applications like gears, rolls and drill bits and crankshafts [73-75].

The procedure of austempering was first developed by Bain and Devenport and practically used for steels in 1930. The resulted microstructure was named after Bain as bainite. Austempering is carried out in the bainitic region. Habitually surface oxidation of specimens or components is evaded by carrying out austenitisation and austempering in molten salt baths [76].

Design of experiments (DOE) has been widely utilized by analysts in wear contemplate as well as in different ranges also. DOE is a statistical technique and an efficient tool. It is used to study multiple variables or factors concurrently. It augments the measure of data picked up from a review and limits the measure of information accumulation [77]. Data about the working of a whole framework and cooperation of variables is given by it, which might be hard to get through testing a solitary component at any given moment keeping others steady. DOE gives data about the response of interconnected components over an extensive variety of qualities without testing every single conceivable esteem [78]. It finds various applications in

the meadow of science and engineering for process development, optimization and validation tests [79]. Automotive, chemical products, medical devices, semiconductor industries have effectively implemented DOE [80]. Researchers, specialists and designers are utilizing this method to decrease time required for any test investigation. Basically, traditional experimental designs are excessively entangled and difficult, making it impossible to utilize. An extensive number of test works must be completed when the quantity of process parameters increment. To take care of this issue, DOE approach utilizing Taguchi system has been effectively utilized by analysts in the investigation of wear conduct of tribological materials.

Taguchi strategy is a capable tool for the plan of excellent frameworks [81, 82]. Taguchi strategy utilizes an extraordinary outline of orthogonal arrays to concentrate the whole parameter space with just few tests. The Taguchi way to deal with experimentation gives a deliberate approach to gather information and to break down the impacts of parameters over some particular response. The strategy consolidates trial and explanatory ideas to decide the parameter with the most grounded impact on the subsequent reaction for a huge change in the general execution. The arrangement of tests is created in Taguchi strategy by the utilization of standard orthogonal exhibits. The exploratory outcomes were then analyzed by using analysis of variance (ANOVA) of the control factors [83, 84].

Novelty of present research work is to develop and study wear behavior of ADI especially at elevated temperatures for wear resistance applications. DOE approach utilizing Taguchi technique has been effectively adopted to study wear and friction. The research findings can help to understand the influence of control parameters such as speed, load and sliding distance and external parameter temperature on wear behaviour and friction of ADI. A well optimized and trained model for wear prediction was also developed using Artificial Neural Network. The specific objectives however are clearly outlined in the next chapter.

1.2 Thesis Outline

The rest of the thesis is organized as follows:

Chapter 2	Incorporates a literature survey to give basic information of the fundamental subjects displayed in this proposal. It convolutes the exploration works completed by different investigators particularly on Austempered Ductile Iron and other related materials.
Chapter 3	Furnishes information about raw materials utilized, production method, test strategies and a depiction of the Taguchi experimental design and MATLAB application in wear study.
Chapter 4	Presents results and discussion on optimization of wear control parameters on ADI at room temperature.
Chapter 5	Presents results and discussion on the elevated temperature wear behavior of ADI.
Chapter 6	Presents results and discussion on optimization of wear control parameters on ADI at elevated temperature.
Chapter 7	Presents results and discussion on the comparative wear behavior of two categories of ADI selected for study.
Chapter 8	Presents results and discussion on prediction of wear using Artificial Neural Networks.
Chapter 9	Presents conclusions from the research findings and scope for further research work.

Chapter 2

LITERATURE REVIEW

2.1 On Ductile Iron (DI)

2.1.1 History of DI

Cast iron was first invented by Chinese archaeologists in the fifth century BC. The needed components like pots, weapons and ploughshare were made by pouring cast iron into mould which was replica of the part. It was in ample use in ancient China since it was in copious and available at cheap rate. However its strength was mediocre to steel. High compressive strength and brittleness were the attributes of the cast. It was unused where sharp edges were the necessity because of its brittle characteristic. It was burly in compression but weak in tension. It was unavailable in western countries till fifteenth century. Canon casting was instigated by Henry VIII in England. Bronze canons were being used before iron canons. Development of casting technique facilitated them to cast iron canons. But it was heavier to bronze. Brass was the crude material for making engine cylinders. Due to the dawn of steam engine by Thomas Newcomen, cast iron increased tremendous market as it was less expensive to brass. Ductile iron (DI) was invented by Keith Millis in 1943. Spheroidal cast iron or SG iron or nodular cast iron is the alternate name for ductile iron. Nodular graphite present in DI helped it be more impact and fatigue resistant contrasted to other varieties of cast iron [85]. Keith Dwight Millis, Norman Boden Pilling and Albert Paul Gangnebin received US patent for DI creation by means of magnesium treatment on October 25, 1949 [85]. Railings, window frames, street lamps etc. were made out of CI in Victorian times. DI developed to extremely sophisticated levels. Compacted graphite iron, SG cast iron were produced from cast iron. Extensive variety of properties was acquired by controlling microstructure in DI. DI was named after the form of graphite. Graphite is in nodules form in DI and flakes in grey iron. Flakes appear as stress focus points within metal matrix whereas round nodules restrain cracks creation imparting ductility to the material and hence the name [86].

2.1.2 Production of DI

2.1.2.1 Raw Materials

Pig iron, steel scrap and returns from foundry are the main raw materials needed. The sulphur content must be under 0.02 by wt % to discover great blend of quality and strength. The manganese substance ought to be between 0.1 to 0.2 % for better ductility. Trace elements like antimony, titanium and lead are kept as low as possible for improved graphite structure [88].

2.1.2.2 Composition Control

Grey iron and unalloyed DI possess same carbon and silicon contents. In unalloyed DI carbon content ranges from 3.2 to 3.6% and silicon from 2.2 to 2.8%. Sulphur is to be in the range of 0.005 to 0.02 % and phosphorous from 0.005 to 0.04 %. Since impurities meddle with the development of graphite nodules, they must be kept as low as possible [87]. Composition of DI should be controlled for better properties.

Carbon content must be reserved in the range indicated in view of the silicon content. Graphite may float if carbon content is over 3.6%. Raw materials introduce silicon content in DI and as well as from alloys containing silicon during inoculation. Silicon and ductility are inversely related. There is a menace of carbides formation in slender sections due lower silicon. This is avoided by having higher silicon levels in thin sections. Silicon increases tensile strength and hardness. Carbon, phosphorus and silicon content collectively identified as carbon equivalent (C_{eq}). This acts as a channel to foundry behavior and also helps in evaluating casting properties. The following formula is commonly used to find its value;

$$C_{eq} = C \% + 1/3(Si \% + P \%)$$

The iron will have eutectic composition at C_{eq} 4.3%. Higher than 4.3% will have graphite nodules in structure and lesser will have dendrites. Steel scrap used as a charge is the main source of manganese. Utmost ductility can be obtained by limiting its content. Especially in heavy sections there is peril of manganese becoming undesirable micro segregation. The content is also accountable for the formation of grain-boundary carbides resulting in lower ductility and toughness [88].

The magnesium amount in the range of 0.04 to 0.06% assists in the formation of spheroidal graphite. Lower magnesium content results in compacted graphite structure with poorer properties while high content endorses carbides formation and

dross defects. The unwanted elements like bismuth, lead, titanium and antimony gets introduced as traces with raw materials charge. Cerium addition neutralises their effects as reported by Hughes [88].

As phosphorous lowers ductility its content is set aside below 0.05%. Aluminium in small traces promotes porosity, dross formation and surface pinhole. Cast iron and steel scrap and inoculants are the main sources of aluminium introduction in DI. Inoculants with lower aluminium content are desirable. Its level is kept as low as 0.01%. Vanadium, boron and chromium promote carbide formation and hence are controlled by vigilant selection of raw materials [88].

2.1.2.3 Desulphurization

Sulphur from molten iron is eliminated by range of compounds such as calcium carbide, calcium cyanide, caustic soda, soda ash, burnt lime etc.. Caustic soda is not suitable because of health hazards. Lime is decreased to Calcium oxide before utilize. Calcium cyanide raises nitrogen in base iron and consequently may induce defects in castings. CaO is extensively used as a desulphurizing compound. Manganese can likewise be utilized with respect to desulphurizing, yet is expensive [88].

2.1.2.4 Spheroidization

The most practically difficult part is to have right proportion of magnesium in the melt with vital consistency. Magnesium has a boiling point of 1091°C. When it is brought into solid metal dissolve at around 1400°C, it vaporizes wildly conveying some cast iron alongside it. To dispose of this trouble, nickel-magnesium combinations are utilized as they sink in liquid metal. However, it is costly and introduces nickel into the melt. Magnesium-ferro-silicon alloys can also be used. Magnesium is added into the melt by sandwich method. Magnesium-ferro-silicon alloys possess low density and therefore float on the melt making the reaction ineffective. To surmount this difficulty, the alloy is put in the pocket made at the base of the ladle and covered with steel plate. Ladle is heated before use. Now melt does not intrude directly on the alloy, instead flows over the sandwich. The cover holds-up the reaction till enough profundity of alloy is built up and also averts floating. To advance magnesium recovery, the ladle is to be filled up as swiftly as possible. The

magnesium revival depends on design of ladle, amount of metal treated and its temperature [89].

2.1.2.5 Inoculation

It provides melt with nuclei onto which solid phases develop during freezing. During freezing, insertion of fines of same phase will result in the formation of nuclei. These act as sites of crystal augmentation, if fines dissolve partly before the start of solidification resulting in heterogeneous nucleation. For graphite spheroids, heterogeneous nuclei are shaped in the inoculation of DI. Inoculation builds up vigorous nodule count. It lessens the formation of principal iron carbides. If not, these carbides generate sharp edges on casting, making it difficult for machining. Inoculation brings in more uniform properties, by reducing reaction rate at leaner sections. It perk ups toughness, wear resistance, tensile strength and machinability. Each material introduced inoculates to some extent. Ferro-silicon alloys with proper chemical composition are favoured for efficient and controlled inoculation. As aluminium endorses hydrogen pinhole defects, the inoculants ought to contain little aluminium. Limiting size of the inoculants is half inch and smallest amount is 1/6th of an inch. Once exposed to open air, its efficacy deteriorates hence it needs to be stored in closed containers. Ladle inoculation, in-stream inoculation and in-mould inoculation are the three modes of inoculation [89, 90].

2.2 On Austempered Ductile Iron (ADI)

2.2.1 Introduction to ADI

Cast iron (CI) is an alloy of carbon and iron. The carbon present is greater than 2%. Silicon is also present in high percentages usually ranging from 2-3%. This turns CI a ternary system. Silicon promotes carbon to precipitate as graphite. It also decreases the carbon content of the eutectic from 4.3%, lessens austenite field area and increases the eutectoid transformation range. This results in the austenite transformation to stable room temperature phase as indicated in figure 2.1 [91].

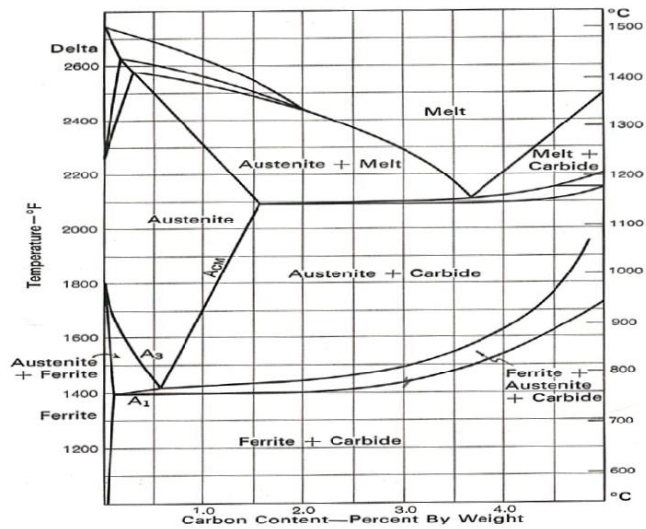


Figure 2.1 Fe -C- Si ternary phase diagram at 2% silicon [91].

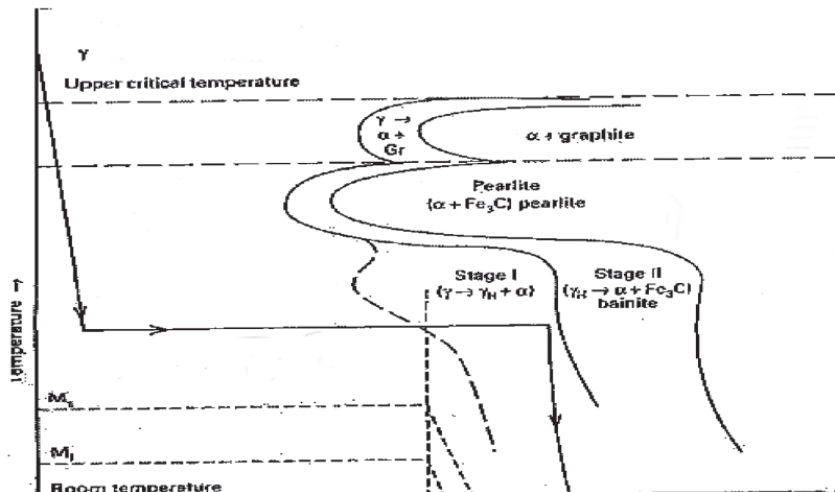


Figure 2.2 Isothermal transformation diagram of a ductile iron composition [91].

Figures 2.1 and 2.2 symbolize Fe -C- Si ternary phase diagram and classic isothermal transformation diagram for ductile iron composition. The diagram (fig. 2.2) illustrates that the austempering completes in two stages.

In the first step, austenite gets transformed into acicular ferrite and soaring carbon soothed austenite. This is the aspired microstructure and provides incredible properties to ADI. This arrangement of acicular ferrite and high carbon soothed austenite is known as ausferrite.

In stage 1;

Austenite \longrightarrow acicular ferrite + high carbon stabilised austenite

In the second step, when austempering time is delayed high carbon austenite decomposes into ferrite and carbide resulting in a brittle material. This structure does not have preference in ADI and needs to be avoided.

In stage 2;

High-carbon stabilised austenite \longrightarrow ferrite + carbide

Most of the desired properties are accomplished on completion of the first stage reaction. Hence proper selection of austempering time plays a vital role [91].

2.2.2 Austempering Cycle

The primary austempering cycle is identical for both ductile iron and steel. The typical austempering cycle has the following chronological operations.

1. Heating of the specimen to austenitisation temperature.
2. Holding it at that temperature for a sufficient time (austenitising)
3. Quenching it in molten salt bath preserved in the temperature range of 200-400°C and holding it for adequate time (austempering).
4. Air cooling of specimen to room temperature.

At the time of austempering, ductile iron undergoes into two stage transformation. However in steel, austenite changes into bainite in a solitary stage transformation. Figure 2.3 depicts schematic diagram of typical austempering cycle for ADI. Cycle times are blotted at the bottom of the diagram.

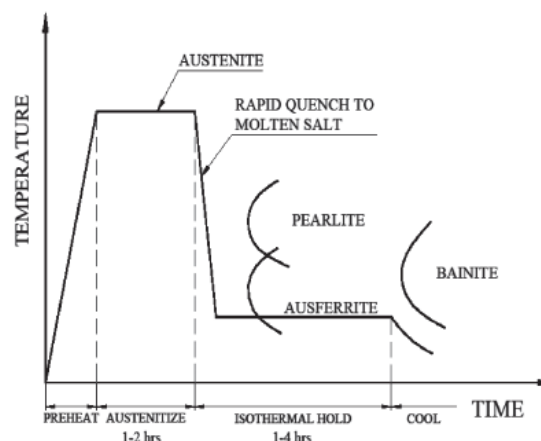


Figure 2.3 Schematic diagram of ADI processing steps [91].

For austempering, 200-400°C is the normal temperature range maintained in a molten salt bath. By fluctuating the austempering time various grades of ADI can be acquired. ADI with grades 3-5 can be manufactured with lower austempering temperatures which will possess high strength and wear resistance. ADI with grades 1-2 can be realised with elevated austempering temperatures which will have high toughness and impact. Since temperature range for grades 1-5 is small, temperature requires to be controlled within a small number of degrees, or else, obtained properties cannot be in range [91].

2.2.3 Production of ADI

Successful production of ADI is not very easy. It needs high-quality DI castings with constant microstructure and chemistry. Reasonable alloying elements in the required extents are expected to thoroughly harden the casting. Information on the appropriate austempering cycle is required as it is one of the deciding factors of ADI properties. Also a unique heat treatment furnace with accurate control of temperature, time and charge transfer is required. Great quality ductile iron is the beginning material required for ADI generation. DI castings are created according to the rules laid by the individual foundries. Quality DI is described in terms of microstructure, consistent chemistry, nodule count and lower levels of casting defects such as porosity, shrinkage, oxide, slag and inclusions. Chemistry decides the ADI cycle parameters. To achieve reproducible results for every batch, chemistry calls for control within limits. Nodule count ought to be over 100/mm² and nodularity above 85%. High nodule counts reduce micro-shrinkage and micro-segregation. Microstructure has to be uniform and consistent. The ferrite and pearlite ratio requires to be maintained in the as cast microstructure. This plays a crucial role for holding dimensional tolerance in machined castings. During austempering, there is certain amount of growth. Level of development is subject to the proportion of ferrite and pearlite. Development will be steady if the proportion is kept up. Microstructure is directed by the processing parameters, chemistry and shake out practice. Defects in castings have to be in low percentages. They influence ductility, strength, performance and machinability of castings. Steady casting practices and chemistry should be taken after every last time. It brings about better quality castings with great nodule count, nodularity, least casting defects with steady microstructure. Consistency is the key for fruitful ADI generation. Uniform microstructure and intensive

hardening is required all through the area thickness. Alloying elements like Cu, Ni, Mn and Mo are put in to thorough harden the whole section thickness. Lesser alloying elements than required for the given segment thickness brings about blended structure (with pearlite) with substandard properties. It is likewise not favourable to include more alloying elements than should be expected to thorough harden. For the most part alloying elements are costly. They will increase the cost of ADI if utilized in excess. Few alloying elements may isolate to cell boundaries amid solidification. It results in lower toughness and ductility. Cu and Si need to be located near the nodules. Ni gets appropriated consistently around the nodules and cell boundaries and consequently should be included higher rates securely. Elements like Mo, Mn, V, Ti, Cr and other carbide formers separate out substantially at the cell boundaries. They diminish ductility and produce problems at the time of machining. So Mo, Mn and other elements are kept below 0.3%. Quality castings, microstructure and reliable chemistry alone won't ensure effective generation of ADI. Heat treatment also plays a vital and basic role. It is essential to know literal liaison between microstructure, chemistry, transformation kinetics, time, temperature parameters and property requirements. Experimentation of austempering procedure won't work for ADI. Heat treatment furnace likewise has a huge role in the fruitful production of ADI. Furnace must be consolidated with the instrument to quench the segments at austenitic temperature inside few moments else it brings about the development of pearlite structure. As different grades of ADI can be produced from a restricted temperature range of 200-400°C, temperature should be controlled in the scope of $\pm 6^\circ\text{C}$. To keep up uniform temperature and to improve severity of quench, salt bath needs to be agitated continuously. There might be peril of salt bath blast and consequently require safe operation and cautious dealing with. Consequently it can be inferred that ADI requires an uncommon heat treatment prepare with legitimate control of different pivotal parameters [91-94].

2.2.4 Microstructure of ADI

Matrix structure in ADI is known as “Ausferrite”. The structure is a blend of acicular ferrite and high carbon balanced out austenite (fig. 2.4). Carbon settled austenite might be as high as 50% at higher austempering temperature. Extensive varieties of properties can be obtained by shifting the blend extents. Structure ends up noticeably refined and better in scale if the austempering temperature is diminished.

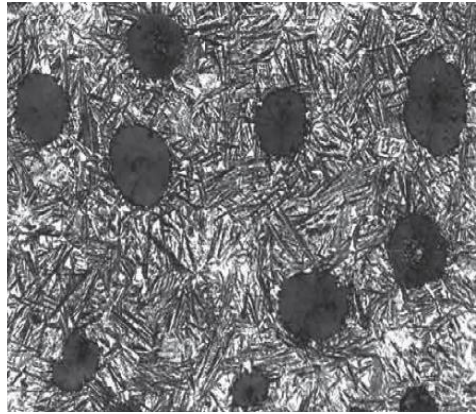


Figure 2.4 Microstructure of ausferrite [91].

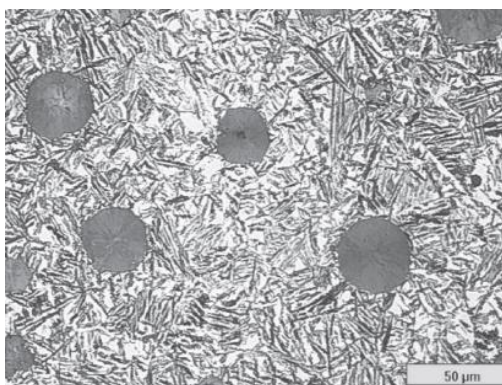
At low temperature, ausferrite structure is stable. At the point when ADI is subjected to normal force, high carbon austenite gets work hardened and changed into martensite making the surface hard and wear safe with an extreme ausferrite matrix.

2.2.5 Properties of ADI

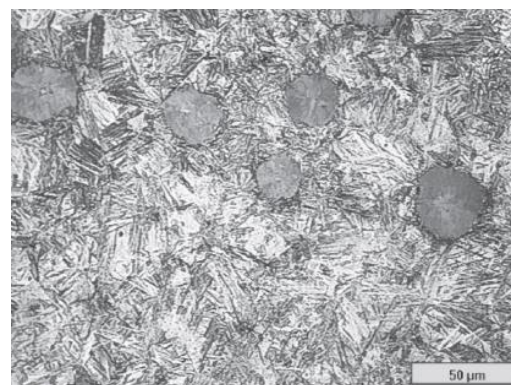
ADI is not a solitary material but rather alludes to a group of heat treated DI. ASTM A-897/897 M-06 (2011) catalogues six categories of ADI. The base properties to be met by each grade are indicated in Table 2.1. Heat treatment parameters decide the range of properties. This decides microstructural size of ausferrite with extents of austenite and ferrite inside the ausferrite. Figure 2.5 depicts the range of microstructures. But, first grade of ADI is an exemption to this rule. It is produced by inter-critical austenitising. This turns into a microstructure that includes ausferrite and pro-eutectoid ferrite. It is generally given as Grade 750 ADI. Any grade of ADI (except grade 750 ADI) can be produced by choosing legitimate extents of alloying elements and austempering temperatures and time. For the most part higher strength and hardness grades of ADI are created with lower austempering temperatures. ADI strength is twice to cast-DI for the specified ductility [92].

Table 2.1 Grades and properties of ADI as per ASTM A897/897M-06
(reapproved 2011) [92]

Grade	Former designation	Tensile strength (MPa)	Yield strength (MPa)	Elongation (%)	Impact energy (J/lb-ft)	Typical hardness (HBW)
750-500-11 (110-70-11)		750 / 110	500 / 70	11	110 / 80	241 - 302
900-650-09 (130-90-09)	Grade 1	900 / 130	650 / 90	9	100 / 75	269 - 341
1050-750-07 (150-110-07)	Grade 2	1050 / 150	750 / 110	7	80 / 60	302 - 375
1200-850-04 (175-125-04)	Grade 3	1200 / 175	850 / 125	4	60 / 45	341 - 444
1400-1100-02 (200-155-02)	Grade 4	1400 / 200	1100 / 155	2	35 / 25	388 - 477
1600-1300-01 (230-185-01)	Grade 5	1600 / 230	1300 / 185	1	20 / 15	402 - 512



(a)



(b)

Figure 2.5 Photomicrographs of the ausferrite microstructure in ADI. grade 900-650-09 ADI is shown in (a) while grade 1600-1300-01 ADI is shown in (b). The grade 900 ADI was produced by austempering at 371°C while grade 1600 ADI was produced by austempering at 260°C. Etched with 5% Nital [92].

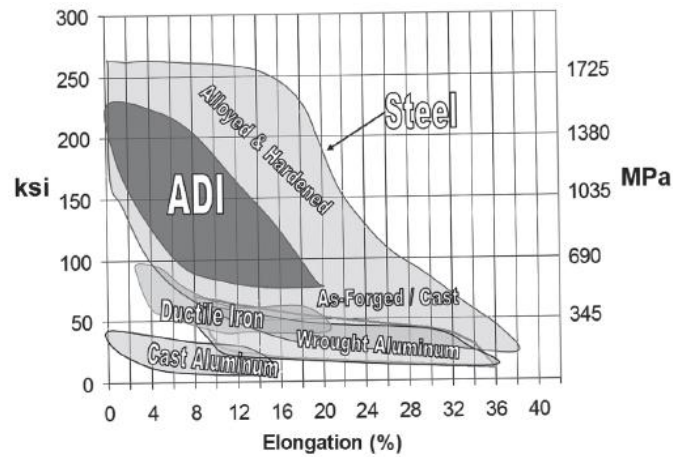


Figure 2.6 Yield strength vs. ductility for various metals [92].

Figure 2.6 shows the association between ductility and yield strength for various metals. Before ADI, steel was the main material accessible with yield strength over 600MPa for designers [92].

2.2.6 Advantages and Disadvantages of ADI

The following are the few advantages and disadvantages listed [92, 93];

Advantages:

- As sufficient time is available for transformation, there is no stress and cracking in quenching.
- It has twice the strength of DI.
- It has properties comparable to steel and also lighter and cheap to steel.
- It has remarkable wear and fatigue resistance.
- It has work hardening aptitude resulting in hard wear-resistant surface with tough core.

Disadvantages:

- Welding is not recommended for austempered ductile iron.
- Lower grades can be machined after heat treatment, but higher grades must be machined before heat treatment.

2.2.7 Applications of ADI

Commercial applications of ADI are gradually increasing since its inception (1970). ADI with grades 1 and 2 are most appropriate in applications which entail good dynamic properties like fracture toughness or fatigue strength. Grades 4 and 5

are considered when wear is of great concern. Grade 3 is preferred when wear and dynamic properties become vital. For thin section sizes, Grade 750 is favoured but needs machining after heat treatment.



Figure 2.7 Constant velocity joint [93].

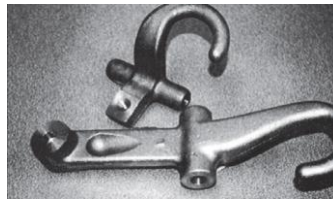


Figure 2.8 Tow hooks [93].

Figures 2.7 and 2.8 represent two eminent automotive sector ADI applications. For constant velocity joints ferritic DI is machined prior to austempering to 45HRC hardness. For sport utility vehicles and trucks, different sizes and shapes of tow hooks with grades 1 and 2 are employed. They are represented in figure 2.8.

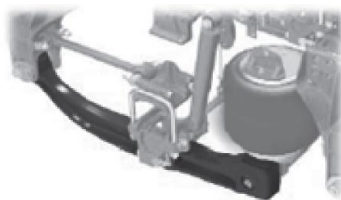


Figure 2.9 An ADI suspension beam that replaced a steel forging and increased durability [93].



Figure 2.10 A sway bar bushing for a heavy truck axle [93].

Figure 2.9 represents an ADI suspension system used in heavy truck vehicles which successfully replaced forged steel. It increased durability by 350% at lower cost. A sway bar bushing is another heavy truck application and is shown in

figure 2.10. Before austempering to grade 3, the component is fully machined. It includes an acme threaded ID and a precision spline.

Majority of the design engineers will have an impression of using materials with low density like aluminium when reduction in weight is considered. Figure 2.11 represents heavy truck vehicle trailer hub replacing aluminium hub at 4% savings in weight as ADI is stronger and 2.3 times stiffer to aluminium. This allows design engineers to reduce thickness at sections.

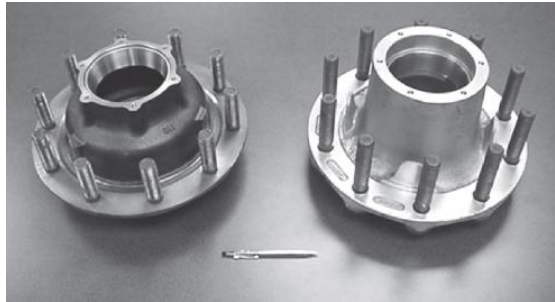


Figure 2.11 An ADI hub along with the competitive aluminium hub that it replaces [93].

In recent years ADI applications in the agricultural sector is enormously increasing. Figures 2.12 and 2.13 show the ground engaging applications of ADI. Figure 2.12 shows a seed boot plant to put seed into the soil. This seed boot weighs 15% less and 65% less in cost to steel weldment and thus replacing it. Also it exhibited remarkable wear performance. Figure 2.13 shows ADI plow point. Grades 4 and 5 are suitable for such ground engaging applications. Other similar applications employ Carbide Austempered Ductile Iron (CADI).



Figure 2.12 Seed boot [94].



Figure 2.13 Plow point [94].

Control arms, brackets, steering knuckles etc. made of ADI find applications in mining and construction vehicles. Figure 2.14 shows a drive wheel used in track system. This one piece casting replaced 84-piece weldment. Different shapes and sizes of gears can be made out of ADI. Some of such examples are shown in figure 2.15.

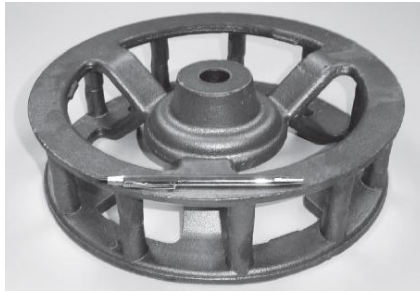
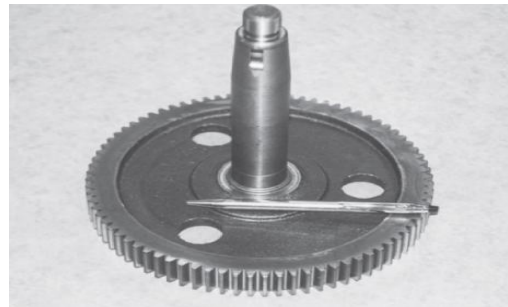


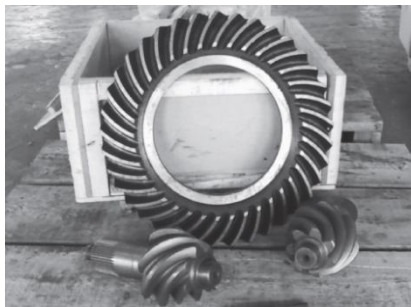
Figure 2.14 A drive wheel for the track system [94].



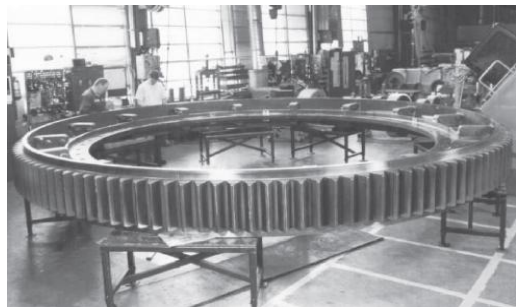
(a)



(b)



(c)



(d)

Figure 2.15 (a) Diesel engine timing gear, (b) Hypoid differential gears and pinions, (c) A one-piece gear and axle for a commercial lawn mower and (d) A large mill gear produced in segments and then assembled after Austempering [95].

2.3 Modes of Wear

Adhesive, abrasive, fatigue and corrosive wear are four modes of wear shown in figure 2.16.

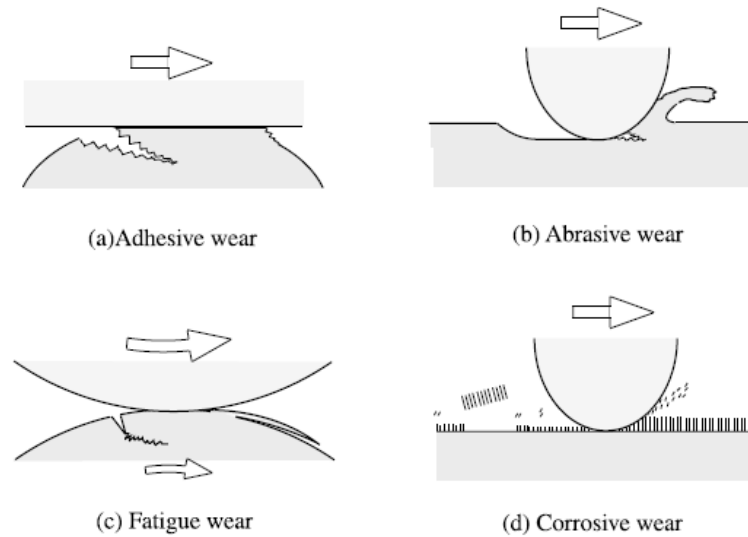


Figure 2.16 Wear modes (a) Adhesive wear (b) Abrasive wear (c) Fatigue wear (d) Corrosive wear [96].

2.3.1 Adhesive Wear

While two surfaces in contact have sufficient adhesive bonding strength and the contact region is subjected to shearing and compression, dislocation causes large plastic deformation. Due to this a crack is instigated in the contact region. It proliferates in the connected fracture mode of shearing and tensile. Wear particle is figured, once the crack reaches the contacts interface and thus forms adhesive wear. This type of wear is known as adhesive wear [96].

2.3.2 Abrasive Wear

The curved or inclined contact surfaces intertwine and ploughing takes place if subjected to sliding. Due to ploughing certain volume of material gets eradicated from the surface. This forms abrasive groove on feeble surface. This kind of wear is known as abrasive wear. In case of ductile material lengthy ribbon like wear unit is produced by micro-cutting mechanism. However in case of brittle material, crack propagation produces wear particle [96].

2.3.3 Fatigue Wear

Wear particles are additionally created by rehashed surface contacts. Wear produced for the contact cycles is known as fatigue wear. High-cycle fatigue mechanism is dominating at higher number of contact cycles. For shorter number of contact cycles, low cycle fatigue mechanism is detected [96].

2.3.4 Corrosive Wear

Electrochemical or chemical interactions of surfaces result in the development of reaction products on surfaces. The reaction products thus formed adhere sturdily to the surface and act as a bulk material. This wear mechanism is similar to that of bulk material. Be that as it may, by and large the behavior of reaction products is particularly not quite same as the bulk material. Wear is unlike for the corroded surfaces. This category of tribochemical wear step up by the corrosive media is known as corrosive wear. A reaction layer created by the tribo-chemical reaction on the surface gets eliminated by friction [96].

2.4 Wear Behavior of ADI

Astounding mechanical properties, for example, high quality, wear resistance, fatigue strength and great ductility turns ADI as an imperative engineering material [97-104]. ADI discovers applications in automobile and engine parts, agricultural implements and gears, majority of which experience wear. ADI possess high wear resistance than tempered and quenched DI as stated by previous investigations [105-108]. Ausferrite microstructure and high carbon in retained austenite provide high resistance to ADI [109]. It is additionally revealed that, strain hardening of austenite and transformation of austenite into martensite during work hardening contributes for wear resistance enhancement. Ausferritic microstructure with carbon prosperous austenite is accountable for this kind behavior. Ductility in conjunction with strain hardening capability of austenite or strain induced martensitic transformation brings in remarkable boost in hardness. Because of this effect, ADI with low initial hardness reveals better wear resistance [110, 111]. Velez et al. [112] and Mohan et al. [113] confirmed that at same hardness level, ADI with fine ausferrite microstructure exhibited better wear resistance than tempered and quenched DI. Daber et al. [114, 115] reported that high austempering temperature produces blocky austenite which gets changed to martensite amid strain hardening. This makes ADI a potential contrasting option to steel having equivalent toughness and strength, more noteworthy damping limit, lower density and with amazing castability. Connecting rod, transmission gears and crankshafts are the other suitable areas of application of ADI [116, 117]. ADI's wear behavior is influenced by the surface graphite nodules and the ability of meta-stable retained austenite at room temperature to change into

martensite during strain hardening [118-121]. Straffelini et al. [119] reported that ADI displayed lower wear coefficient and COF to nitride steel in dry rolling-sliding wear. As attributed by authors it was because of the smearing of graphite on surface acting as a lubricant between wear surfaces in contact. Wear mechanism maps portrayed by Lim and Ashby [122] were used to establish the wear mechanisms. Graphical presentations of wear rate and mechanisms in steel / steel tribo contacts for a wide range of sliding speeds and loads was given by the latter authors. Surface properties can be improved by changing either microstructure or composition of surface by using surface engineering techniques such as mechanical, thermal, chemical or thermo-chemical treatments. Tan et al. [123] reported laser hardening improved surface hardness and abrasive wear resistance of nodular cast irons. It was attributed to the predominant martensitic structure formed in the hardened zone. Lu and Zhang [124] reported that austempered and laser hardened Cu-Mo ADI exhibited relatively high sliding wear resistance as compared to DI. They attributed this to the conversion of retained austenite into martensite through strain hardening and martensite that was attained during laser processing. Further to this, Xue et al. [125] reported that contact fatigue resistance was lofty for ADI and laser hardened ADI compared to induction hardened steel.

Fatigue strength of automotive components may be developed by conventional mechanical surface treatment such as shot peening. Here spherical media are assailed onto the surface of material which generates a layer of compressive left over stress and induce lofty dislocation densities [126]. The layer created enhances the resistance to crack initiation and proliferation thus improving the life of components. Shot peened surface turn into rough due to the formation of dimples by the striking of spherical media in turn changes components wear resistance. Ohba et al. [127] observed high COF at the beginning of test and work hardened surface in rolling contact fatigue tests on ADI. Ho et al. [128] showed shot peening decreased the wear rate of hardened 4340 steel and did not perk up the sliding wear resistance of annealed 1018 steel. On the other hand, Vaxevanidis et al. [129] reported that tribological behavior of steel was improved by shot peening. Studies [130-134] showed the improvement in fatigue bending strength by shot peening.

Investigations on the role of graphite nodules and matrix hardness in ADI were also carried out [135, 136]. In addition the transition from mild oxidative wear to severe wear by delamination under the influence of various tribological parameters

such as sliding distance, load and speed was studied by few authors [137-139]. Gears will have rolling-sliding contact with extensive contact pressures because of the line contact. Hence investigations were carried out on the rolling-sliding wear behavior and reported that wear by delamination turned to be severe in the course of time and also wear behavior of ADI was compared with nitride steel [140]. Sugisghita et al. [141] studied dry rolling-sliding wear behavior of nodular cast iron having ferritic-pearlitic matrix microstructure with particular emphasis on the role of graphite nodules. It was found that during rolling-sliding graphitic squeeze films were formed due to the release of graphite nodules. In delaminative form of wear surface and subsurface regions are subjected to extensive plastic shear stresses. Under such circumstances microstructure plays a predominant role to withstand the conditions as it has the ability to strain harden and retained austenite may change to martensite [142-144]. Like so, material develops an ability to bear the contact load to contrast wear [145, 146]. Perez et al. [147] by treating Cu-Ni-Mo ADI with little variation in austempering temperature and time showed the optimum wear behavior of the material. Kumari et al. [148] demonstrated that fine ausferrite microstructure advanced wear resistance. Tribo-oxidation controls dry sliding wear. Here surface asperities or debris created during sliding gets oxidised and a protective scale is formed by the agglomerated oxide particles [149, 150]. Wear is due to the fragmentation of these scales and thus it is typically mild [151-153]. Working parameters such as sliding distance, applied load and sliding speed determine transition from mild oxidative wear to ruthless delamination. A critical combination of speed and load prevents the formation of oxide scale by delaminating the surface material [154-156]. Riahi et al. [157] produced wear map for grey cast iron which displays speed-load boundary between gentle oxidative and severe wear by delamination. Lu et al. [145] reported that because of oxidation at low loads wear was mild and wear resistance improved with creation of strain tempered martensite in subsurface regions. Haseeb et al. [146] reported the contribution of strain induced retained austenite transformation and strain hardening for the oxidative wear resistance of ADI. Also supremacy of ADI was emphasized by the authors in comparison with tempered and nodular cast irons at the same hardness level. Fordyce and Allen [156] showed that matrix hardness and sliding speed are proportional to oxidative wear resistance of ADI. Authors also brought to light the formation of hard white and patchy layers on worn surfaces but however their part was not discussed on

the wear process. Microstructural studies on embrittled ADI when in contact with moisture [158], influence of welding [159] and stress corrosion cracking behavior [160] were carried out.

ADI swung to be a critical engineering material with amazing properties. These include good wear resistance, good fatigue strength, high tensile strength with good ductility [161-170]. Agricultural implements, automobile and engine parts, gears are subjected to rolling and sliding wear [171-174]. Investigations [175, 176] reported that ADI has much improved wear resistance to cast iron. Ahmadabadi et al. [177] also reported that ADI's wear resistance is superior to grey cast iron and concluded that presence of ferrite and high carbon austenite conveyed wear resistance to it. It has been reported that [178-180] that strain hardening of austenite and formation of strain induced martensite made ADI enhanced wear resistant. ADI possesses improved wear resistance to martensitic steels with similar hardness [181]. Even small hardness ADI exhibits better wear resistance if strain hardening occurs or strain induced martensite results [182]. Velez et al. [183] reported that fine ausferrite ADI exhibits good wear resistance to tempered and quenched irons at the same hardness level. He relayed this to martensitic transformation or strain hardening. Mohan et al. [184] too reported that fine ausferritic matrix ADI has good wear resistance to tempered martensitic matrix at same hardness level. The ductility and austenite strain hardening capability or martensitic transformation significantly increase hardness. Zhou et al. [185] reported that abrasive wear resistance of martensitic matrix DI also relies on volume fraction of austenite. Daber and Rao [186] and also Daber et al [187] investigated on the effect of microstructure morphology on strain induced martensitic formation. They found that higher austempering temperatures develop blocky martensite which undergoes strain induced martensitic transformation. It was revealed by a two step austempering. Low austempering temperature generates fine ausferrite and higher produces coarse ausferrite.

Boutorabi et al. [188] studied wear behavior of ADI containing aluminium and showed that it was a complex function of austempering time and temperature. Ahmadabadi et al. [189] reported that ADI having 0.75% Mn austempered at 375°C has substandard wear resistance to ADI austempered at 315°C. He observed lower wear rate in ADI with lower nodule count than in higher. Influence of heat treating variables such as austenitising time and temperature and austempering time and

temperature on mechanical properties is well set up as indicated by the literature on ADI [190-199].

Most commonly encountered industrial problem is wear by abrasion which leads to recurrent replacement of parts. Penetration of asperities or hard particles onto surface roots wear by abrasion and material gets displaced in the form of slivers or elongated chips. These hard particles are made amid the wear procedure or might be presented by the tainting from environs. Wear is not an innate property of material. Rather it relies on tribological framework, for example, microstructure, rough coarseness estimate, test conditions and environment [200-203]. Rebaso et al. [204] conducted investigations on thin wall DI prepared from plates having thickness ranging from 2.5mm to 12mm. It was observed that nodule count was proportional to abrasive wear. Moore et al. [205] found that subsurface plastic region was reliant on abrasive grit size and applied load.

There is an incongruous opinion on the wear behavior of ADI with respect to retained austenite and hardness. One such opinion is that small austempering temperatures produce ADI with lofty hardness and retained austenite in small volumes with superior wear properties [206]. Other researchers conveyed modest effect of initial hardness on wear resistance. Johanson et al. [207] reported that the amount and quality of retained austenite has predominant effect on wear resistance than initial hardness. It was also reported that transformation of austenite to martensite was due to the surface stresses and thus was responsible for increase in wear resistance of surface.

ADI manufacturers are generally hesitant to use unalloyed DI due to quality issues. Alloying elements for instance Ni, Cu, Mo or Mn in proper ratios are generally preferred to spurn pearlite nose of CCT curve. This is attained with little effect on the transformation of first stage ausferrite. An impediment in the austenite stabilization results in martensite formation when cooled to room temperature [208]. It is significant to know relationship between material properties and its wear behavior with respect to the operational conditions. It is necessary in design and materials selection for tribological applications [209].

2.5 Taguchi Method

The requirement of optimization is to get best outcome. Input parameters are adjusted to optimize output for enhanced performance. In general, optimization techniques are viewed as universal and local techniques. Particle Swarm Optimization (PSO), Genetic Algorithm (GA), Simulated Annealing (SA) and Taguchi's technique are the global optimization techniques. Gradient-based technique is the local optimization technique [210]. The techniques have been used over decades to enhance the performance of materials. Researchers [211-214] have also applied these techniques in the machining processes. Investigators [215-218] used the techniques for enhancing the performance of composite materials. Investigators [219-248] worked on the optimization of various test parameters in dry sliding wear, turning, milling, hardening processes.

A Kacal et al., [219] used Taguchi system to optimize finish turning process parameters of ADI. L_{18} orthogonal exhibit was utilized for plan of experiments. ANOVA was carried out to know the factors influencing cutting force and surface roughness. S/N ratio analysis carried out, suggested the combination of optimum process parameters. H. B. Bhaskar et al., [220] employed Taguchi technique to optimize factors such as speed, sliding distance and load for aluminium metal matrix composites in dry sliding wear test. Rama Rao. S. et al., [221] utilized Taguchi method to optimize control factors such as feed rate, voltage and electrolyte concentration on the material removal rate of Al/5%SiC composites in machining. Radhakrishnan et al., [222] used Taguchi system to optimize process factors in dry sliding wear of Al-2219-SiC particulate composites. Vinod Kumar et al., [223] completed improvement of tribological execution parameters of Al-6061T6 combination strengthened with SiC, Al_2O_3 15% and graphite particulates of weight rate of 10% on wear and friction properties. Uvaraja et al., [224] optimized dry sliding wear process parameters of SiC and B_4C particulates reinforced LM24 alloy matrix composite using Taguchi method. Hemanthkumar et al., [225] optimized wear test parameters of Al-Cu-Mg / Titanium dioxide particle reinforced composites using Taguchi technique. Basavarajappa et al., [226] studied wear influencing parameters on glass epoxy polymer composites and optimized them using Taguchi method. Hemanth Kumar.T.R et al., [227] carried out simultaneous optimization of tribological parameters on Al-Cu-Mg-Fe-Ni alloy under dry sliding wear test. Senthil kumar et al., [228] applied

Taguchi optimization technique on HVOF sprayed (WC-12% CO and Al₂O₃-13% TiO₂) coating on AISI 1040 steel substrate in dry sliding wear. Gopalsamy et al., [229] utilized Taguchi strategy to discover ideal process parameters in end processing of hardened steel AISI H13 with Tin covered P10 carbide embed. Bharat et al., [230] optimized wear process parameters along with reinforcement content of LM25/flyash Composite. Radhika et al., [231] optimized parameters influencing wear rate of AlSi10 Mg alloy reinforced with 9 wt% alumina and 3 wt% graphite using Taguchi system. Panchakshari et al., [232] optimized cryogenic treatment parameters in the wear study of Al/Al₂O₃ metal matrix composites. Rajesh et al., [233] has shown the use of Taguchi method for minimising wear rate and friction coefficient of red mud based aluminium MMCs. Taguchi method was used by Dinesh Kumar et al. [234] to optimize EDM process parameters of EN-353 steel. Oji et al., [235] employed Taguchi's optimization technique and optimized sand casting process parameters such as pouring temperature, mould temperature and runner size. Vijayanand et al., [236] applied Taguchi's Grey Relational analysis in the dry sliding wear parameters optimization on SiC reinforced Al-6082 alloy. Ganpat et al., [237] optimized aluminium silicon titanium alloy's dry sliding wear process parameters. Taskesen et al., [238] worked on the optimization of drilling process parameters for B4C reinforced Al-alloy using Taguchi method. Srinivasa et al., [239] optimized dry sliding wear behavior of Titanium Oxide (TiO₂) particulate filled e-glass fibre reinforced composites in the unsaturated polyester resin matrix. Ashok et al., [240] investigated on the optimization of tribological parameters of Al 6061 reinforced with 10% SiC fabricated by stir casting route under dry sliding conditions. Vinod Kumar et al., [241] studied effect of wear control parameters on wear rate and friction coefficient of Al6061T6 alloys and optimized them using Taguchi method. K.N.P. Prasad et al., [242] carried out wear process parameters optimization of LM6 Al-flyash composite prepared by squeeze casting. Madeva et al., [243] optimized dry sliding wear process parameters of Al6061-SiC particulate composites and showed that load has mainly astounding impact on rate of wear than different parameters. Rachit et al., [244] studied on the dry sliding wear optimization of SiC(10%) and graphite (5%) reinforced Al alloy produced by stir casting process. Abhay et al., [245] optimized parameters in crossed cylinder test on new and used lubricating oils using Taguchi method. Kochure et al., [245] found the best working parameters such as

input power, traverse speed etc. of induction hardening of EN8 D steel. Darshan et al., [246] found that the normal load was the most significant factor in the dry sliding wear test of bismaleimide nanocomposites on the basis of Taguchi's results. Ferit et al., [247] obtained optimal combinations of wear testing parameters of boronised AISI 1040 steel and developed wear resistance model. Aslan et al., [248] developed prediction models for dry sliding weight loss and coefficient of friction for polyamide-6 composites and optimized testing parameters using Taguchi method. Literature suggests that Taguchi method is the most preferred method in Tribology study.

2.6 Artificial Neural Networks

Artificial Neural Network (ANN) is stimulated by biological nerve system. Over numerous years this is being utilized to take care of an assortment of complex issues in field of science and engineering. This computational technique has the competence to simulate any correlation which frequently is hard to explain with the physical model. It has the inclination to learn by case and recognizes examples of variety in a progression of info yield esteems. This incredible ability of modelling helps in the study of obscure problems which may be difficult to solve by present mathematical approaches or physical theories. In recent times, ANN approach was set up in the study of wear behavior of metals and alloys, polymers and composites. ANNs depend on the course of action and working of the organic sensory system. Neurons are essential building blocks or units of brain. A neuron accepts a number of input signals but will create only one yield signal at a time. Motivated by these natural neurons, ANN comprises of basic components which work in parallel. ANN is the simple collection of ancient artificial neurons. The gathering happens by making layers that are later associated by each other to frame a system of neurons. They show aptitudes like learning, generalisation and abstraction. The systems in this manner framed are utilized as models for the procedures whose information/yield information is accessible. The neural system is prepared with the information and yield information in approach to limit the error between real yield and the anticipated yield by ANN. The model can then be utilized for various purposes like distinguishing proof and estimation. Back propagation network comprises of many quantities of interconnected neurons. The neurons are organized in layers (input layer, yield layer,

at least one concealed layer(s)) between the input and yield layer. Every neuron in the input layer is associated with each neuron in concealed layer, which thus is associated with each neuron in the yield layer. This topology brings about a system normally known as the Multi-Layer Preceptor (MLP) in which there is no association between the neurons in a same layer. Input layer neurons obtain input signal from each training pattern. The output from input neurons is accepted by the neurons in the concealed layer. Then the signal darts through a nonlinear function. This creates output of each neuron of the hidden (concealed) layer. The yield from neurons of the last shrouded layer thus is sent as an input to each yield neuron. At that point an examination between the anticipated yield and craved yield is made. The error is sent back to enhance prediction. Number of neurons in each layer, number of shrouded layers, activation function to nonlinearise input-yield relationship, learning rate, training algorithms and other significant parameters utilized as a part of the system characterizes the ANN architecture. An ANN mathematical model which symbolizes the structure shown in figure 2.17 is written as;

$$y = f(U) = W_o * \tanh(W_i * U + B_i) + b_o \text{-----Eqn. 2.1}$$

where y is the yield of the neural network model, U is the column vector of magnitude p including p inputs of the process, W_o is the row vector of magnitude n which enfolds the weights of the neural network model from the concealed layer to the output, W_i signifies matrix which includes the weights of the neural network model from the inputs to the concealed layer. This matrix possesses n rows and p columns. B_i is a column vector of magnitude n. This restrains biases of hidden layer from input layer. b_o is the bias from hidden layer to yield of the neural network model [249-255].

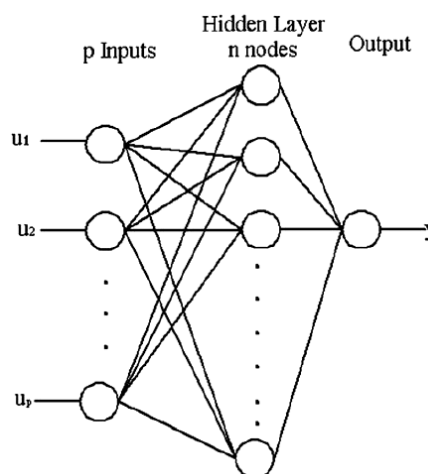


Figure 2.17 Structure of a back propagation neural network

As of late, ANN is discovering applications in the field of tribology. Sudharshan et al. [256] utilized ANN to anticipate abrasive wear properties of graphite filled and unfilled carbon fabric reinforced epoxy composites. He utilized 3-5-1 back propagation neural network to foresee weight loss. Durmus et al. [257] anticipated surface harshness and weight loss due to wear of AA6351 aluminum alloy utilizing ANN. In his experimental study, he contrasted trial esteems and the anticipated esteems and had demonstrated the occurrence between the two. Velten et al. [258] anticipated and dissected the wear conduct of fibre strengthened polymer bearing materials utilizing "back propagation ANN with Levenberg-Marquardt" algorithm. Cetinel et al. [259] anticipated the impact of Mo coating on the wear manner of metals utilizing ANN system.

2.7 The Knowledge Gap in Earlier Investigations

Extensive literature survey carried out above, unveils following knowledge gap in research reported so far;

1. ADI has wide applications yet its maximum capacity usage in tribological applications is restricted due to the non-introduction of bunches of shrouded data.
2. Very little work has been done on this material contrasted with different materials particularly aluminium composites because of the poor ADI production sites in India. A significant part of the work on ADI has been done on the laboratory samples prepared.
3. A significant part of the distributed research gives an account of ADI are done at the room temperature dry sliding conditions. Hoisted temperature dry sliding wear study of the material under review has not been concentrated up until now. Additionally the work on the optimization of picked ADI's wear controls parameters at higher temperature working conditions has not been accounted for up until this point.
4. Many reviews conveyed so far on the dry sliding wear test of ADI and utilization of factual techniques for ADI wear study is exceptionally restricted. Taguchi strategy is the most favoured technique to study quality, execution and cost as it is straightforward and productive. Likewise it has a precise way to deal with study.

5. Impact of sliding speed and applied load on the wear properties of ADI at raised temperature has not been contemplated on chosen ADI with chemical composition.
6. Artificial neural network technique has not been concentrated so far on the dry sliding wear conduct of ADI at room and hoisted temperature.

2.8 Objectives of the Present Work

Knowledge gap recapitulated above has helped to frame the objectives of the present work. The objectives are outlined as follows.

1. To fabricate two categories of ADIs for wear study. First ADI is austempered at 345°C and the second at 380°C.
2. To optimize the control parameters influencing wear conduct of ADI at room temperature.
3. To study consequence of sliding speed on dry sliding wear at elevated temperature.
4. To study effect of applied load on dry sliding wear at elevated temperature.
5. To study effect of various factors such as speed, load and temperature on dry sliding wear behavior of ADI.
6. To predict order of influence of control factors under study.
7. To use Taguchi's experimental design and ANOVA for wear control parameters optimization and analysis.
8. To obtain regression models for wear rate and friction coefficient.
9. To study wear surface using SEM.
10. To obtain most suitable operating conditions at room and elevated temperatures.
11. To use artificial neural network technique to foretell dry sliding wear properties of ADI at room and elevated temperature.

Chapter summary

This chapter has provided;

- An in-depth review of previous experimental investigations and research findings on various facets of ADI reported by Researchers.

- Review on the analysis of the investigations using Design of Experiments with Taguchi method on wide variety of materials and in various fields.
- Usefulness of the ANN model for the prediction of results.
- The knowledge in previous research work
- The objectives of the present work

The next chapter refers to materials and methods in production of ADI, experimental planning and procedure, Taguchi method and Artificial Neural Network methodology.

Chapter 3

MATERIALS AND METHODS

3.1 Introduction

A conduction of wear and friction test on materials includes an extensive number of factors. A few of these are process parameters and others are external parameters. Together the idiom coined for these variables is control factors. Assortment of apparatus for the conduction of test is one of the most difficult tasks. It ends up being the best equipment contingent on the degree to which it emulates the real working conditions. Be that as it may, in light of the literature review larger part of the researchers lead investigates wear and friction utilizing Friction and Wear Monitor (TR-20-LE) testing machine. This equipment has turned out to be all around acknowledged for leading wear study. The equipment comprised of collate to hold the test specimen against a hardened disc affected by connected load. The contact pin surface might be circular, level or any geometry in light of real wear component. Frictional force and temperature are consistently observed amid wear test on a Friction and Wear Monitor machine. The material removed during the test was calculated by the difference in weights before and after the test utilizing a high precision digital weighing scale. A transform in wear mechanism was observed with the change in frictional load value during conduction. Amid the early phases of trial, more changes were observed. Friction and wear were affected by the key factors such as sliding speed, load, sliding distance and temperature. The test comes about differ definitely in the early phases of experimentation and achieve relentless state or balance conditions throughout time. The results attained during equilibrium situations were better. Shear strains were generated close to the sliding surfaces during sliding showing in changes of surface hardness. Worn out surface was subjected to most extreme strain with higher hardness esteems. These work hardening impacts were measured by measuring the estimations of surface hardness prior and afterward the wear tests [260].

The basic practice to quantify surface temperature is to penetrate an opening of little diameter close to the surface subjected to wear on the round and hollow surface and entrenching a thermocouple. The mounted thermocouple gave the correct

estimation of temperature at the surface when it broke amid running. The output was observed consistently amid the test.

A vast number of ways are available to study the worn out surfaces and wear debris. Amongst the accessible methods, Scanning Electron Microscopy (SEM), Optical Microscopy, X-ray Diffractometer (XRD) and X-ray analysis (EDAX) are frequently used. These present information on the wear mechanism, composition and subsurface conditions of ADI. The surface and subsurface can likewise be investigated.

3.2 Selection of ADI for the Present Investigation

The present trial examinations were done on ADI. The ADI was produced by subjecting DI to austempering cycle. The chemical composition of DI is shown in Table 3.1. It was determined by Optical Spectrometer.

Table 3.1 Chemical composition of ductile iron

Element	Ceq	C	Si	Mn	P	S	Cr
Wt %	4.36	3.52	2.50	0.161	0.037	0.014	0.027
Element	Ni	Mo	Al	Cu	Ti	Mg	Fe
Wt %	0.151	0.421	0.017	0.78	0.026	0.054	92.2

Method used: IS 228; Optical Spectrometry

Good quality DI with the above chemical composition was selected for the fabrication of ADI. Consistent chemistry, microstructure, lower casting defects and nodule count decides the quality. The specimen is viewed for a nodule count greater than 100 per mm² and nodularity over 85% to cast ductile iron. Two ADIs were delivered for the present examination by changing the asutempering cycle parameters.

3.3 Preparation of the Sample

DI castings were produced in a foundry utilizing 500kg medium frequency induction furnace. The raw materials utilized as a part of the casting are S.G. Pig Iron, Carbon (most extreme 3.4%), Silicon 1.5 to 2.5%, Manganese 0.3%, Phosphorous 0.015%, CRCA scrap (Carbon-0.1%, Si - 0.1% max., Mn-0.3%, P-0.025%), Fe-Si-Mg and uncommon earth components like Barium and Cerium. Molten metal was filled the shell mould at 1420°C to cast the example test bar showed up in figure 3.1. The

specimens for the exploratory work were then machined to the required size of $\phi 10\text{mm}$ and 30 mm length showed up in figure 3.2.



Figure 3.1 Ductile iron test bar



Figure 3.2 Test specimen

The specimen were heated to austenitization temperature of 870°C in a furnace with heating rate of $180^{\circ}\text{C}/\text{hour}$ and solutionised for a hour and a half. They were then transferred into the salt bath hisalt 1150, held at temperature 345°C and held for 150 minutes and afterward air cooled. The ADI thus prepared was designtaed as ADI1.

Another few samples were heated to austenitization temperature of 870°C in the same furnace with similar rate of heating. It was solutionised for 120 minutes. The specimens were austempered at 380°C for 180 minutes and air cooled later. The ADI thus prepared was designated as ADI2.

To take a measure of the surface temperature an opening of diameter 2mm was penetrated to a profundity of 3mm at a depth of 5mm from the test surface as appeared in figure 3.3. The tip of the Iron-Constantan thermocouple was embedded in the hole by a light punch. The thermocouple was appropriately fitted into the penetrated gap by filling the hole with silver and after that brazed to the specimen. The thermocouple utilized and the arrangements for temperature measurement along with wear track are shown in figures 3.4 and 3.5 respectively.

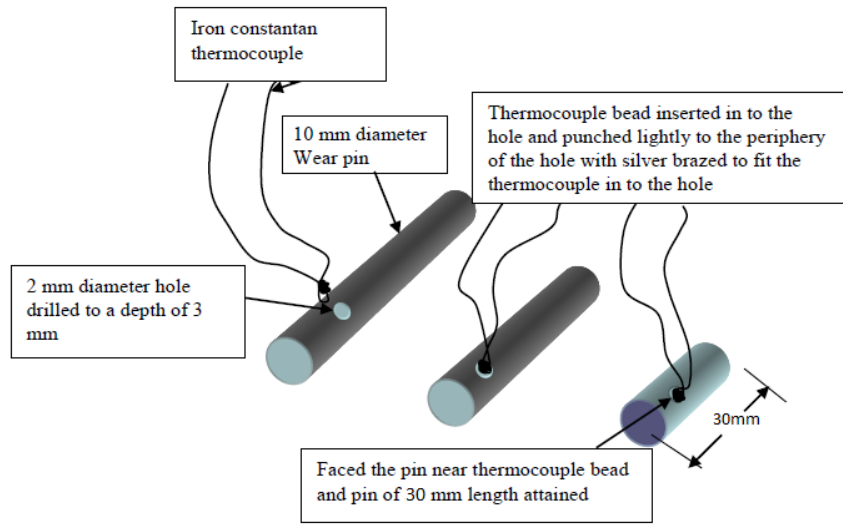


Figure 3.3 Wear test pin



Figure 3.4 Thermocouple mounted on test specimen



Figure 3.5 Friction temperature wear measurement and wear track on disc

3.4 Experimental Set up and Procedure

DUCOM wear testing machine (TR-20-LE) was utilized to assess the dry sliding wear attributes. Figures 3.6 and 3.7 depict the photographic sight and schematic figure of the machine respectively. The chemical composition and physical and thermal properties of the disc material (manufactured by DUCOM Bengaluru, as per ASTM G-99) are pointed out in tables 3.2 and 3.3 respectively. Dry sliding wear trials were conducted as per ASTM G99-95a standards. The equipment specifications are specified in table 3.4. Pin was cleaned with acetone. Initial mass was assessed with digital weighing scale with least count of 0.1mg. The pin was held pushed against turning steel disc (EN-32) with a hardness of 65HRC amid the test. Tests were performed by run orchestrate delivered by Taguchi procedure. Around completion of each test, pin was again cleaned with acetone and its ultimate mass was assessed. Disc

was moreover cleaned towards the completion of each test. The difference between fundamental and last mass of pin gave mass loss due to sliding wear. The volume loss was found out using density of ADI. The wear rate of ADI pins was then calculated. Indicator on Friction and Wear screen machine showed frictional drive in Newton with assistance of sensor appended on the arm of stacking. The test duration was computed based on the sliding distance, speed and track diameter. The disc was coerced with constant speed during the entire duration of test. The variables preferred for the wear study based on extensive literature were load, sliding distance, sliding speed, and temperature.



Figure 3.6 DUCOM pin-on-disc wear testing machine (TR-20-LE)

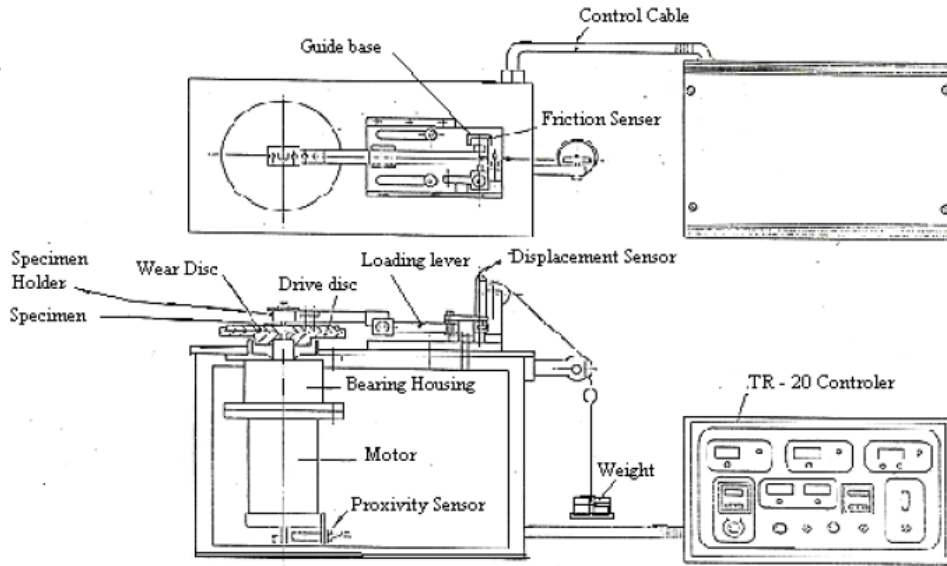


Figure 3.7 Schematic diagram of wear and friction monitor [269]

Table 3.2 Disc material chemical composition (AISI316 austenitic) [269]

Element	C	Mn	S	P	Si	Cr	Ni	Mo
Composition %	0.008	2.0	0.03	0.045	1.0	16.0-18.0	10.0-14.0	2.0-3.0

Table 3.3 Disc material physical and thermal properties [269]

Physical properties		Modulus of elasticity		Thermal properties			
Melting temperature	Density in g/cm^3	Tension GPa	Torsion GPa	Specific heat 0-100°C in J/kgK	Electrical resistivity 20°C in Ωm	Temp. in °C	Thermal conductivity in W/mK
1370-1400	6.0	193	77	500	74	100-500	16.3-21.5

Table 3.4 Wear and friction monitor machine specifications [269]

Parameter		Units	Min.	Max.	Remarks
Pin / ball diameter		Mm	3	12	Round or square pin
Wear track diameter		Mm	10	18	Disc dia. 100 mm
Disc rotation speed		Rpm	1	2000	0.1rpm least count
Normal load		N	0	60	50 Mn least count
Frictional force		N	0	20	5Mn least count
Temperature		°C	Ambient	800	1°C least count
Wear measurement range		mm	0	2000	0.1µm least count
Disc oscillation	Stroke angle	Degrees			
	Oscillation frequency	Hz	0.1	5	
Preset Timer		Hr/Min/Sec	99/59/59		
Power		V/kVA/Ph/Hz	230/10/1/50		

3.5 Estimation of the Set up Parameters for the Experimental Study

The sliding speed in rpm and test span were required to be determined for every one of the tests to feed as input to the equipment. The employed relations and computations are detailed below;

Sliding speed is given by

$$S = (\pi d_t N) / 60 \text{ -----Eqn. 3.1}$$

Where,

S-Sliding speed in m/s,

d_t -Track diameter in m,

N-Speed of disc in r.p.m.

The above equation is rewritten as;

$$N = S * 60 / \pi d_t \text{ -----Eqn. 3.2}$$

Thus the disc speed in rpm was calculated for the selected sliding speed and track diameter.

The test duration is given by

$$t = D*60/S \text{ -----Eqn. 3.3}$$

Where,

t- Test duration in minutes

D- Sliding distance in m

Thus the required test duration was selected based on speed and sliding distance.

3.6 Measurement of Surface Temperature and Estimation of Flash Temperature

The thermocouple mounted on each of the specimen during the test was applied for the measurement of surface temperature of pin. The temperature was observed continuously during the intact duration of test. Hardness of the underlying material dwindles with the load. This amplifies the contact temperature in fastidious the flash temperature. It is the highest temperature attained for an extremely short time during sliding at the contacting asperities. Ashby et al. [261] proposed an approach to calculate the flash temperature.

$$T_f = T_s + \frac{\mu F v}{A_r} \left(\frac{1}{k_1/l_1 + k_2/l_2} \right) \text{ -----Eqn. 3.4}$$

Where,

T_f- Flash temperature

T_s- Experimental surface temperature

F- Applied load

v- Sliding speed

k₁, k₂- Thermal conductivities of the mating materials

l₁, l₂- Equivalent diffusion distances

A_r- Real area of contact

A_r can be approximated by the following expression [261];

$$A_r = \frac{F}{H\sqrt{1 + 12\mu^2}} \text{ -----Eqn. 3.5}$$

Where,

H- Microhardness of ADI

Ashby [85] gave the relation $l_1=l_2=0.01/H$ to estimate the distances l_1 and l_2 expressed in m and H in kg/mm^2 (it is obtained that $l_1=l_2=21.2\mu\text{m}$). An oxide scale is formed on the surface of pin. Hence k_2 is calculated using the following relation [154];

$$k_2 = \frac{k_s k_o}{(1 - (t/l_2))k_o + (t/l_2)k_s} \text{-----Eqn.3.6}$$

Where k_s and k_o are the thermal conductivities of ADI ($k_s=36\text{W/mK}$ [262]) and of the iron oxide ($k_o=3.2\text{W/mK}$ [263]) and t is the thickness of scale. Based on experimental observations and reported data [154], t was selected as $10\mu\text{m}$. The calculated value of k_2 was 6W/mK . Thus the T_f values were calculated.

3.7 Heat Flux

Heat was engendered at the contacting surfaces due to friction when the pin slides on disc. The heat flux is the heat generated due to friction per unit surface area per unit time measured in J/sm^2 . It is given by

$$q = \mu W S/A \text{-----Eqn. 3.7}$$

Where, μ - Coefficient of friction, W -Normal force on the pin, S -Sliding speed and A -Nominal contact area i.e. the area at the pin end surface.

A minute amount of this generated heat was conducted through the pin and rest was lost to atmosphere by convection and radiation [264].

3.8 Metallographic Studies on ADI

Specimen with aspects 10mm diameter and 5mm thickness were cut from the sample specimens (plain as well as tested) for metallographic examinations. Samples were prepared as per the paradigm metallographic procedure. 2% nital solution (2ml HNO_3 + 98ml ethanol) was used as an etchant for revealing the surface microstructures. The ADI microstructures were captured using Scanning Electron Microscope (figure 3.8). Towards the end of sliding wear tests the worn out surfaces of specimen were inspected by SEM to understand the wear mechanisms. Wear mechanisms predominant during the tests are one of the important criterions to influence the wear rate of material [265].

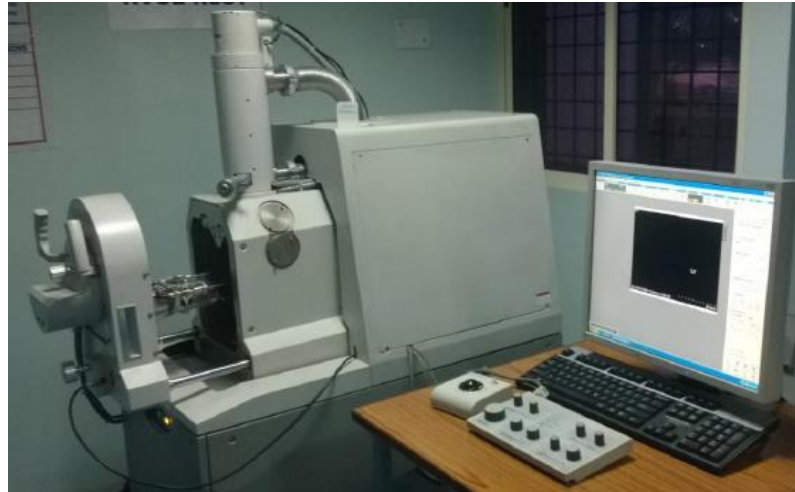


Figure 3.8 Scanning electron microscope

3.9 Wear Debris

To appreciate wear mechanism, debris analysis was also carried out. A variation in the shape and size of wear debris was observed based on load, speed and distance of sliding. The wear debris was characterised by Scanning Electron Microscopy.

3.10 Surface and Subsurface Hardness

To comprehend hardenability and work hardening impacts of the material, hardness tests were conducted by Vicker's hardness testing machine (figure 3.9). A load of 50kg was applied on the specimen using a diamond pyramid cone indenter and 20s dwelling time was appropriate for the study. The hardness was measured in Vicker's Pyramid Number (HV). The specimen was segmented and at every 1mm depth of the specimen the hardness was measured. The sectioned specimens and indentation on surface are depicted in figures 3.10 and 3.11 respectively.



Figure 3.9 Vicker's hardness tester



Figure 3.10 Sectioned specimen for hardenability test

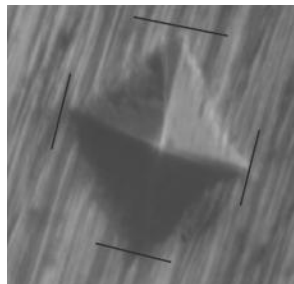


Figure 3.11 Indentation made by the indenter on test surface

3.11 Measurement of Surface Roughness

Time make TR100 surface roughness tester (figure 3.12) was used for the measurement of surface roughness. The probe travels in forward and reverse direction. Roughness value was indicated during the reverse motion of the probe. Three readings were averaged out to curtail the error during measurement. The evaluations were observed for parallel and across the worn out surface.



Figure 3.12 Surface roughness measuring instrument

3.12 Taguchi Method

In the investigation at hand an L_9 orthogonal cluster was picked, which has nine rows and three columns. Preference of orthogonal cluster depends on the condition that degrees of opportunity for the orthogonal exhibit ought to be more noteworthy than or equivalent to, entirety of factors [81]. Choice of orthogonal cluster depends on influencing factors, number of levels for factors, desired exploratory assurance or cost imperatives. Response variable contemplated was wear rate and coefficient of friction. Tests were driven in view of run order spawned by Taguchi method and outcomes were procured. Examination of trial data was finished using MINITAB15 software, extraordinarily designed for DOE applications. Basically, customary trial outline methodologies are excessively confused and difficult, making it impossible to utilize. Countless works must be completed when quantity of control parameters increment. To take care of this issue, DOE approach utilizing Taguchi system has been effectively utilized by analysts in investigation of wear conduct of tribological materials. Taguchi technique is an effective tool for outline of fantastic frameworks [81, 82]. It utilizes an exceptional plan of orthogonal exhibits to ponder whole parameter space with just few analyses. Taguchi technique gives an organized approach to gather information and to investigate impacts of parameters over some particular response. The strategy has exploratory and diagnostic ideas to decide factor with most grounded impact on subsequent rejoinder for a noteworthy change in general execution. The arrangement of investigations was created in Taguchi technique by utilization of standard orthogonal exhibits. Experimental results were

then analyzed by using Analysis of Variance (ANOVA) of affecting parameters [83, 84].

The means connected for Taguchi optimization in this exploratory work are as per the following [221].

1. Decide on noise and control factors
2. Pick Taguchi orthogonal array
3. Perform experimentation
4. Weight loss measurement
5. Analyze results (Signal-to-noise ratio)
6. Envisage most favorable performance
7. Confirmation experimentation

In this work, impact of four variables was examined considering three parameters at any given moment appropriate for L_9 orthogonal cluster. Arrangement of investigations was created utilizing orthogonal exhibit for different working conditions. Working conditions chosen for test contemplate were sliding speed, applied load, sliding distance and temperature.

3.13 Artificial Neural Networks

Lately, ANN is picking up significance in many fields including forecast and function estimation. ANN resembles a data handling innovation. It handles complex nonlinear relations existing between the information and yield factors. In the present investigation, ANN with three neurons in the information layer, ten and twelve neurons in single concealed layer and one neuron in output layer was considered. The model anticipated the objective esteems for the differing estimations of information parameters. By the experimentation approach in light of the mean square error esteem the quantity of neurons in the concealed layer were decided. It was discovered that the single shrouded layer with ten and twelve neurons for the arrangement of examinations was generally appropriate. For concealed neurons nonlinear tangent sigmoid function has been utilized. For yield neurons linear activation function was exercised. The validation error was observed during the training procedure. During the initial phase of training, generally the error diminished like training set error. The error on the validation set began rising when network started once again to fit information. The preparation was ceased if the validation error incremented for a

specific number of iterations. Biases and weights at the base number of validation error were returned. In this investigation, the weight loss and coefficient of friction for ADI were anticipated by the Neural Network Tool enclosed MATLAB 2011b utilizing Levenberg-Marquardt algorithm. The system execution was assessed for the informational index utilizing mean square error and regression as a quality measure. Mean squared error value and regression were acquired unswervingly from NN training session [266].

Chapter summary

This chapter has provided;

- Facets of material chosen for investigation and its heat treatment parameters
- The different testing methods and equipment involved in the study to determine the properties of materials
- Details of Taguchi system for the optimization of process factors and to study influence of parameters on wear behavior.
- ANN methodology for prediction of results

The next chapter consigns to results and discussion on wear behavior of ADI under the influence of various parameters (both process and external parameters).

Chapter 4

RESULTS AND DISCUSSION – I

OPTIMIZATION OF WEAR CONTROL PARAMETERS AT ROOM TEMPERATURE

4.1 Parameters and Levels

Based on the literature survey, three factors namely sliding speed or speed (S), applied load or load (L) and sliding distance (D) had been preferred for the experimental wear study on ADI1. DI was considered for comparison purposes. The factors have been chosen at three levels as shown in Table 4.1.

Table 4.1 Parameters and their levels

Level	Load, L (N)	Sliding speed, S (m/s)	Sliding distance, D (m)
1	19.62	1.047	1257
2	29.43	2.095	2514
3	39.24	3.142	3770

4.2 Plan of Experiments

Plan of experiments were generated by DOE using Taguchi method. The present study employed an L_9 orthogonal array. It is indicated in table 4.2. Orthogonal array was generated by utilizing statistical software MINITAB15. It has nine rows and three columns. The run order thus generated by Taguchi method is specified in table 4.3. The response variable decided on was wear rate. It is not a material property but rather relies upon the working conditions, resulting microstructure after heat treatment and environmental factors. The test table 4.3 shows an arrangement of working conditions decided for contemplate.

Table 4.2 Taguchi L₉ orthogonal array

Experiment no.	Column 1	Column 2	Column 3
1	1	1	1
2	1	2	2
3	1	3	3
4	2	1	2
5	2	2	3
6	2	3	1
7	3	1	3
8	3	2	1
9	3	3	2

Table 4.3 Plan of experiments

Experiment no.	Load, L (N)	Speed, S (m/s)	Sliding distance, D (m)
1	19.62	1.047	1257
2	19.62	2.095	2514
3	19.62	3.142	3770
4	29.43	1.047	2514
5	29.43	2.095	3770
6	29.43	3.142	1257
7	39.24	1.047	3770
8	39.24	2.095	1257
9	39.24	3.142	2514

4.3 Influence of Parameters on Wear Rate

4.3.1 Experimental Results of Wear Rate

The experimental dry sliding wear test results of DI and ADI1 are tabulated in table 4.4 and 4.5. The loss in weight was converted into loss in volume by dividing with the density of material. The density (ρ) of ADI is 7.1g/cm^3 . The wear rate was articulated in m^3/m which designates volume loss per unit sliding distance. Detailed calculation for first result is shown below and others are tabulated.

$$\text{Weight loss, } W_o = W_i - W_f = 16.1555 - 16.1554 = 0.0011\text{g}$$

$$\begin{aligned} \text{Volume loss per unit sliding distance, } V_o &= (W_o / \rho \times D) \times 10^{-6} \\ &= (0.0011 / 7.1 \times 1257) \times 10^{-6} \\ &= 0.12325 \times 10^{-12} \text{ m}^3/\text{m} \end{aligned}$$

Table 4.4 Experimental results of DI

Expt. No.	Load, L (N)	Speed, S (m/s)	Sliding distance, D (m)	Initial weight, W _i (g)	Final weight, W _f (g)	Weight loss, W _o (g)	Wear rate, W _r (m ³ /m) x10 ⁻¹²
1	19.62	1.047	1257	16.1555	16.1544	0.0011	0.12325
2	19.62	2.095	2514	15.8791	15.8786	0.0005	0.02801
3	19.62	3.142	3770	15.9505	15.9495	0.0010	0.03736
4	29.43	1.047	2514	15.1085	15.1030	0.0055	0.30813
5	29.43	2.095	3770	14.6403	14.6381	0.0022	0.08219
6	29.43	3.142	1257	16.4767	16.4754	0.0013	0.14566
7	39.24	1.047	3770	16.2030	16.1918	0.0112	0.41840
8	39.24	2.095	1257	15.6364	15.6349	0.0015	0.16807
9	39.24	3.142	2514	16.3270	16.3254	0.0016	0.08964

Table 4.5 Experimental results of ADI1

Expt. No.	Load, L (N)	Speed, S (m/s)	Sliding distance, D (m)	Initial weight, W _i (g)	Final weight, W _f (g)	Weight loss, W _o (g)	Wear rate, W _r , (m ³ /m) x10 ⁻¹²
1	19.62	1.047	1257	15.7932	15.7923	0.0009	0.10084
2	19.62	2.095	2514	15.8358	15.8357	0.0011	0.06163
3	19.62	3.142	3770	15.7144	15.7140	0.0004	0.01494
4	29.43	1.047	2514	15.9411	15.9383	0.0028	0.15687
5	29.43	2.095	3770	15.9458	15.9442	0.0016	0.05978
6	29.43	3.142	1257	15.9195	15.9190	0.0005	0.08964
7	39.24	1.047	3770	15.7439	15.7422	0.0017	0.06351
8	39.24	2.095	1257	16.2064	16.2058	0.0006	0.14566
9	39.24	3.142	2514	16.1810	16.1790	0.0020	0.11205

4.3.2 S/N Ratio Analysis

The sway of control factors was examined utilizing Signal to Noise Ratio (SNR) analysis. Factor with uppermost SNR dependably yields ideal quality with littlest measure of fluctuation [270]. Smaller is better type wear quality trait was chosen for analysis. The response for SNR is given by the following equation.

$$\eta = -10 \log_{10} \left\{ \frac{1}{n} \sum_{i=1}^n y_i^2 \right\} \text{-----Eqn. 4.1}$$

Response for SNR was evaluated for all eighteen tests (9 tests on ADI and 9 on DI) using eqn. 4.1. SNR for DI and ADI1 is represented in table 4.6 and 4.7 respectively. Its retort analysis for DI is shown in table 4.8. It shows that applied load is the most significant and influential factor among all three factors. Second most influential factor is sliding speed and last sliding distance. Figure 4.1 portrays mean of SNR of DI for wear rate graphically. Figure 4.2 speaks to Main Effects Plot (MEP) for mean wear rate. Examination of test outcomes show that parameter combination given in table 4.9 gave least wear rate for DI.

Table 4.6 S/N ratio for DI

Expt. No.	Load, L (N)	Speed, S (m/s)	Sliding distance, D (m)	Wear rate of DI (m ³ /m) x10 ⁻¹²	S/N ratio (db)
1	19.62	1.047	1257	0.12325	18.1843
2	19.62	2.095	2514	0.02801	31.0537
3	19.62	3.142	3770	0.03736	28.5519
4	29.43	1.047	2514	0.30813	10.2253
5	29.43	2.095	3770	0.08219	21.7036
6	29.43	3.142	1257	0.14566	16.7332
7	39.24	1.047	3770	0.41840	7.56820
8	39.24	2.095	1257	0.16807	15.4902
9	39.24	3.142	2514	0.08964	20.9500

Table 4.7 S/N ratio for ADI1

Expt . No.	Load, L (N)	Speed, S (m/s)	Sliding distance, D (m)	Wear rate of DI (m ³ /m) x10 ⁻¹²	S/N ratio (db)
1	19.62	1.047	1257	0.10084	19.9273
2	19.62	2.095	2514	0.06163	24.2042
3	19.62	3.142	3770	0.01494	36.5130
4	29.43	1.047	2514	0.15687	16.0892
5	29.43	2.095	3770	0.05978	24.4689
6	29.43	3.142	1257	0.08964	20.9500
7	39.24	1.047	3770	0.06351	23.9432
8	39.24	2.095	1257	0.14566	16.7332
9	39.24	3.142	2514	0.11205	19.0118

Table 4.8 Response table of DI for S/N ratios - smaller is better (wear rate)

Level	Load (N)	Speed (m/s)	Sliding distance (m)
1	25.93	11.99	16.80
2	16.22	22.75	20.74
3	14.67	22.08	19.27
Delta	11.26	10.76	3.94
Rank	1	2	3

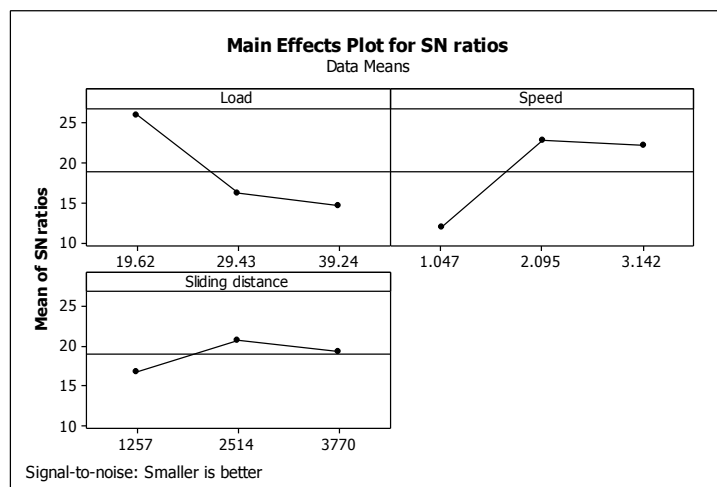


Figure 4.1 Main effects plot of DI for S/N ratios-wear rate

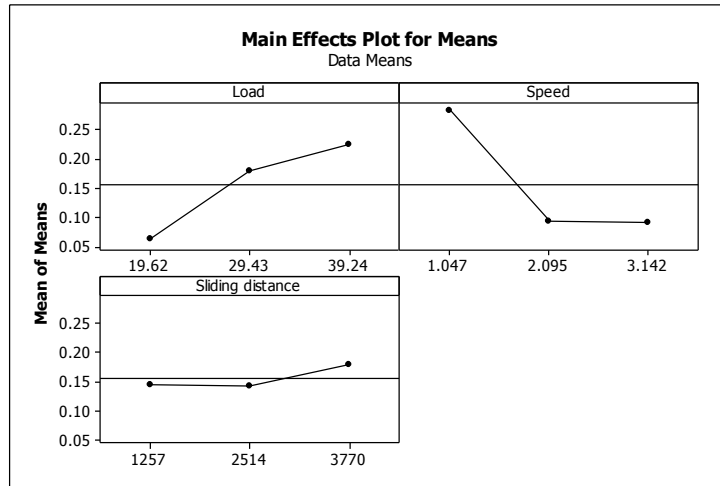


Figure 4.2 Main effects plot of DI for means-wear rate

Table 4.9 Optimized operating conditions of DI for wear rate

Load, L (N)	Speed, S (m/s)	Sliding distance, D (m)
19.62	2.095	2514

The SNR analysis for ADI1 is revealed in table 4.10. Sliding distance is the most significant and influential factor among three factors. Load is second influential factor followed by speed. Figure 4.3 shows ADI1's MEP for SNR. Figure 4.4 depicts MEP for mean wear rate. From analysis of test results, it is found that factor combinations given in table 4.11 gave bare minimum wear rate for ADI1.

Table 4.10 Response table of ADI1 for S/N ratios-smaller is better (wear rate)

Level	Load (N)	Speed (m/s)	Sliding distance (m)
1	26.88	19.99	19.20
2	20.50	21.80	19.77
3	19.90	25.49	28.31
Delta	6.99	5.51	9.10
Rank	2	3	1

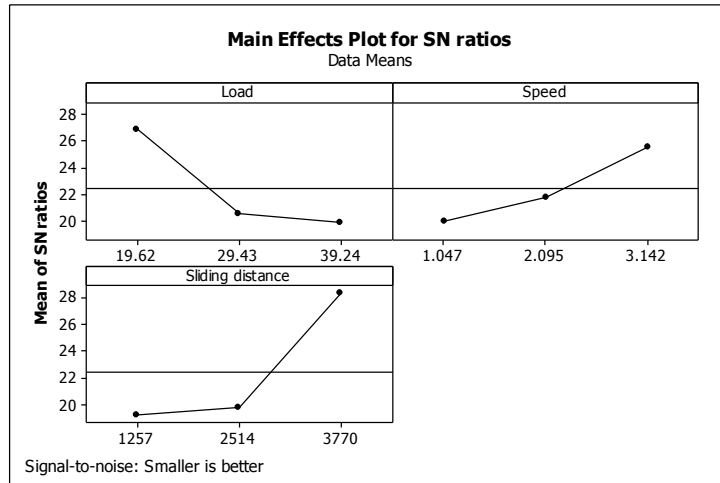


Figure 4.3 Main effects plot of ADI1 for S/N ratios-wear rate

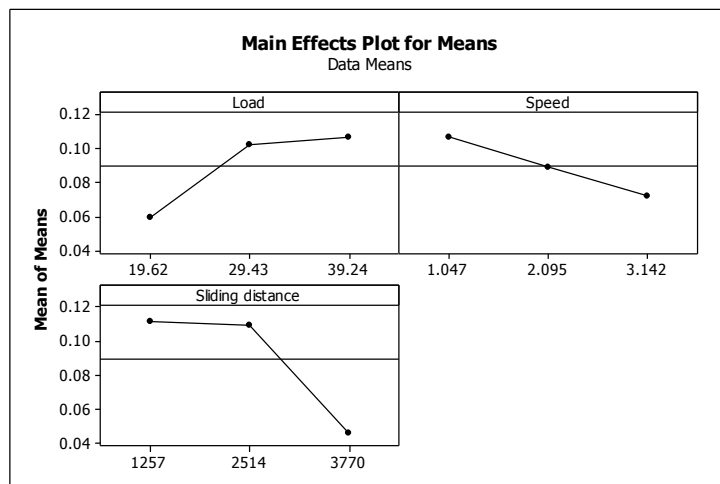


Figure 4.4 Main effects plot of ADI1 for means-wear rate

Table 4.11 Optimized operating conditions of ADI1 for minimum wear rate

Load, L (N)	Speed, S (m/s)	Sliding distance, D (m)
19.62	3.142	3770

4.3.3 Analysis of Variance for Wear Rate

Analysis of Variance (ANOVA) was made use of to analyse experimental outcomes. It is beneficial in investigating sway of parameters considered for study. The confidence level preferred for evaluation of analysis was 95% and significance level $\alpha=0.05$.

Table 4.12 shows ANOVA results for wear rate of DI. The last segment of table demonstrates rate commitment (P %) of each of the factors on response (wear rate). It shows level of impact on outcomes. Outcomes from table 4.12 for DI show that load (47.20%) and speed (46.02%) have practically equivalent and noteworthy on wear rate. Sliding distance (5.06%) has least impact because of reduction in wear rate due to work hardening effects. Table 4.13 demonstrates ANOVA outcomes on wear rate of ADI1. Results confirm that sliding distance (51.92%) has uppermost influence on wear rate of ADI1. Second most affecting component is load (29.88%). Wear rate is least affected by speed (15.70%).

Table 4.12 Analysis of variance for S/N ratios-wear rate (DI)

Source	DOF	Seq. SS	Adj. SS	Adj. MS	F-test	P-value	Percentage Contribution (%)
Load	2	223.475	223.475	111.737	27.03	0.036	47.20
Speed	2	217.877	217.877	108.939	26.35	0.037	46.02
Sliding distance	2	23.794	23.794	11.897	2.88	0.258	5.06
Error	2	8.268	8.268	4.134			1.72
Total	8	473.415					100

Notes: DOF, Degrees of Freedom; Seq. SS, Sequential sum of squares; Adj. SS, Adjusted sum of squares; Adj. MS, Adjusted mean squares.

Table 4.13 Analysis of variance for S/N ratios-wear rate (ADI1)

Source	DOF	Seq. SS	Adj. SS	Adj. MS	F-test	P-value	Percentage Contribution (%)
Load	2	89.854	89.854	44.927	11.97	0.077	29.88
Speed	2	47.214	47.214	23.607	6.29	0.137	15.70
Sliding distance	2	156.148	156.14	78.074	20.80	0.046	51.92
Error	2	7.057	8	3.753			2.50
Total	8	300.722	7.057				100

Proportion of disclosed variety to aggregate variety is known as coefficient of assurance (R^2). It is a measure of level of fit. A superior model has R^2 approaching solidarity. It fits real information. Figured estimation of R^2 for this model of ADI1 wear test has an estimation of 0.975. It is satisfactory as it is near solidarity. It reveals that 97.5% changeability in information can be clarified by this model. Thusly this model gives sensibly great clarification of connection between the response and impacting factors.

4.3.4 Regression Analysis

A linear regression model (LRM) relates response of two or more variables. It fits linear expression to monitored data [18, 19]. Utilizing MINITAB15 software a LRM was produced in light of exploratory information. It sets up a relationship between terms acquired from ANOVA. Accompanying are regression equations developed both for DI and ADI1.

$$\text{Wear rate (DI)} = (0.0706 + 0.008282 * L - 0.09184 * S + 0.00001339 * D) 10^{-12} \text{ -----Eqn. 4.2}$$

$$\text{Wear rate (ADI1)} = (0.11837 + 0.002443 * L - 0.01664 * S - 0.00002625 * D) 10^{-12} \text{ ---Eqn. 4.3}$$

Wear rate of DI and ADI1 can be anticipated utilizing above expressions. Constant in expression is residue. A regression coefficient of 0.975 was obtained for model. This esteem demonstrates that wear information accumulated was not scattered. From LRM 4.2, it is watched that wear of DI is specifically corresponding to load and sliding distance and conversely relative to speed. From eqn. 4.3, it is watched that wear rate of ADI1 is straightforwardly relative to load and conversely corresponding to speed and distance. Load in two expressions is positive and points to that wear rate increases with load.

4.3.5 Confirmation Test

The LRM accomplished was validated by conducting confirmation tests. Parameter levels decided for affirmation tests must be not same as prior parameter levels utilized for investigation. Affirmation tests parameter levels are presented in table 4.14. Table 4.15 demonstrates test outcomes for affirmation tests done. Wear rate in m^3/m is figured from LRM given by eqn. 4.3. Affirmation test outcomes and results acquired from condition are presented to in table 4.16.

Table 4.14 Parameters used in the confirmation wear test

Test no.	Load L, (N)	Sliding speed S, (m/s)	Sliding Distance D, (m)
1	9.81	1.31	1571
2	29.43	2.62	3142
3	49.05	3.93	4713

Table 4.15 Experimental confirmation test results

Test no.	Load L, (N)	Sliding speed S, (m/s)	Sliding Distance D, (m)	Initial weight, W_i (g)	Final weight, W_f (g)	Weight loss, W_o (g)	Wear rate of ADI1 (m^3/m) $\times 10^{-12}$
1	9.81	1.31	1571	16.1359	16.1350	0.0009	0.08069
2	29.43	2.62	3142	15.7865	15.7842	0.0023	0.10310
3	49.05	3.93	4713	15.1632	15.1615	0.0017	0.05080

Table 4.16 Confirmation wear test results and their comparison with regression model

Test no.	Experimental wear rate (m^3/m) $\times 10^{-12}$	Regression model – predicted wear rate (m^3/m) $\times 10^{-12}$	Error (%)
1	0.08069	0.07930	1.72
2	0.10310	0.10543	2.21
3	0.05080	0.04909	3.37

Error between investigational and values gained from LRM is less than 4%. Hence obtained LRM from experimental facts is an effective and feasible way to predict wear rate of ADI1.

4.4 Influence of Parameters on Coefficient of Friction (COF)

An investigation on frictional conduct of DI and ADI1 was likewise completed alongside dry sliding wear contemplate. Parameters, their levels and arrangement of examinations picked were same as that of wear study. Response undependable contemplated was Coefficient of Friction, μ (COF).

4.4.1 Experimental Results of COF

Frictional load was glimpsed in each of the investigations directed for wear study about from friction monitor associated with trial set up. Table 4.17 demonstrates got frictional loads in examination and computed COF esteems utilizing eqn. 4.4. The COF is figured by accompanying equation.

$$COF = \text{Frictional Force} / \text{Applied Load} \text{ -----Eqn. 4.4}$$

Table 4.17 Orthogonal array of Taguchi and experimental results of COF

Expt. no.	Load, L (N)	Speed, S (m/s)	Sliding distance, D (m)	Frictional load of DI (N)	COF	Frictional force of ADI1 (N)	COF
1	19.62	1.047	1257	10.6	0.5403	8.8	0.4485
2	19.62	2.095	2514	9.5	0.4842	10.9	0.5556
3	19.62	3.142	3770	10.9	0.5556	7.4	0.3772
4	29.43	1.047	2514	14.1	0.4791	12.3	0.4179
5	29.43	2.095	3770	8.4	0.2854	12.7	0.4315
6	29.43	3.142	1257	18.5	0.6286	6.2	0.2107
7	39.24	1.047	3770	18.1	0.4613	19.3	0.4918
8	39.24	2.095	1257	19.6	0.4995	18.8	0.4791
9	39.24	3.142	2514	26.2	0.6677	23.2	0.5912

4.4.2 S/N Ratio Analysis

The sway of control factors was evaluated by SNR response analysis. Ideal quality with least fluctuation is acquired for most elevated estimation of SNR. Smaller is better sort quality trademark was picked in investigation of COF. SNR values for DI and ADI1 are displayed in table 4.18 and 4.19 respectively.

Table 4.18 S/N ratios for DI

Expt. no.	Load, L (N)	Speed, S (m/s)	Sliding distance, D (m)	Coefficient of friction	S/N ratio
1	19.62	1.047	1257	0.5403	5.3479
2	19.62	2.095	2514	0.4842	6.2995
3	19.62	3.142	3770	0.5556	5.1055
4	29.43	1.047	2514	0.4791	6.3914
5	29.43	2.095	3770	0.2854	10.8902
6	29.43	3.142	1257	0.6286	4.0324
7	39.24	1.047	3770	0.4613	6.7210
8	39.24	2.095	1257	0.4995	6.0295
9	39.24	3.142	2514	0.6677	3.5086

Table 4.19 S/N ratios for ADI1

Expt. no.	Load, L (N)	Speed, S (m/s)	Sliding distance, D (m)	Coefficient of friction	S/N ratio
1	19.62	1.047	1257	0.4485	6.9643
2	19.62	2.095	2514	0.5556	5.1055
3	19.62	3.142	3770	0.3772	8.4693
4	29.43	1.047	2514	0.4179	7.5777
5	29.43	2.095	3770	0.4315	7.2997
6	29.43	3.142	1257	0.2107	13.5280
7	39.24	1.047	3770	0.4918	6.1634
8	39.24	2.095	1257	0.4791	6.3914
9	39.24	3.142	2514	0.5912	4.5648

It demonstrates that speed is most critical and compelling variable for COF of DI. Second most impacting variable is sliding distance followed by load. Figure 4.5 portrays mean of SNR for COF of DI and figure 4.6 demonstrates plot of main effects for mean COF. Investigation of results demonstrates ideal working conditions for least COF of DI and is appeared in table 4.21.

Table 4.20 Response table of DI for S/N ratios-smaller is better (COF)

Level	Load (N)	Speed (m/s)	Sliding distance (m)
1	5.584	6.153	5.137
2	7.105	7.740	5.400
3	5.420	4.215	7.572
Delta	1.685	3.524	2.436
Rank	3	1	2

SNR response examination for ADI1 is depicted to in table 4.22. It uncovers that connected load is most critical and persuasive variable among three elements considered for contemplate. Second most affecting element is sliding distance. Speed is least impacting component in correlation with other two. Figure 4.7 portrays mean of SNR plot for COF and figure 4.8 MEP for mean COF of ADI1.

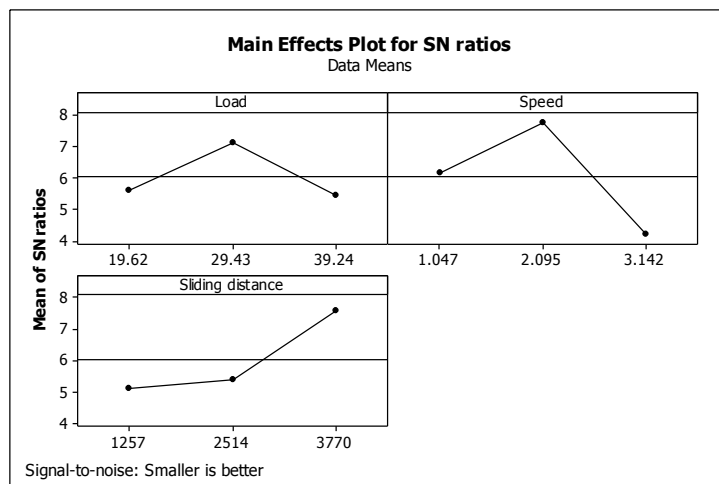


Figure 4.5 Main effects plot of DI for S/N ratios-coefficient of friction

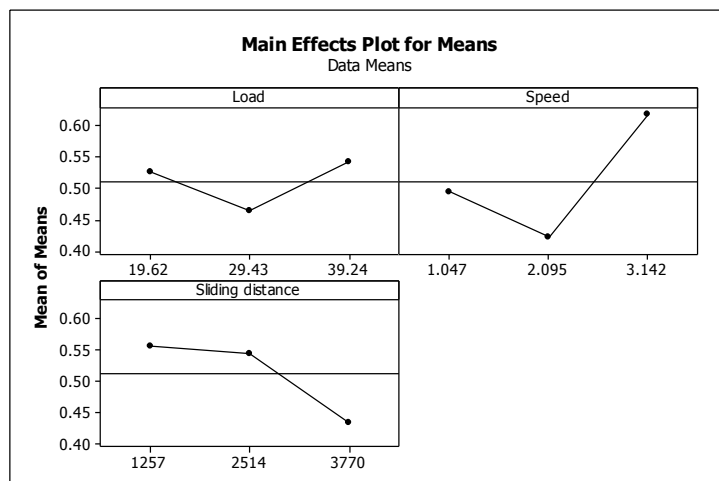


Figure 4.6 Main effects plot of DI for means-coefficient of friction

Table 4.21 Optimized operating conditions of DI for COF

Load, L (N)	Speed, S (m/s)	Sliding distance, D (m)
29.43	2.095	3770

Table 4.22 Response table of ADI1 for S/N ratios - smaller is better (COF)

Level	Load (N)	Speed (m/s)	Sliding distance (m)
1	6.846	6.902	8.961
2	9.468	6.266	5.749
3	5.707	8.854	7.311
Delta	3.762	2.589	3.212
Rank	1	3	2

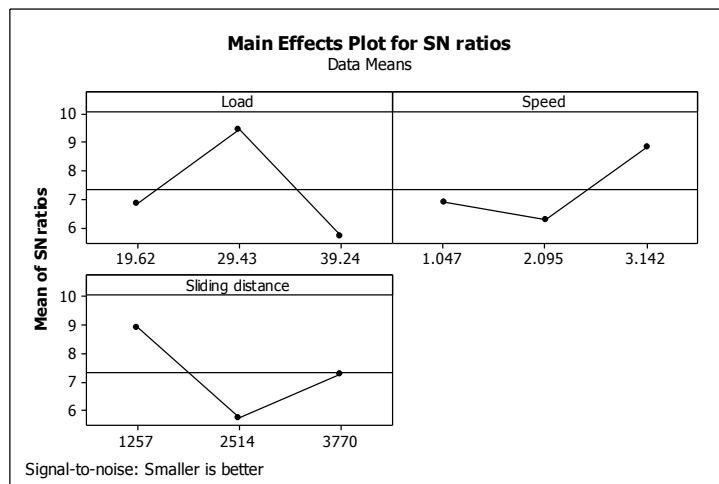


Figure 4.7 Main effects plot of ADI1 for S/N ratios-coefficient of friction

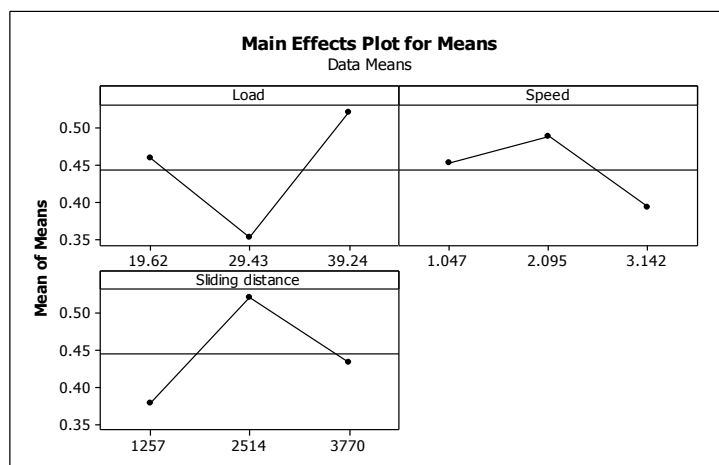


Figure 4.8 Main effects plot of ADI1 for means-coefficient of friction

Examination of results indicates optimum operating conditions for bare minimum COF of ADI1 and is shown in table 4.23.

Table 4.23 Optimized operating conditions of ADI1 for minimum COF

Load, L (N)	Speed, S (m/s)	Sliding distance, D (m)
29.43	3.142	1257

4.4.3 Analysis of Variance of COF

ANOVA was utilized in analysis of experimental results. Influence of factors employed for study was investigated. Confidence echelon chosen for study was 95% with connotation level of $\alpha=0.05$. Tables 4.24 and 4.25 depict ANOVA results for COF of DI and ADI1.

Table 4.24 Analysis of variance for S/N ratios - COF (DI)

Source	DOF	Seq. SS	Adj. SS	Adj. MS	F-test	P-value	Percentage Contribution (%)
Load	2	5.1779	5.1779	2.5890	3.76	0.210	14.40
Speed	2	18.6926	18.6926	9.3463	13.56	0.069	51.97
Sliding distance	2	10.7211	10.7211	5.3605	7.78	0.114	29.81
Error	8	35.9705		0.6895			3.82
Total							100

Notes: DOF, Degrees of Freedom; Seq. SS, Sequential sum of squares; Adj. SS, Adjusted sum of squares; Adj. MS, Adjusted mean squares.

Table 4.25 Analysis of variance for S/N ratios - COF (ADI1)

Source	DOF	Seq. SS	Adj. SS	Adj. MS	F-test	P-value	Percentage Contribution (%)
Load	2	22.327	22.327	11.163	3.71	0.212	40.78
Speed	2	10.916	10.916	5.458	1.81	0.356	19.94
Sliding distance	2	15.479	15.479	7.739	2.57	0.280	28.27
Error	2	6.023	6.023	3.012			11.01
Total	8	54.745					100

Impact of parameters considered for examination was explored. Certainty level decided for examination, was 95% with noteworthiness level of $\alpha=0.05$. Tables 4.24 and 4.25 delineate ANOVA results of COF for DI and ADI1. Last section in table demonstrates percentage contribution (P %) of every one of the factors on the response (COF). It indicates level of impact on outcomes. It reveals that speed (51.97%) has the most astounding impact on COF of DI. Sliding distance has an impact of 29.81% taken after by load with 14.40%. Most astounding affecting component for COF of ADI1 is load (40.78%). Sliding distance has an impact of 28.27% taken after by speed with 19.94%.

4.4.4 Regression Model

LRMs were developed for DI and ADI1 with response as COF using MINITAB15 software and are given by equations (4.5) and (4.6).

$$COF (DI) = 0.4855 + 0.000823 * L + 0.05904 * S - 0.00004856 * D \text{ -----Eqn. 4.5}$$

$$COF (ADI1) = 0.3600 + 0.003074 * L - 0.0285 * S + 0.00002153 * D \text{ -----Eqn. 4.6}$$

Above equations can be utilized to envisage COF of DI and ADI1 for given operating conditions. Invariable in LRM is residual. A regression coefficient of 0.90 was achieved for model. It signifies that friction information was not scattered. From eqn. 4.5, it is discovered that COF of DI is specifically corresponding to load and speed. It is contrarily relative to sliding distance. It is found from eqn. 4.6 that COF of ADI1 is specifically corresponding to load and sliding distance. It is contrarily identified with speed. Positive load in two conditions shows that as load builds COF increments both for DI and ADI1.

4.4.5 Confirmation Test

Parameter levels selected for confirmation test other than used before are indicated in table 4.26. Confirmation tests were carried out for ADI1. Table 4.27 illustrates experimental results for confirmation tests carried out. COF is calculated using eqn. 4.6.

Table 4.26 Parameters used in the confirmation friction test

Test no.	Load L, (N)	Sliding speed S, (m/s)	Sliding Distance D, (m)
1	9.81	1.31	1571
2	29.43	2.62	3142
3	49.05	3.93	4713

Table 4.27 Experimental confirmation test results

Test no.	Load L, (N)	Sliding speed S, (m/s)	Sliding Distance D, (m)	Frictional Load of DI (N)
1	9.81	1.31	1571	3.9
2	29.43	2.62	3142	9.6
3	49.05	3.93	4713	16.6

Table 4.28 Confirmation friction test results and comparison with regression model

Test no.	Experimental COF	Regression model – predicted COF	Error (%)
1	0.3975	0.3866	2.74
2	0.3262	0.3081	5.55
3	0.3384	0.3615	6.39

A correlation was made between exploratory COF and figured COF utilizing expression 4.6. Error between two was computed and is appeared in table 4.28. This error is less than 7%. Consequently developed LRM symbolizes an effective and viable way to predict COF of ADI1 for given operating circumstances.

Chapter 5

RESULTS AND DISCUSSION – II

STUDY OF WEAR BEHAVIOR AT ELEVATED TEMPERATURE

This chapter presents effect of sliding speed, applied load and temperature on wear behavior of ADI2 under dry sliding conditions. Process parameters load, sliding speed, sliding distance and external parameter temperature were selected for wear study.

5.1 Experimental Results and Discussion

Experiments were performed at Room Temperature (RT) and Elevated Temperature (ET) of 150°C for various speeds varying from 1.5 to 6 m/s at constant load of 34.335N and sliding distance of 2000m. Experiments were also conducted at RT and ET for various loads varying from 9.81 to 49.05 N at constant speed of 3.5 m/s and sliding distance of 3000m. Collate of wear testing machine was changed to conduct tests at ET. Selected sliding speeds can be categorised into low (1.5 to 2.5 m/s) and high (4 and 6 m/s). Wear test was performed as per ASTM G99a standard and weight loss was calculated. It was translated into volume loss considering a density value of 7.1g/cm³ for ADI. Results of experimentation are presented in table 5.1 and hardness test outcomes are tabulated in table 5.2.

Table 5.1 Experimental results

Expt. No.	Load, L, (N)	Speed, S, (m/s)	Speed, N (rpm)	Sliding Distance, D (m)	Temp., T (°C)	Time (mins.)	Initial weight, W _i (g)	Final weight, W _f (g)	Weight loss, W _o (g)	Wear rate (m ³ /m) x10 ⁻¹²	Frictional Load, (N)	Coefficient of Friction, μ	Specific wear rate, k m ³ /Nm x10 ⁻¹²	Surface temp., °C	Estimated flash temp., °C	Heat Flux q=μWS/A kJ/sm ²
	(1)	(2)	(3)	(4)	(5)	(6)	(7)	(8)	(9)	(10)	(11)	(12)	(13)	(14)	(15)	(16)
1	34.335	1.5	239	2000	ET	22.22	15.862	15.85	0.012	0.8451	17.4	0.5068	0.0230	194	448	332.29
2	34.335	2	319	2000	ET	16.67	15.8549	15.8437	0.0112	0.7887	15.9	0.4631	0.0246	204	513	404.85
3	34.335	2.5	398	2000	ET	13.33	14.8329	14.8205	0.0124	0.8732	14.1	0.4107	0.0254	210	553	448.80
4	34.335	4	637	2000	ET	8.33	15.4747	15.4545	0.0202	1.4225	11.2	0.3262	0.0414	215	651	570.34
5	34.335	6	955	2000	ET	5.56	15.3832	15.2872	0.096	6.7606	10.1	0.2942	0.1969	220	809	771.59
6	34.335	1.5	239	2000	RT	22.22	15.8615	15.839	0.0092	0.6479	20.9	0.6087	0.0029	75	380	399.10
7	34.335	2	319	2000	RT	16.67	15.0548	15.0478	0.007	0.4930	17.4	0.5068	0.0049	96	434	443.05
8	34.335	2.5	398	2000	RT	13.33	15.725	15.7204	0.0046	0.3239	14.9	0.4340	0.0094	103	465	474.26
9	34.335	4	637	2000	RT	8.33	14.7896	14.7872	0.0024	0.1690	13.4	0.3903	0.0144	108	629	682.42
10	34.335	6	955	2000	RT	5.56	15.5935	15.5921	0.0014	0.0986	12.2	0.3553	0.0461	111	823	931.83
11	9.81	3.5	557	3000	ET	14.29	15.4421	15.4214	0.0207	0.9718	3.3	0.3364	0.0499	186	298	147.04
12	19.62	3.5	557	3000	ET	14.29	15.4419	15.4182	0.0237	1.1126	7.8	0.3976	0.0567	196	461	347.59
13	29.43	3.5	557	3000	ET	14.29	15.4363	15.3996	0.0367	1.7230	10.4	0.3534	0.0585	219	573	463.42
14	39.24	3.5	557	3000	ET	14.29	15.6266	15.5849	0.0417	1.9577	14.2	0.3619	0.0857	231	714	632.76

Expt. No.	Load, L, (N)	Speed, S, (m/s)	Speed, N (rpm)	Sliding Distance, D (m)	Temp., T (°C)	Time (mins.)	Initial weight, W _i (g)	Final weight, W _f (g)	Weight loss, W _o (g)	Wear rate (m ³ /m) x10 ⁻¹²	Frictional Load, (N)	Coefficient of Friction, μ	Specific wear rate, k m ³ /Nm x10 ⁻¹²	Surface temp., °C	Estimated flash temp., °C	Heat Flux q=μWS/A kJ/sm ²
15	49.05	3.5	557	3000	ET	14.29	15.325	15.2355	0.0895	4.2018	15.7	0.3201	0.0991	239	773	699.59
16	9.81	3.5	557	3000	RT	14.29	14.2149	14.2129	0.002	0.0939	4.2	0.4281	0.0078	82	225	187.13
17	19.62	3.5	557	3000	RT	14.29	14.3930	14.3881	0.0049	0.2300	9.1	0.4638	0.0085	100	410	405.46
18	29.43	3.5	557	3000	RT	14.29	14.8114	14.806	0.0054	0.2535	11.3	0.3840	0.0086	136	521	503.55
19	39.24	3.5	557	3000	RT	14.29	14.8638	14.8567	0.0071	0.3333	14.6	0.3721	0.0096	152	649	650.59
20	49.05	3.5	557	3000	RT	14.29	15.6132	15.605	0.0082	0.3850	21.1	0.4302	0.0117	179	897	940.22

RT-Room Temperature, ET-Elevated Temperature of 150°C

Table 5.2 Hardenability test results

Expt. No.	Load L, (N)	Speed S, (m/s)	Sliding Distance, D (m)	Temp., T (°C)	Distance from worn out surface, mm					
					0	1	2	3	4	5
					Hardness, HV					
S1	34.335	1.5	2000	ET	414	429	438	454	462	472
S3	34.335	2.5	2000	ET	352	378	413	431	452	468
S5	34.335	6	2000	ET	284	305	340	385	436	452
S6	34.335	1.5	2000	RT	502	495	490	479	472	470
S8	34.335	2.5	2000	RT	521	513	492	486	472	468
S10	34.335	6	2000	RT	533	521	509	495	483	483
L1	9.81	3.5	3000	ET	434	438	444	450	456	483
L3	29.43	3.5	3000	ET	391	394	401	434	456	479
L5	49.05	3.5	3000	ET	242	295	342	385	416	452
L6	9.81	3.5	3000	RT	523	504	492	486	475	470
L8	29.43	3.5	3000	RT	549	536	495	490	483	472
L10	49.05	3.5	3000	RT	597	565	509	490	482	478

Table 5.3 Results of surface roughness measured on worn surfaces

Expt. No.	Load L, (N)	Speed S, (m/s)	Sliding Distance, D (m)	Temp., T (°C)	Surface roughness Ra (µm) [parallel to wear track]	Surface roughness Ra (µm) [across wear track]
1	34.335	1.5	2000	ET	0.18	0.47
2	34.335	2	2000	ET	0.15	0.41
3	34.335	2.5	2000	ET	0.26	0.37
4	34.335	4	2000	ET	0.14	0.26
5	34.335	6	2000	ET	0.09	0.18
6	34.335	1.5	2000	RT	0.42	0.56
7	34.335	2	2000	RT	0.26	0.37
8	34.335	2.5	2000	RT	0.31	0.42
9	34.335	4	2000	RT	0.14	0.27
10	34.335	6	2000	RT	0.11	0.21
11	9.81	3.5	3000	ET	0.27	0.41
12	19.62	3.5	3000	ET	0.34	0.47
13	29.43	3.5	3000	ET	0.22	0.36
14	39.24	3.5	3000	ET	0.29	0.42
15	49.05	3.5	3000	ET	0.16	0.25
16	9.81	3.5	3000	RT	0.24	0.38
17	19.62	3.5	3000	RT	0.19	0.32
18	29.43	3.5	3000	RT	0.23	0.47
19	39.24	3.5	3000	RT	0.33	0.51
20	49.05	3.5	3000	RT	0.35	0.68

5.1.1 Effect of Sliding Speed on Wear Rate

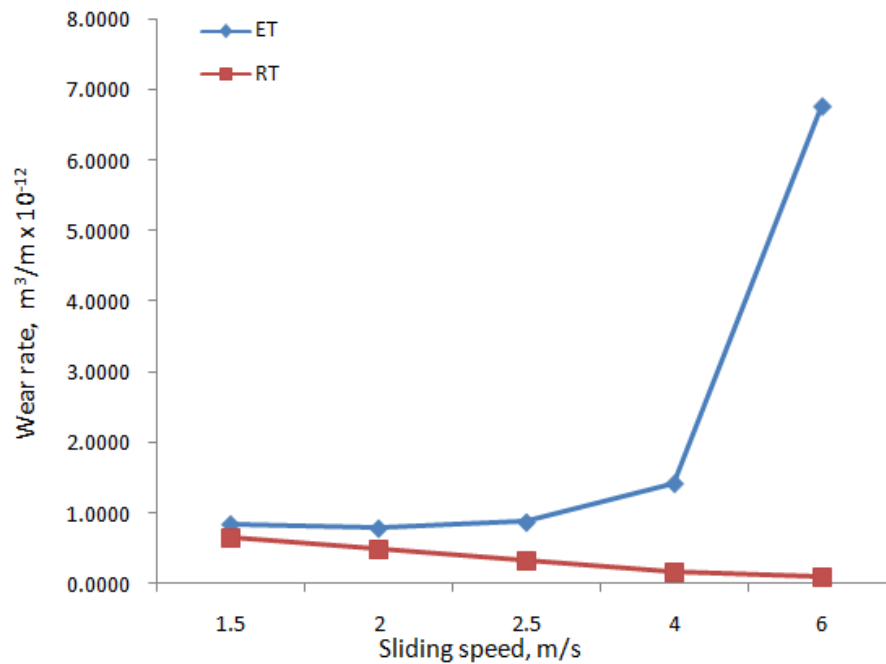


Figure 5.1 Experimental wear rates as a function of sliding speed

Weight loss attained its steady state subsequent to running through a small sliding distance of less than 250m. In figure 5.1 investigational steady rates of wear are reported against sliding speed. In concurrence with [119, 267] wear rate is observed to decline with sliding speed for RT operating conditions. However, reverse tendency is observed at ET. Wear rate at RT is at its acme for a small sliding speed of 1.5m/s and has been reduced with increase in sliding speed. For remaining sliding speeds from 2m/s to 6m/s wear rate has turned out to be almost steady. Wear rate observed at ET is steady for sliding speeds from 1.5m/s to 2.5m/s. It increases for a sliding speed of 4m/s but reached its peak value at a sliding distance of 6m/s. Wear rate observed for a small sliding speed temperature does not have any role on wear rate. However, its role is predominant at higher sliding speeds. Sliding speed and temperature has much greater influence on wear rate. Specific wear rate defined as, “volumetric loss per unit sliding distance per unit load” varied between 0.0029×10^{-12} to $0.0461 \times 10^{-12} \text{ m}^2/\text{N}$ at RT and 0.023×10^{-12} to $0.1969 \times 10^{-12} \text{ m}^2/\text{N}$ at ET. The values are emblematic of a meek oxidative wear at RT [122, 150].

5.1.2 Effect of Sliding Speed on Coefficient of Friction

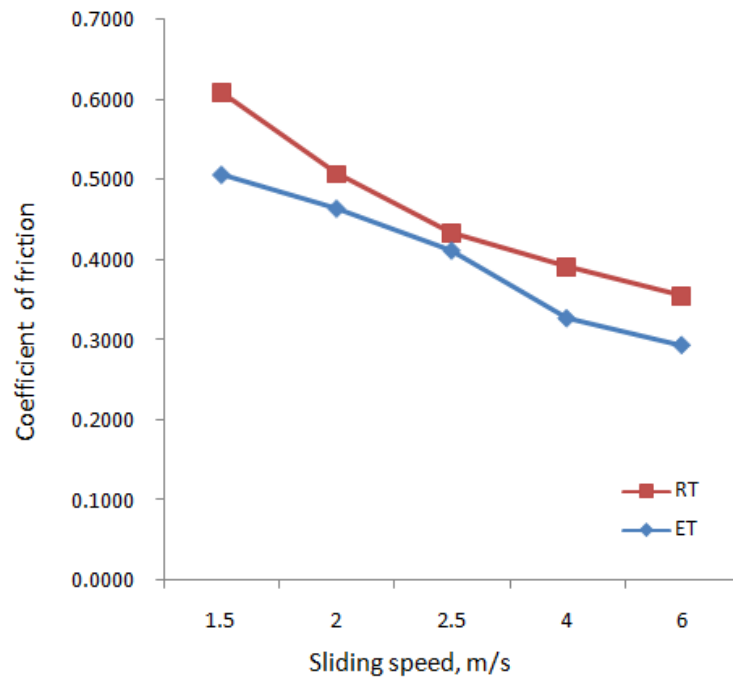


Figure 5.2 Coefficient of friction as a function of sliding speed

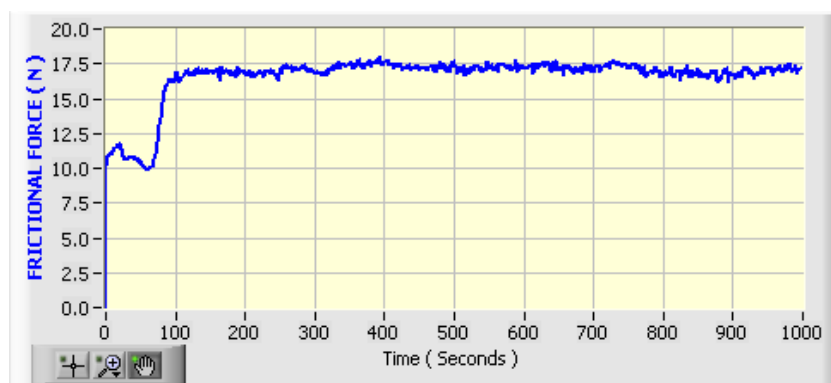


Figure 5.3 Frictional force as function of time

Steady state frictional load is observed in all tests. COF is calculated considering normal load. In figure 5.2 friction coefficients under steady state are reported as a function of speed. Steady state was attained after an average sliding distance of 500m. In figure 5.3 represents steady state frictional force in N as a function of time. COF is seen to dwindle with sliding speed both at RT and ET. As observed, wear rate decreased with sliding speed at RT is in agreement with drop in value of COF with sliding speed. However, reverse is observed at ET though COF decreases.

5.1.3 Effect of Sliding Speed on Surface and Flash Temperature

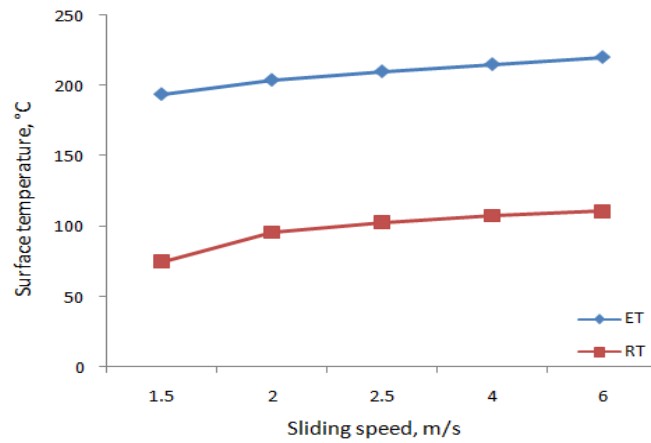


Figure 5.4 Surface temperature as a function of sliding speed

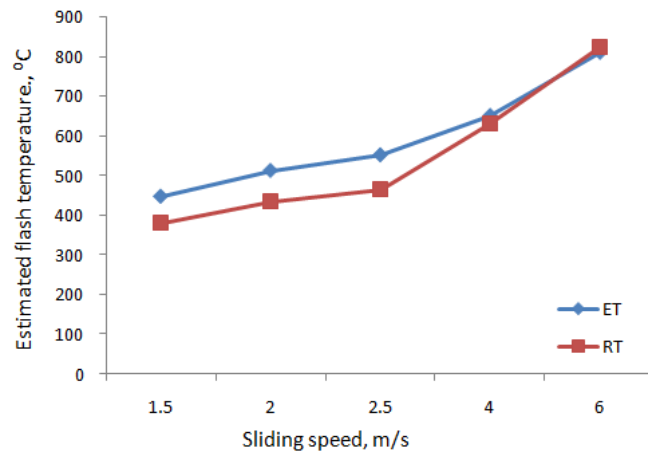


Figure 5.5 Estimated flash temperature as a function of sliding speed

In Figure 5.4 noted contact temperatures are depicted against speed of sliding at RT and ET. Correspondingly to COF, steady-state readings were reached after a sliding distance of 500m. It is observed that surface temperature increased with speed though COF decreased. Thus sliding speed has a role in increasing surface temperature due to local heating.

Flash temperature is temperature attained at contacting asperities for a very short time during sliding. Figure 5.5 depicts calculated flash temperatures for various speeds. Its value increases with sliding speed. It is very high in higher speed regimes and results in thermal softening at asperities. Highest flash temperature observed is 823°C, for a speed of 6m/s at RT.

5.1.4 Effect of Sliding Speed on Hardness

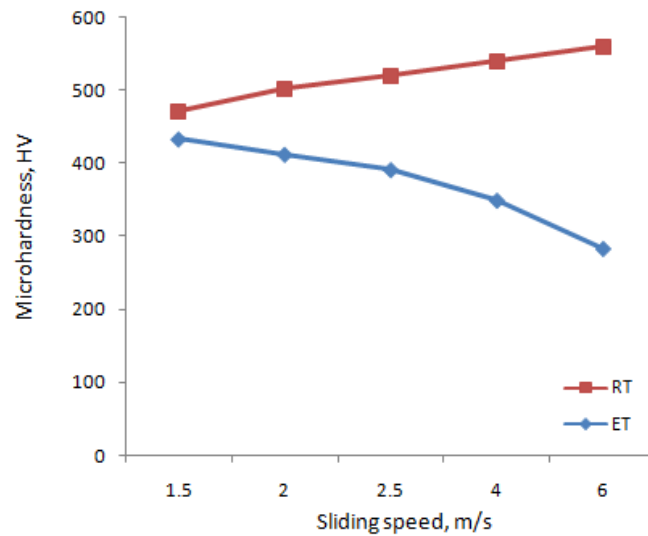


Figure 5.6 Microhardness as a function of sliding speed

In figure 5.6, microhardness is reported against speed at RT and ET. Microhardness on wear tracks increases considerably with increase in sliding speed. Increase in hardness is an indication of work hardening effects with translation of retained austenite (formed during as tempering) to martensite. This is in harmony with report by Daber [115]. However, reverse trend is observed at ET indicating prohibition of change of retained austenite to martensite. This supports increase in wear rate observed for ET.

5.1.5 Effect of Wear Rate and Specific Wear Rate for Varying Speed

In figure 5.7 and 5.8 wear rate and specific wear rate are reported against sliding speed at RT and ET. Results at RT infer that from a sliding speed of 1.5m/s, wear rate decreased drastically and slightly decreased further with speed, whereas, specific wear rate is constant with sliding speed. There is a drastic increase in wear rate at high sliding speed of 6m/s at ET.

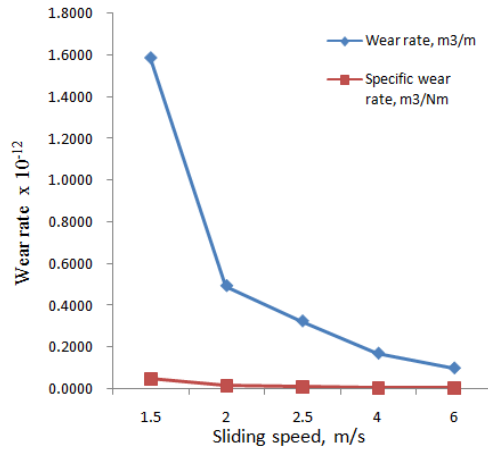


Figure 5.7 Wear rate and specific wear rate as a function of sliding speed at RT

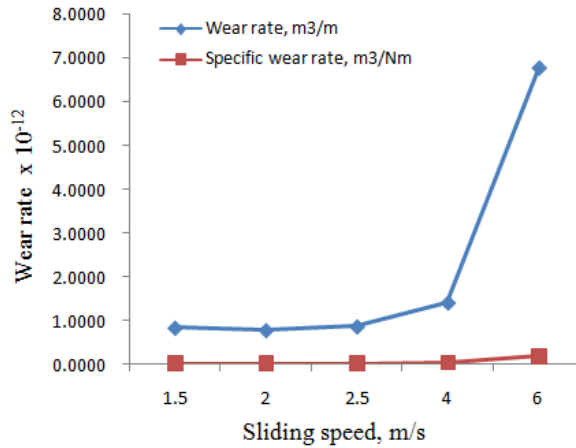


Figure 5.8 Wear rate and specific wear rate as a function of sliding speed at ET

However, specific wear rate remained constant at all speeds except for a slight boost for a sliding speed of 6m/s. Minimum gap between specific wear rate and wear rate is observed for a sliding speed of 6m/s at RT. This indicates oxidative wear mechanism as evidenced by Tikotkar [22]. Specific wear rate varied from 0.023×10^{-12} to $0.1969 \times 10^{-12} \text{ m}^2/\text{N}$ at ET and from 0.029×10^{-12} to $0.0461 \times 10^{-12} \text{ m}^2/\text{N}$ at RT. Most types of wear are consequences of ill temper contacts. It has been hypothesized by Archard [22] that aggregate volume is relative to genuine contact times distance of sliding.

5.1.6 Effect of Sliding Speed and Load on Heat Flux

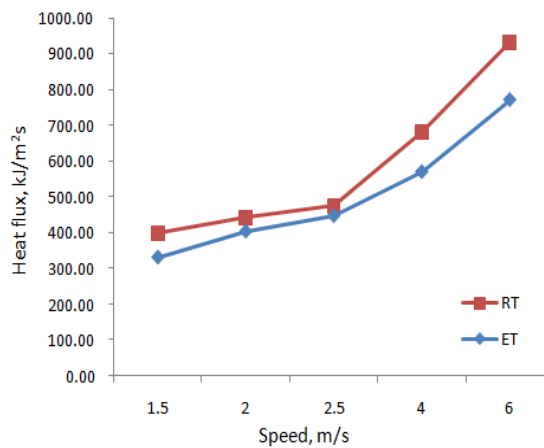


Figure 5.9 Heat flux as a function of sliding speed

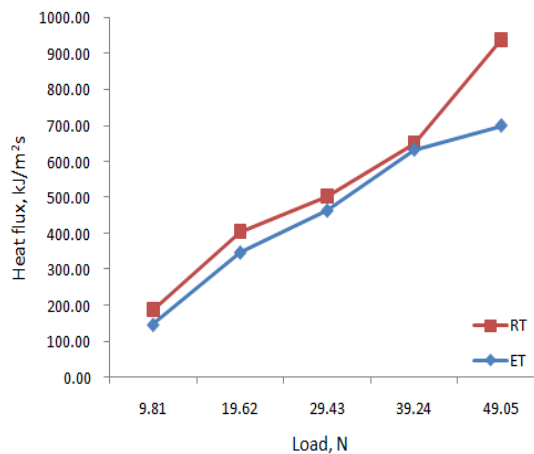


Figure 5.10 Heat flux as a function of applied load

Heat is generated due to friction during sliding and temperature of pin increases. Figure 5.8 shows variation of heat flux with sliding speed and figure 5.9 depicts variation of heat flux with applied load. Heat flux varies from 399.1kJ/sm² to 931.83kJ/sm² at RT and from 332.29kJ/sm² to 771.59kJ/sm² at ET for increasing speed from 1.5m/s to 6m/s. Variation in heat flux is maximum at lower and higher speeds. At a speed of 2.5m/s, heat flux is almost same at RT and ET. Heat flux varies from 187.13kJ/sm² to 940.22kJ/sm² at RT and from 147kJ/sm² to 700 kJ/sm² at ET for increasing load from 9.81N to 49.05N. Variation in heat flux is maximum at the highest load of 49.05N. Friction is less at ET than RT at all operating conditions. Hence heat flux observed is less at ET than RT.

5.1.7 Effect of Applied Load on Wear Rate

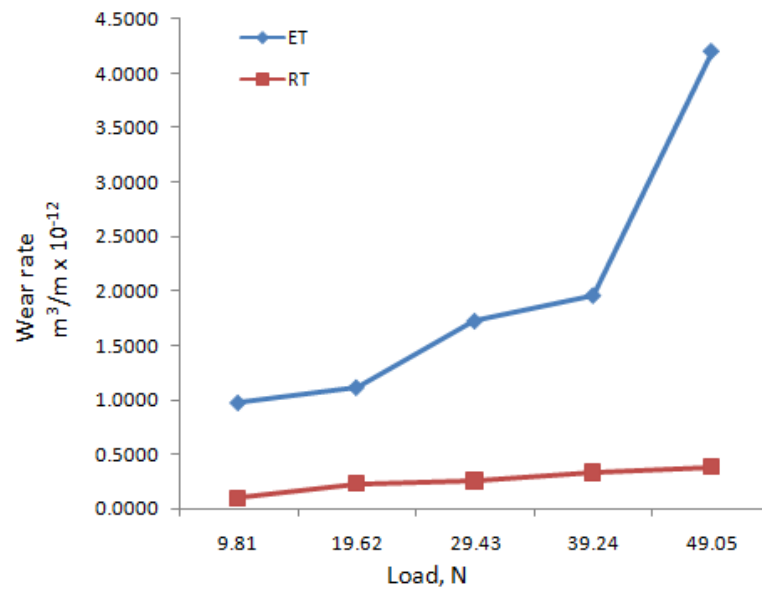


Figure 5.11 Experimental wear rates as a function of applied load

Loss by wear arrived at steady state past running through tiny sliding distance of less than 500m. In figure 5.11 experimental wear rates under steady circumstances are reported as a function of applied load. In concord with [119], wear rates are found to increase with load for RT conditions. Wear rate augmented drastically with load at ET. Gap between wear rates at RT and ET is almost same for loads of 9.81N and 19.62N. This gap increases beyond for a load of 19.62N and as observed from experimental results, it is maximum for a load of 49.05N. Applied load in combination with temperature has a predominant consequence on wear rate. Hence, material does not have application at higher loads and ET conditions.

5.1.8 Effect of Applied Load on Friction

Steady state frictional load was observed in all the tests. In figure 5.12 steady state COF are reported against applied load. It reached steady state after about 300m of sliding distance on an average. In figure 5.13 represents steady state frictional force in N dependent on load. Figure 5.14 shows frictional force as a function of time. As observed, COF is least for a load of 39.24N and maximum for a load of 19.62N at RT.

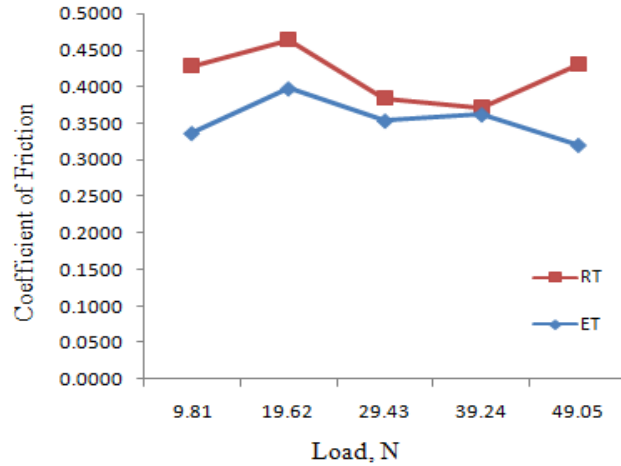


Figure 5.12 Coefficient of friction as a function of applied load

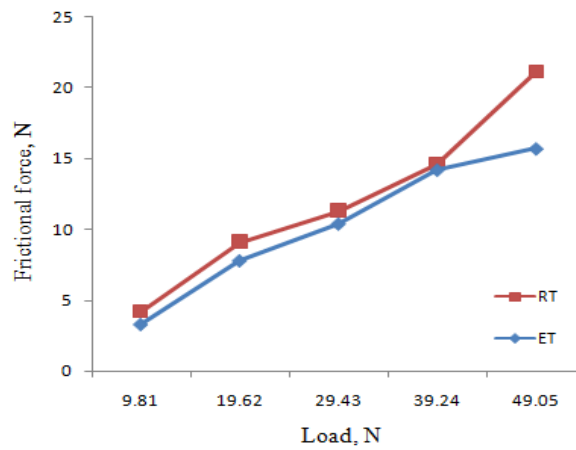


Figure 5.13 Frictional force as a function of applied load

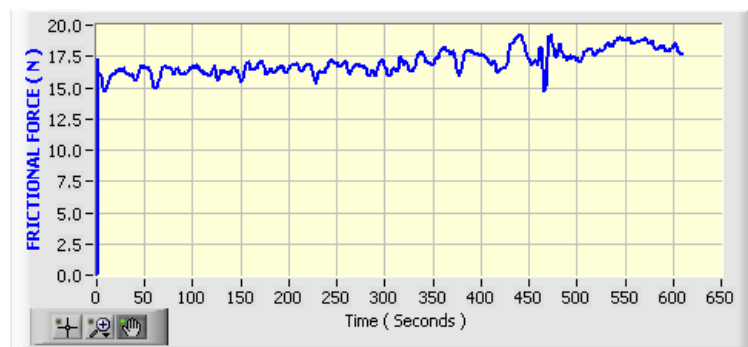


Figure 5.14 Frictional force as function of time

Gap between COF at RT and ET is same at stumpy and high applied loads. COF at a load of 39.24N is almost same for RT and ET. As seen from figure 5.13, frictional force increases with load both at RT and ET conditions. Frictional force at ET gets reduced compared to RT irrespective of applied load. Frictional force for a load of 39.24N is almost same both at RT and ET. Maximum gap between frictional forces is observed for a load of 49.05N.

5.1.9 Effect of Applied Load on Surface and Flash Temperature

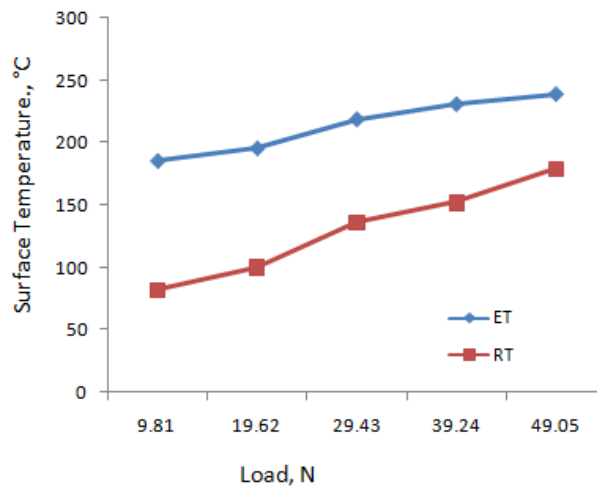


Figure 5.15 Surface temperature as a function of applied load

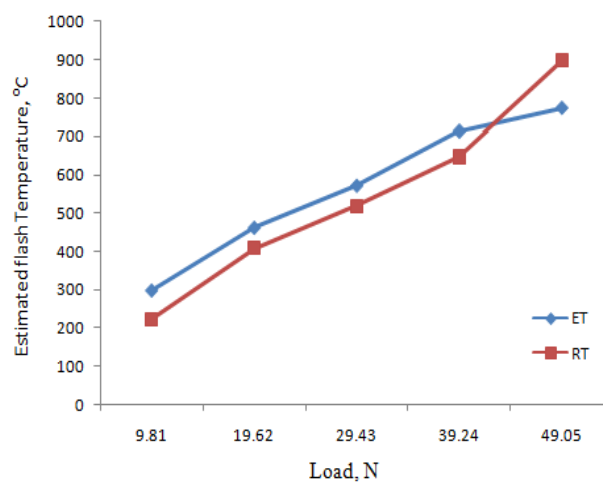


Figure 5.16 Estimated flash temperature as a function of applied load

In figure 5.15 noted contact temperatures are displayed against load at RT and ET. Similarly to COF, steady values were attained after a sliding distance of 300m. It was observed that surface temperature increased with load due to increase in frictional force with load. Thus applied load along with sliding speed selected for study has a major role in increasing surface temperature due to local heating.

Figure 5.16 shows estimated flash temperatures for various loads. This value increases almost linearly both at ET and RT. Gap between two is constant from a load of 9.81N to 39.24N. Highest value of flash temperature (897°C) is observed for a load of 49.05N.

5.1.10 Effect of Applied Load on Hardness

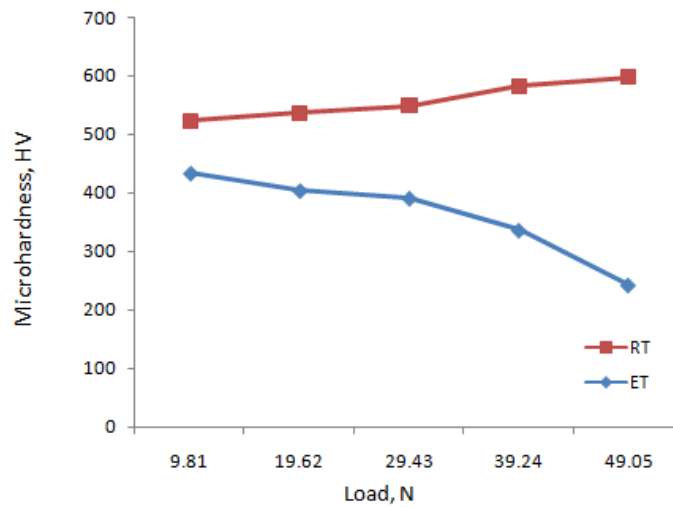


Figure 5.17 Microhardness as a function of applied load

In figure 5.17, microhardness is reported against load at RT and ET. Microhardness on wear tracks augments with load at RT. Increase in hardness is an indication of enhancement in work hardening effects. However, it decreases with load at ET. It decreases considerably at higher loads. For lower loads, gap between hardness values is less and increases with load. This gap is highest for the highest load. Conversion of retained austenite into martensite is prohibited as ADI becomes soft at ET thus decreasing hardness.

5.1.11 Effect of Wear Rate and Specific Wear Rate for Varying Loads

In figure 5.18 and 5.19 wear rate and specific wear rate are reported against load at RT and ET. The specific wear rate is same at 9.81N and 19.62N. This decreases at 29.43N and further remains same till 49.05N at RT. As observed, wear rate increases with load. Gap between two is least at 9.81N load and maximum at 49.05N at RT. Specific wear rate is more at 9.81 N and 49.05 N and almost same from 19.62N to 39.24N at ET.

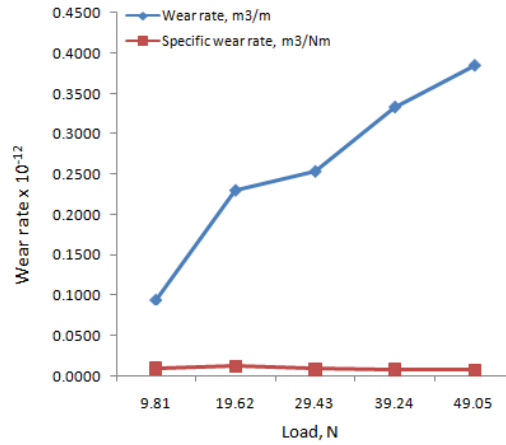


Figure 5.18 Wear rate and specific wear rate as a function of applied load at RT

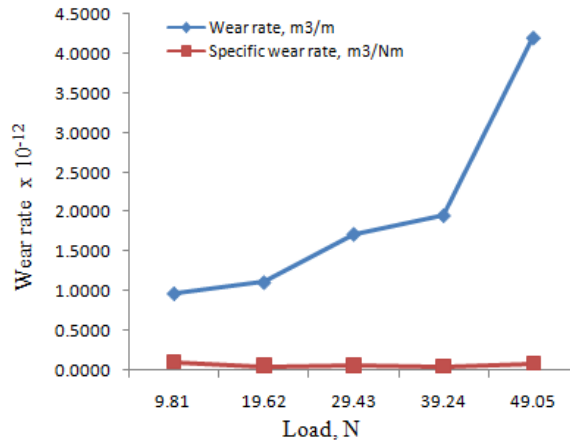


Figure 5.19 Wear rate and specific wear rate as a function of applied load at ET

Gap increases with load at ET. It is least both at RT and ET indicating oxidative wear mechanism as evidenced by Tikotkar [22]. Specific wear rate varied from 0.0499×10^{-12} to $0.0991 \times 10^{-12} \text{ m}^2/\text{N}$ at ET and from 0.0078×10^{-12} to $0.0117 \times 10^{-12} \text{ m}^2/\text{N}$ at RT.

5.1.12 Hardenability

Figure 5.20 depicts deviation in microhardness with depth of specimen from worn surface at RT and ET subjected to same operating conditions. As observed from graphs, microhardness decreases for RT specimens. However, reverse trend is seen in specimens operated at ET. This is because specimen becomes soft subjected to higher temperatures and hardness decreases removing more material from surface.

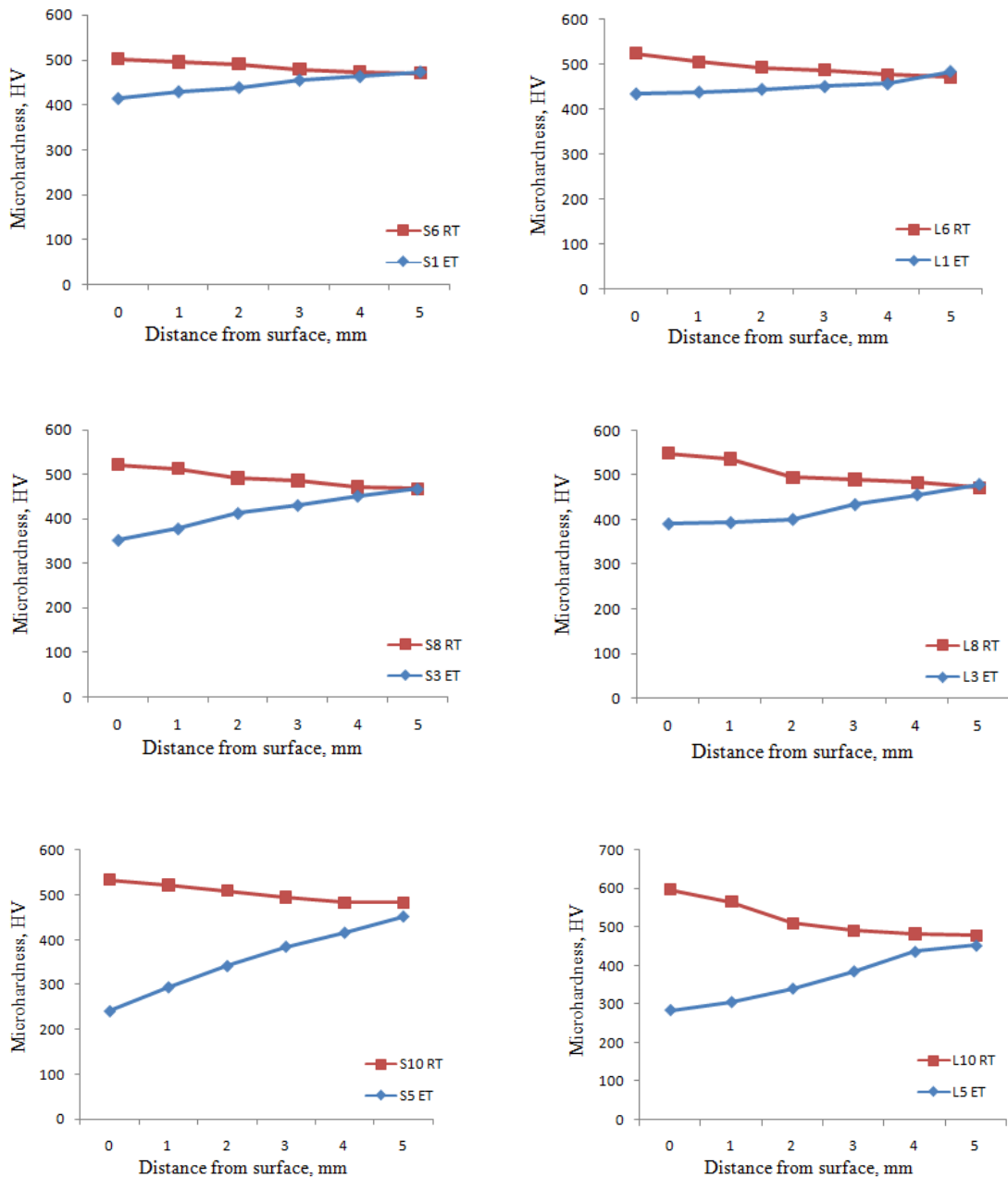


Figure 5.20 Microhardness profiles from worn surface for RT and ET specimens

5.1.13 Morphology of Worn Surfaces

It is observed from SEM micrographs of DI, ADI1 and ADI2 (figs. 5.21, 5.22, 5.23) that graphite nodules of almost same size have been distributed uniformly on the surface. Microscopic examination of worn surfaces was carried out to recognize type of wear process. Micrographs of SEM of worn surfaces are shown in figures 5.24 to 5.41. The morphology of worn surface (fig.5.27) clearly shows the sliding marks which run more or less parallel to one another. Dark patches (fig.5.36) which are scattered on the surface are also observed. Patches were not removed even when the

test surface was cleaned with water. They may indicate oxidized layers. A transfer layer representing greyish area is also occasionally seen (fig.5.32). The dark patches present on the worn surfaces which are presumed to be oxides indicate oxidation wear in the present working conditions. The published wear data on steel was systematically analyzed by Lim and Ashby [154]. They showed that the wear mechanisms vary for different values of the normalised pressure defined as $p_o = W / (A_n * H_o)$ where p_o stands for the normalised wear pressure, A_n is the nominal contact area, W is the normal applied load and H_o is the hardness at RT. For normalized lower pressure range of (10^{-2} to 10^{-4}) to 1.5m/s, the wear mechanism map indicates oxidational wear. Figure 5.30 reveals worn surface subjected to severe damage and affected the subsurface damage as well. The wear tracks show plastically deformed metal distensions and chips (fig. 5.28). Spalled layers and large voids which resemble delamination are observed on the surface. They illustrate the occurrence of severe wear (fig. 5.24). Figure 5.29 shows plastically deformed chip. It appears that the graphite nodules have been plucked out from the surface during sliding. White and greyish layers are visible within the wear track correspond to iron oxide and parent metal. Part of the oxide layer is smeared on the surface appearing as a flake (fig. 5.36). Probably the major cause for abrasion is the oxide chips. This is commonly associated with unlubricated sliding wear. Fast oxidation occurs during sliding due to heat generation in friction. Oxide layers are observed as islands on the surface (fig. 5.26). The separation of these layers result in mild wear. Rough cracked surface with irregular patches or layers seen on the surface indicate wear debris adhesion (fig. 5.24). The graphite nodules distort into elliptical shapes under the applied load. Metal to metal contact is reduced by the presence of these nodules resulting in reduction of friction. The worn out surfaces are also characterised by the valleys or ploughing marks along the wear area. It is also evident that the graphite nodules underwent plastic deformation and elongated in the direction of wear. As observed the preferential sites for wear initiation is the graphite metal interfaces. They develop crack after severe plastic deformation at the interfaces. Wear debris is formed when these cracks grow towards the wear surface. Fatigue of oxide film and heat generation during friction also results in debris. This results in the weakening of bonding strength between the substrate and oxide film and delamination of the oxide layer occurs. The observations are in agreement with the theory of delamination presented by Ahmadabadi et al. [92], Prado et al. [27], Hemanth et al. [268]. These authors

recommend that wear rate is emphatically affected by material characteristic imperviousness to shape sub-surface splits, and by resulting crack development and formation of debris. Tongue formation and plastic flow (figs. 5.24, 5.28) indicate occurrence of wear by adhesion and delamination and are in agreement with Ritha kumari et al. [148]. Wear behavior is influenced by the hardness and strain hardening when sample is subjected to plastic flow and tear. Longer time and higher loads are required to tear the hard material from the surface. Material subjected to strain hardening flows to a greater extent making it very difficult to tear. As observed from the SEM images at ET few spots on the surface are subjected to severe plastic deformation. These spots were plucked out of the surface by adhesion making pits and grooves on the surface. This process predominates at ET resulting in severe wear. This type of wear accelerates at higher loads and speeds at ET rendering the material non-functional at ET operating conditions.

5.1.14 Wear Debris Analysis

Figure 5.42 shows SEM images of wear debris gathered for specimen operated at ET with speed of 3.5m/s, load of 49.05N and sliding distance of 3000m. The collected debris shows some amount of oxidation. Oxide reddish brown powder generated indicates oxidational wear mechanism under present operating conditions and is in agreement with Gangasani et al. [270]. The brittle iron oxide is removed off easily from the surface. Because of asperities in the route of rotation load is compressive with shear constituent. Pin surface gets gashed from the asperities present on the hardened disc. The amount of material removed by this gashing action is very small as the disc has a smooth surface and is well polished.

SEM Micrographs of DI, ADI1 and ADI2

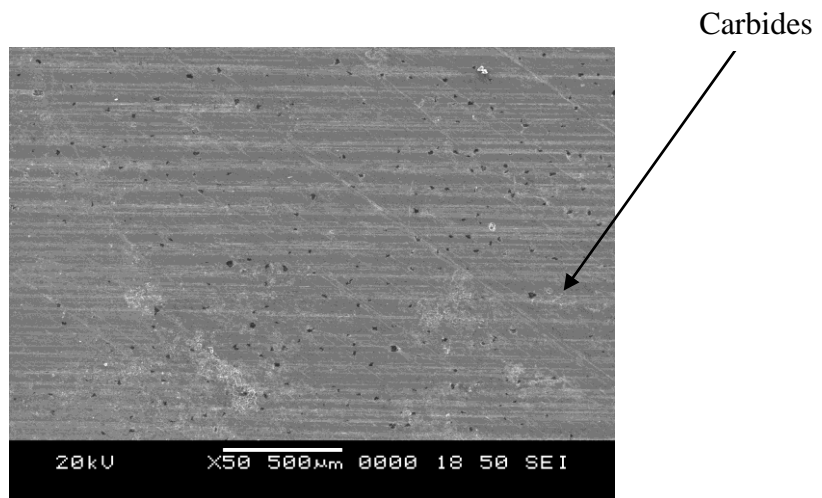


Figure 5.21 SEM micrograph of DI

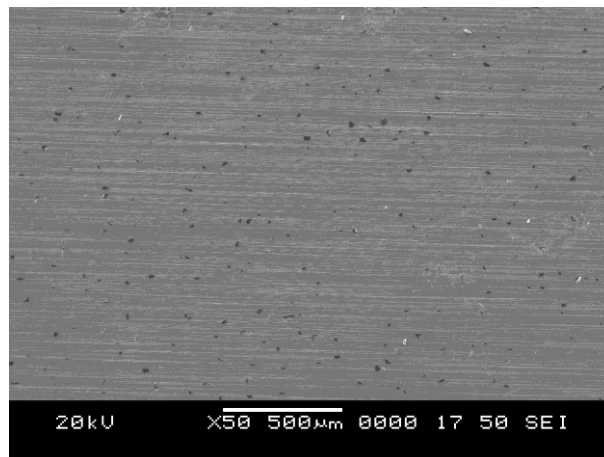


Figure 5.22 SEM micrograph of ADI1

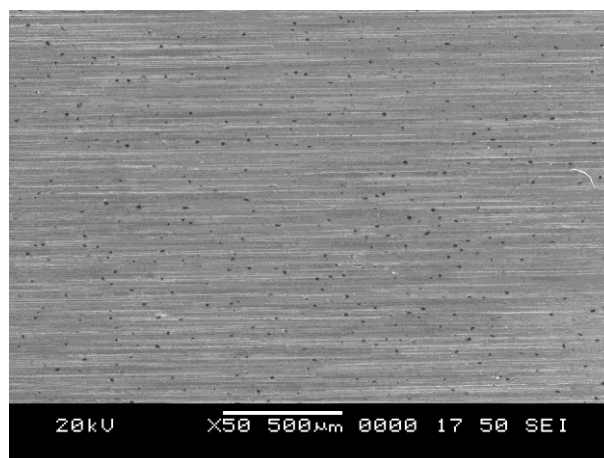


Figure 5.23 SEM micrograph of ADI2

SEM Micrographs at RT

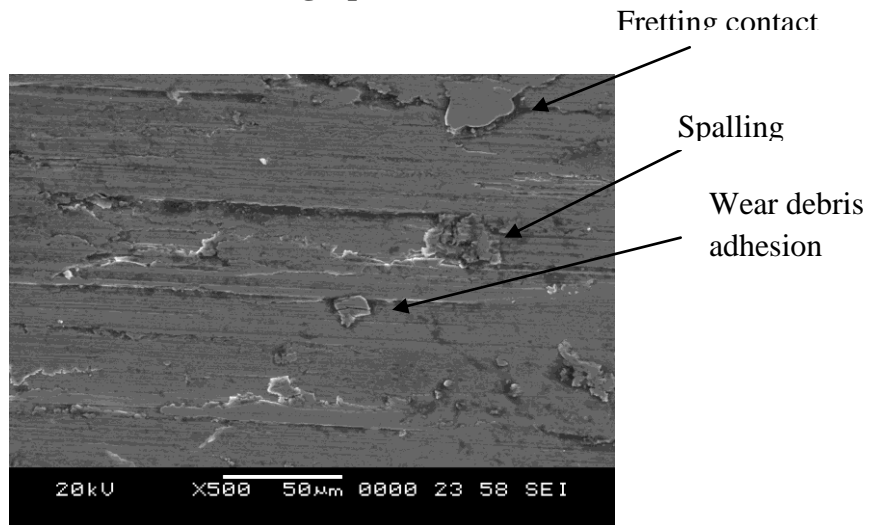


Figure 5.24 SEM micrograph at L=34.335N, S=6m/s, D=2000m

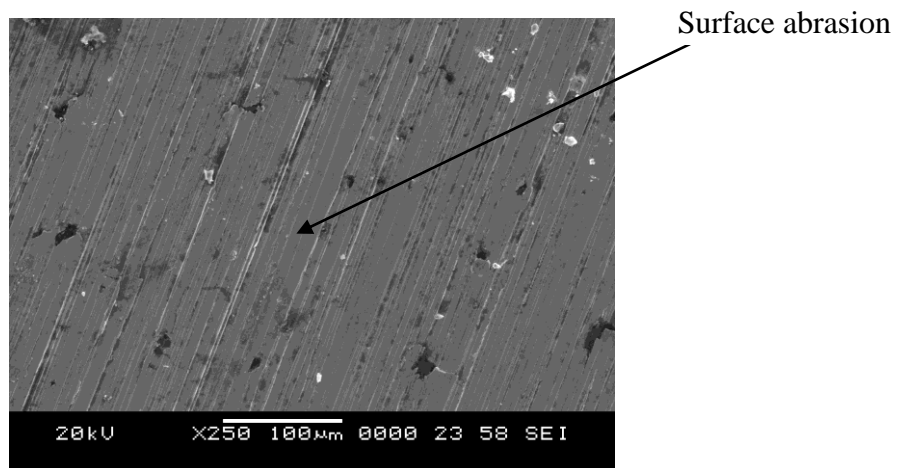


Figure 5.25 SEM micrograph at L=34.335N, S=4m/s, D=2000m

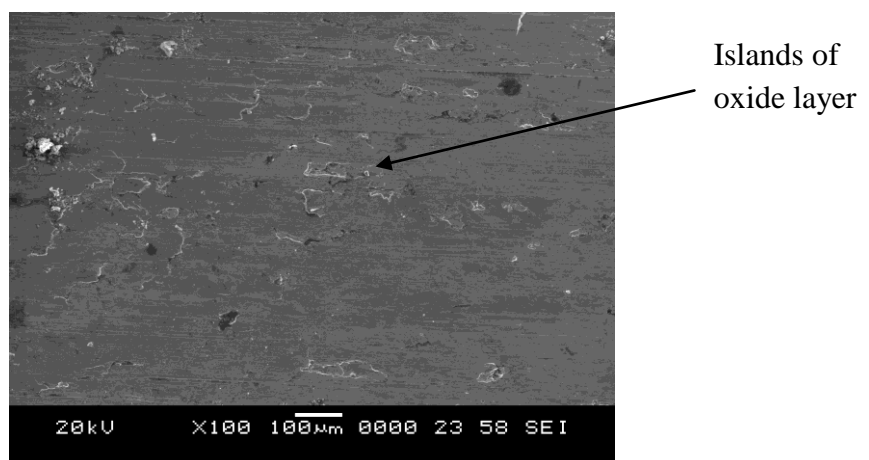


Figure 5.26 SEM micrograph at L=9.81N, S=3.5m/s, D=3000m

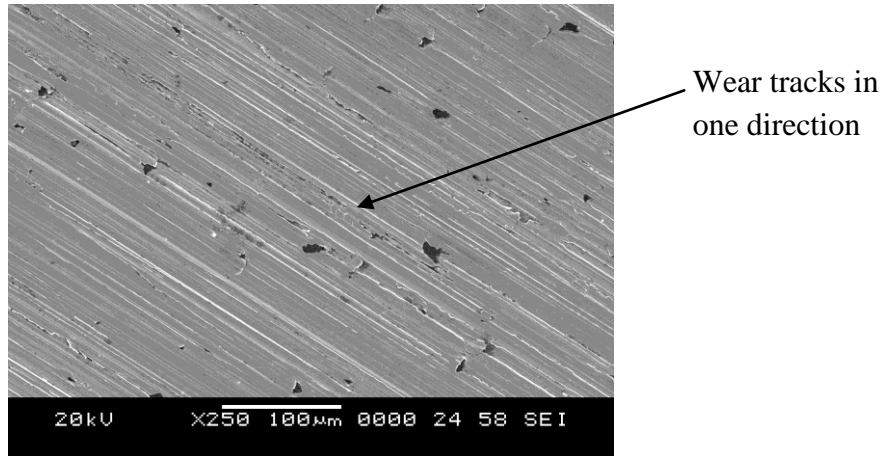


Figure 5.27 SEM micrograph at L=34.335N, S=2.5m/s, D=2000m

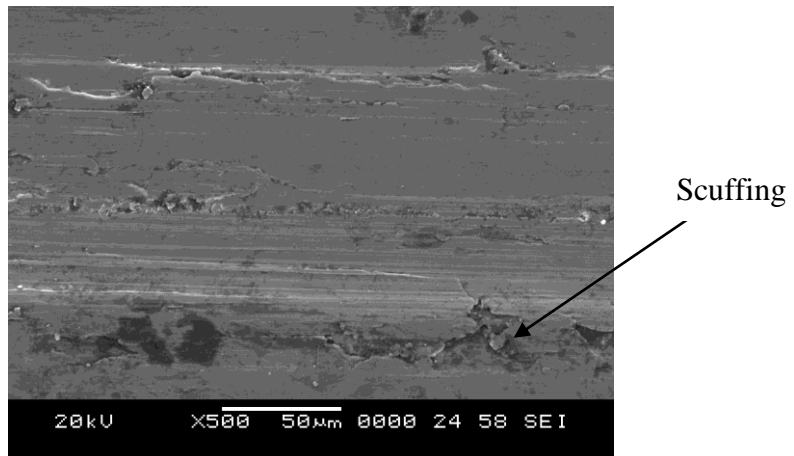


Figure 5.28 SEM micrograph at L=49.05N, S=3.5m/s, D=3000m

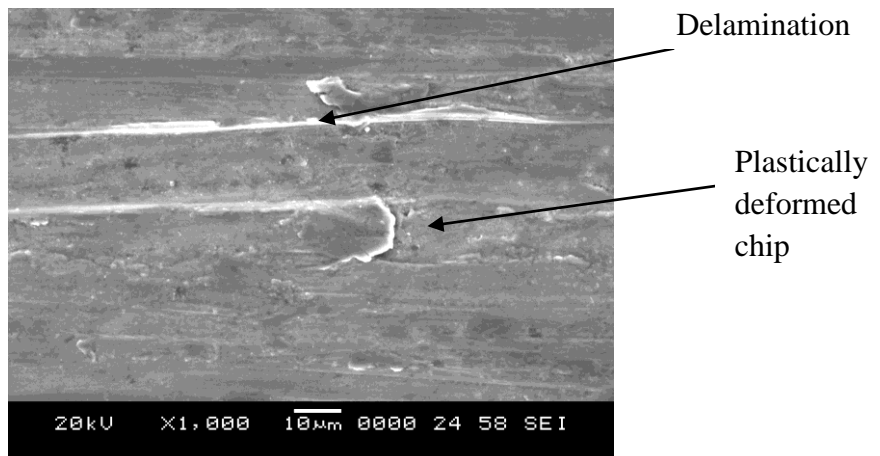


Figure 5.29 SEM micrograph at L=34.335N, S=1.5m/s, D=2000m

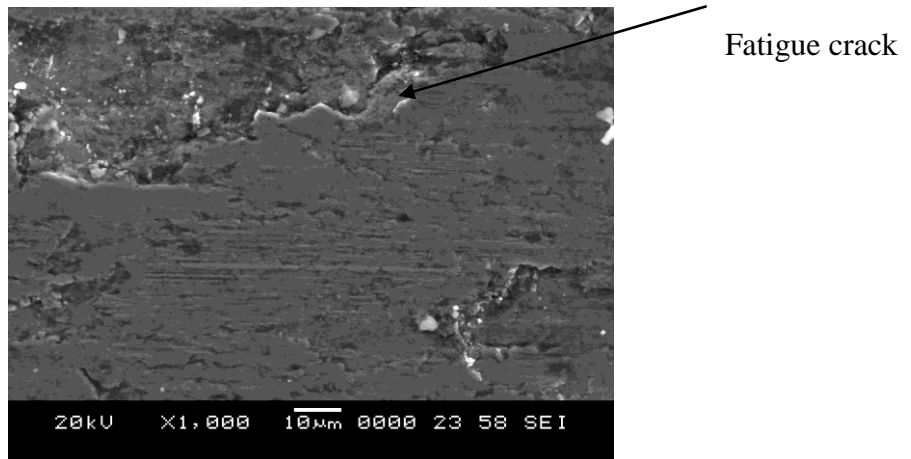


Figure 5.30 SEM micrograph at L=19.62N, S=3.5m/s, D=3000m

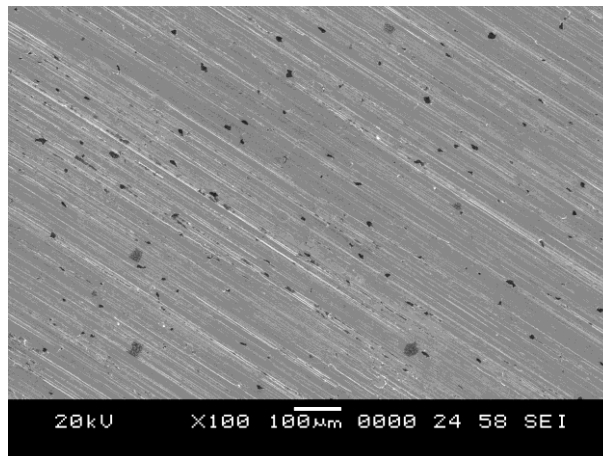


Figure 5.31 SEM micrograph at L=34.335N, S=2m/s, D=2000m

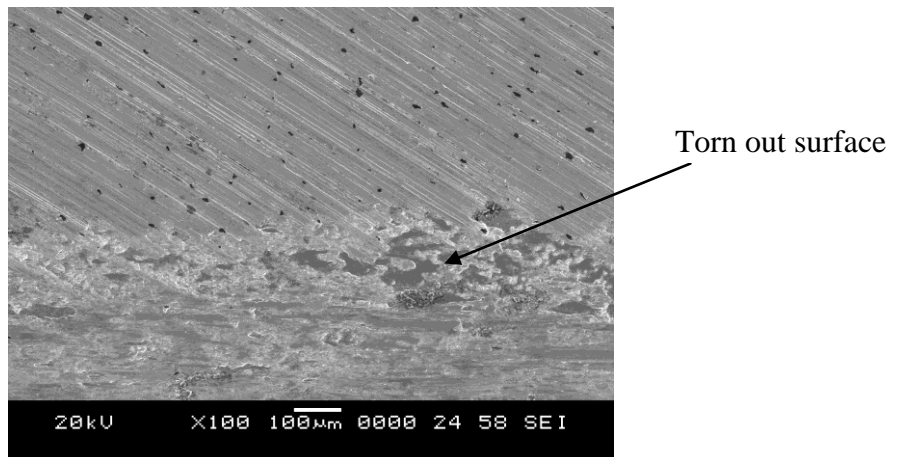


Figure 5.32 SEM micrograph at L=39.24, S=3.5m/s, D=3000m

SEM Micrographs at ET

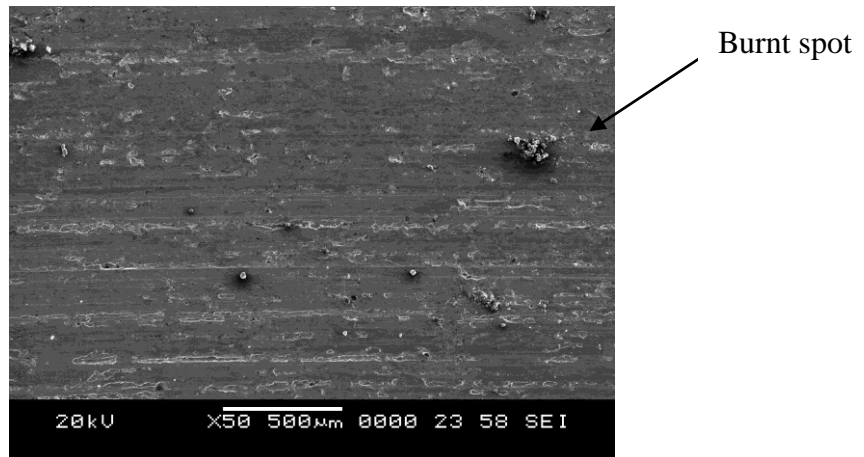


Figure 5.33 SEM micrograph at L=34.335N, S=1.5m/s, D=2000m

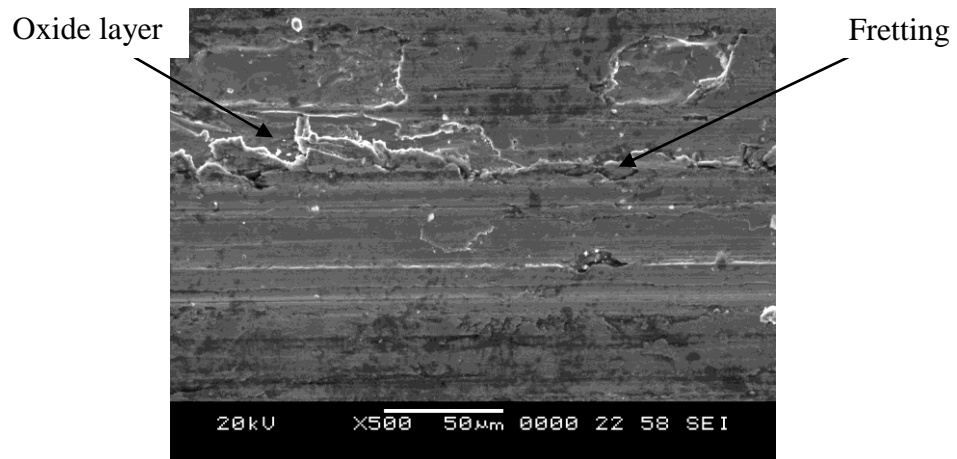


Figure 5.34 SEM micrograph at L=9.81N, S=3.5m/s, D=3000m

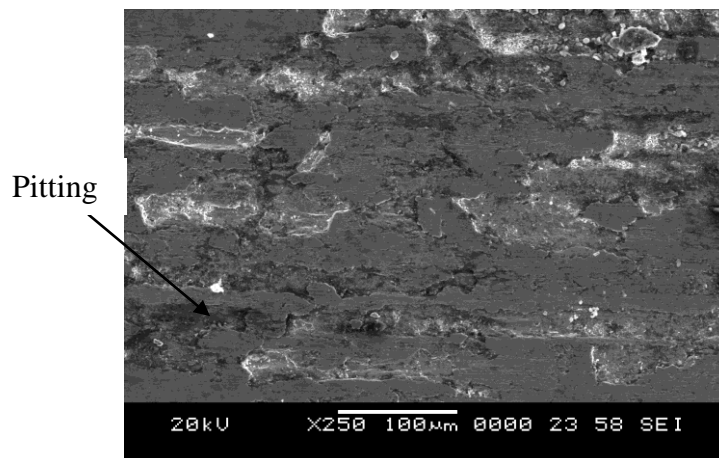


Figure 5.35 SEM micrograph at L=19.62N, S=3.5m/s, D=3000m

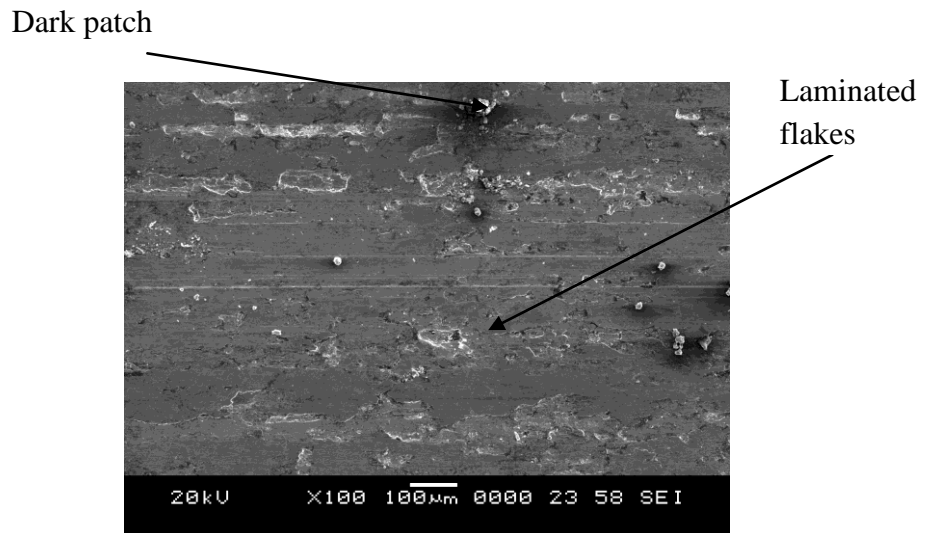


Figure 5.36 SEM micrograph at L=34.335N, S=6m/s, D=2000m

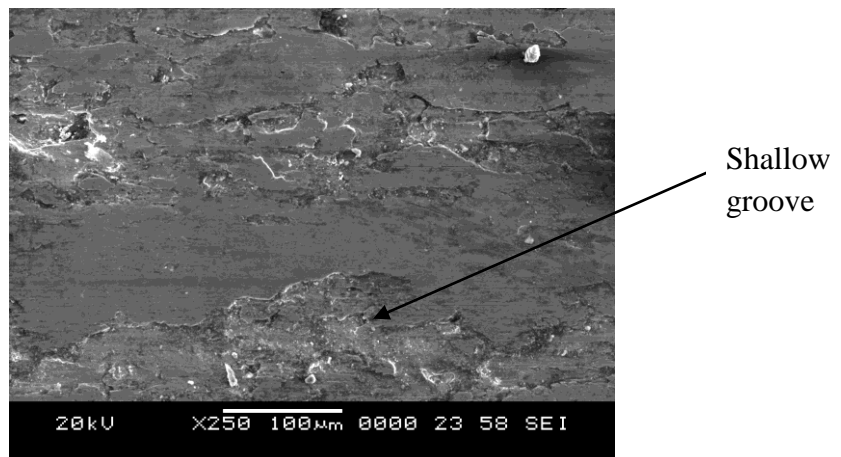


Figure 5.37 SEM micrograph at L=49.05N, S=3.5m/s, D=3000m

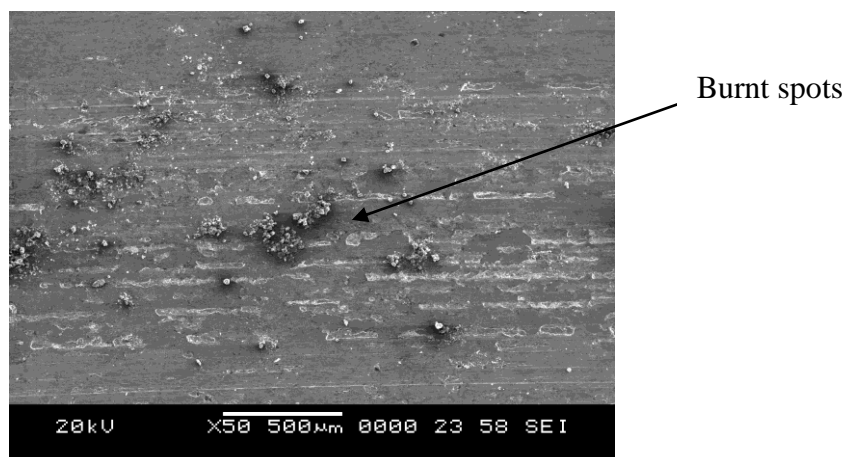


Figure 5.38 SEM micrograph at L=34.335N, S=2m/s, D=2000m

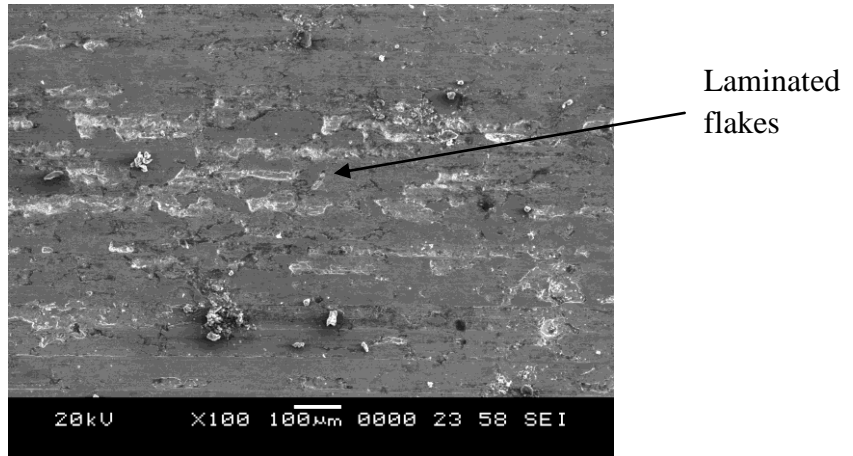


Figure 5.39 SEM micrograph at L=34.335N, S=4m/s, D=2000m

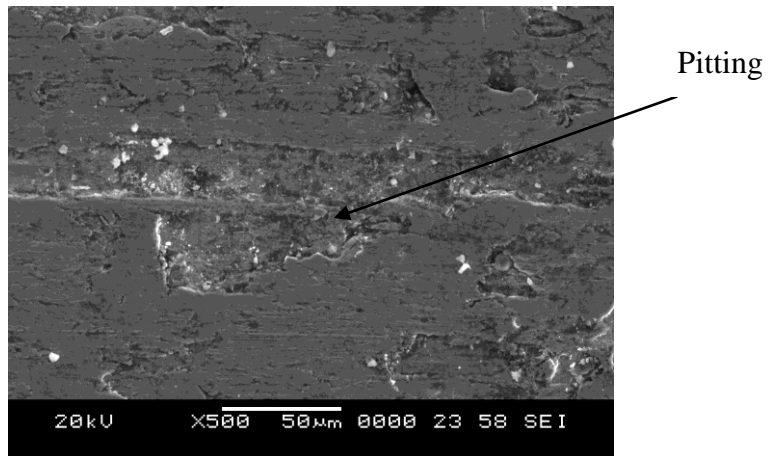


Figure 5.40 SEM micrograph at L=39.24N, S=3.5m/s, D=3000m

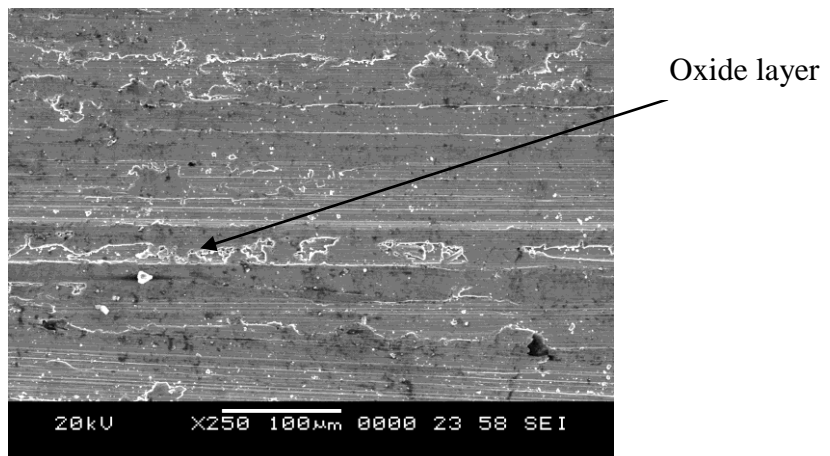
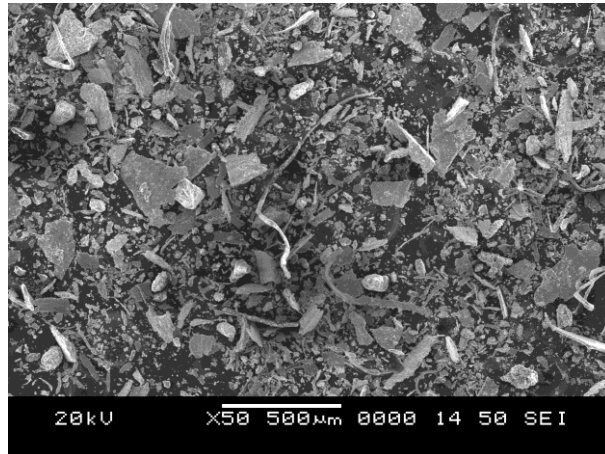
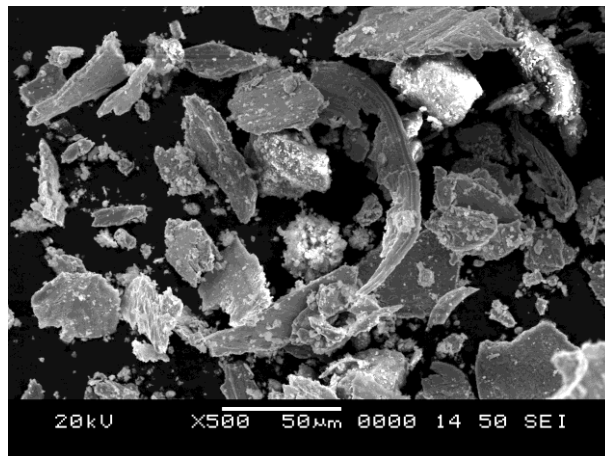


Figure 5.41 SEM micrograph at L=34.335N, S=2.5m/s, D=2000m

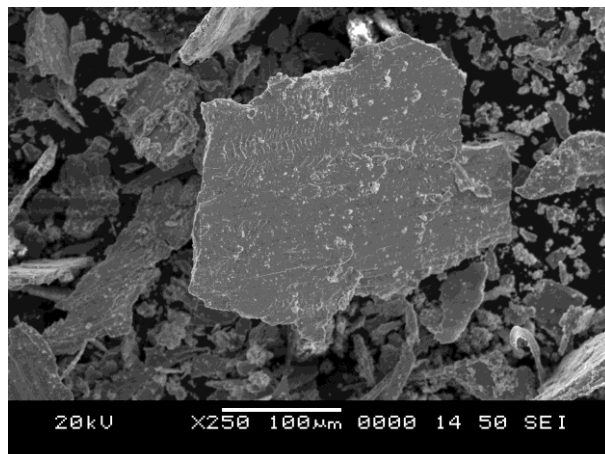
Wear Debris



(a)



(b)



(c)

Figure 5.42 (a), (b), (c) SEM micrographs of wear debris at $L=49.05\text{N}$, $S=3.5\text{m/s}$, $D=3000\text{m}$

5.1.15 Effect of Temperature on Weight Loss and COF

Weight loss as observed from experimental results increased with sliding speed and hence when expressed as a % increase in weight loss between ET and RT conditions, an increase in the % weight loss is observed for all speeds (fig. 5.43). Percentage weight loss increased from 23.33 to 98.54%.

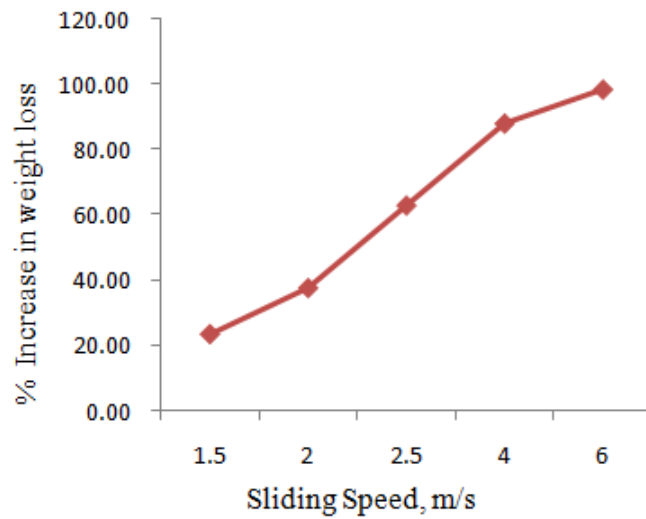


Figure 5.43 Percentage weight loss as a function of sliding speed

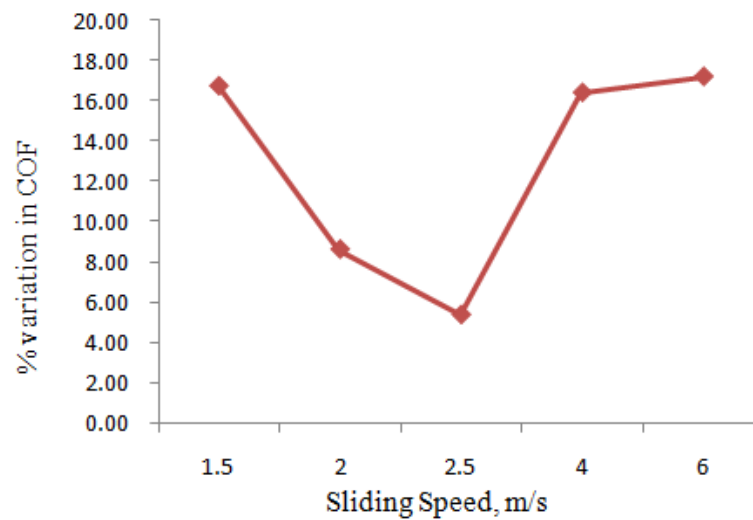


Figure 5.44 Percentage variation in COF as a function of sliding speed

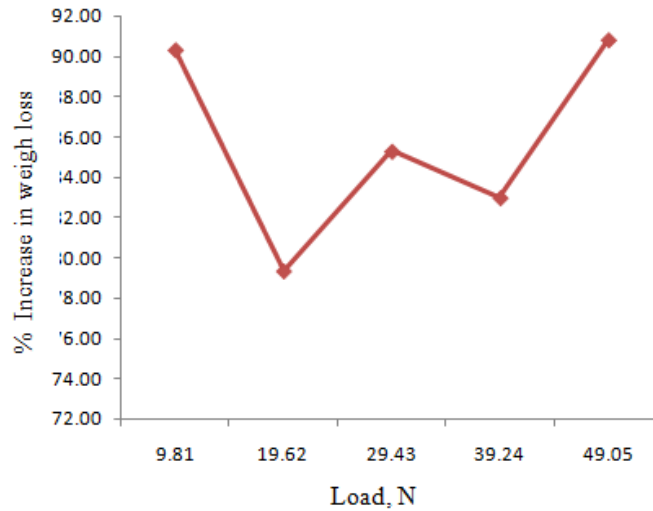


Figure 5.45 Percentage variations in weight loss as a function of load

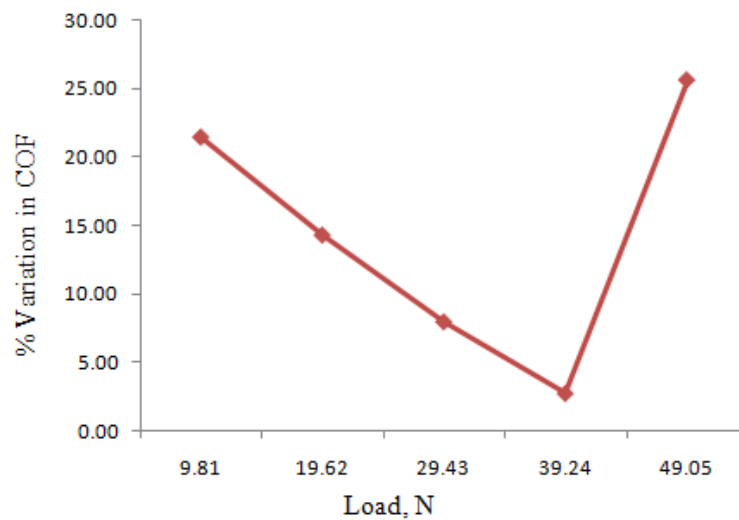


Figure 5.46 Percentage variations in COF as a function of load

However, with increase in applied load the % increase in weight loss fluctuates as observed from fig. 5.44. This value is high for lowest and highest load. The % increase in weight loss varied from 79.32% to 90.84%. As seen from fig. 5.45, % variation in COF between ET and RT conditions rise and falls for various speeds. Minimum % variation is observed for a speed of 2.5m/s. The maximum variation is for a speed of 6m/s. It varied from 5.37 to 17.21%. Fig. 5.46 depicts % COF variation as a function of load. The minimum variation is observed for a load of 39.24N and maximum for 49.05N. It varied from 2.74 to 25.59%.

Chapter 6

RESULTS AND DISCUSSION – III

OPTIMIZATION OF WEAR CONTROL PARAMETERS AT ELEVATED TEMPERATURE

6.1 Parameters and Levels

The experimental investigations were executed on ADI2 as per the plan of experiments. Based on the literature assessment three parameters namely speed, load and temperature have been chosen at three levels and are indicated in table 6.1.

Table 6.1 Parameters and their levels

Level	Load, L [N]	Sliding Speed, S [m/s]	Temperature, T [°C]
1	9.81	1.75	100
2	19.62	3.25	150
3	29.43	5.50	200

6.2 Plan of Experiments

Table 6.2 Plan of experiments

Expt. No.	Load [N]	Sliding speed [m/s]	Temperature [°C]
1	9.81	1.75	100
2	9.81	3.25	150
3	9.81	5.50	200
4	19.62	1.75	150
5	19.62	3.25	200
6	19.62	5.50	100
7	29.43	1.75	200
8	29.43	3.25	100
9	29.43	5.50	150

The experimental investigations here, made use of an L_9 orthogonal array as used in earlier analysis. DOE by means of Taguchi method was employed to generate plan of experiments and is shown in table 6.2. Statistical software MINITAB15 was applied for the analysis.

6.3. Influence of Parameters on Wear Rate

The experiments were performed as per the developed plan of experiments for a constant sliding distance of 2500m. The weight loss was computed by the difference in weights prior and after the test. It was translated into volume loss. The results and computed wear rate are tabulated in table 6.3. The wear control parameters were analysed with S/N ratio and ANOVA.

Table 6.3 Experimental results of wear rate

Expt. No.	Load [N]	Sliding speed [m/s]	Temp. [°C]	Initial weight, W_i (g)	Final weight, W_f (g)	Weight loss, W_o (g)	Wear rate, $m^3/m \times 10^{-12}$
1	9.81	1.75	100	15.9989	15.9978	0.0011	0.0062
2	9.81	3.25	150	15.6579	15.6555	0.0024	0.0135
3	9.81	5.50	200	15.8196	15.8133	0.0063	0.0355
4	19.62	1.75	150	15.8584	15.8553	0.0031	0.0175
5	19.62	3.25	200	15.4775	15.4699	0.0076	0.0428
6	19.62	5.50	100	16.3417	16.3380	0.0037	0.0208
7	29.43	1.75	200	15.5024	15.4928	0.0096	0.0541
8	29.43	3.25	100	15.4226	15.4155	0.0071	0.0400
9	29.43	5.50	150	15.6519	15.6438	0.0081	0.0456

6.3.1 S/N Ratio Analysis

Influence of control factors on wear rate was established using SNR. The factor with highest SNR provides smallest amount of wear rate [271]. SNR for wear rate is illustrated in Table 6.4.

Table 6.4 S/N ratio for wear rate

Expt. No.	Load [N]	Sliding speed [m/s]	Temperature [°C]	Wear rate [m ³ /m]x10 ⁻¹²	S/N ratio [dB]
1	9.81	1.75	100	0.0062	44.15
2	9.81	3.25	150	0.0135	37.39
3	9.81	5.50	200	0.0355	29.00
4	19.62	1.75	150	0.0175	35.14
5	19.62	3.25	200	0.0428	27.37
6	19.62	5.50	100	0.0208	33.64
7	29.43	1.75	200	0.0541	25.34
8	29.43	3.25	100	0.0400	27.96
9	29.43	5.50	150	0.0456	26.82

Response table for SNR of wear rate is appeared in Table 6.5. The distinction between the most extreme and least estimations of SNR provides delta. Reviewing of elements was done in understanding to delta esteem. The component for the record estimation of delta has the most noteworthy influence on wear rate. It is established that load has significant effect on wear rate sought after by temperature and sliding speed.

Table 6.5 Response table for S/N ratio-wear rate

Level	Load [N]	Sliding speed [m/s]	Temperature [°C]
1	36.85	34.88	35.25
2	32.05	30.91	33.12
3	26.71	29.82	27.23
Delta	10.14	5.06	8.02
Rank	1	3	2

The MEP for mean wear rate is revealed in figure 6.1. Plot infers that wear rate boosts with increment in load, speed and temperature. It is observed that speed has a direct impact on wear unlike RT conditions. As temperature rises, material turns into soft and hence additional material was removed from the pin surface. As speed

increases at ET, thermal softening becomes predominant resulting in acceleration of material removal rate. The MEP for SNR is shown in fig. 6.2.

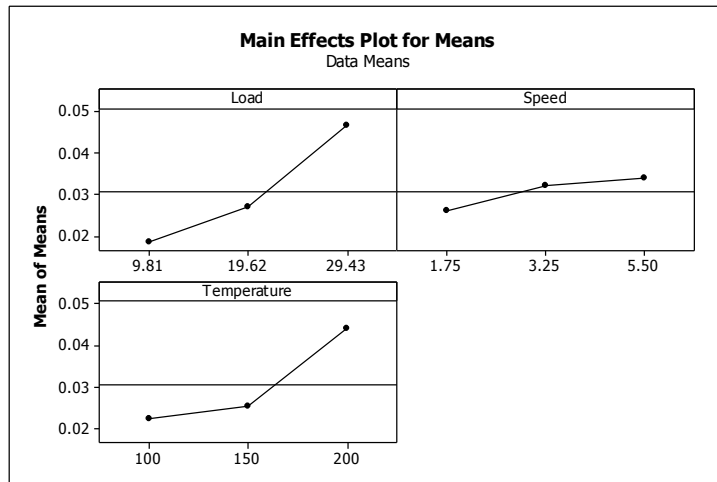


Figure 6.1 Main effects plot for means-wear rate

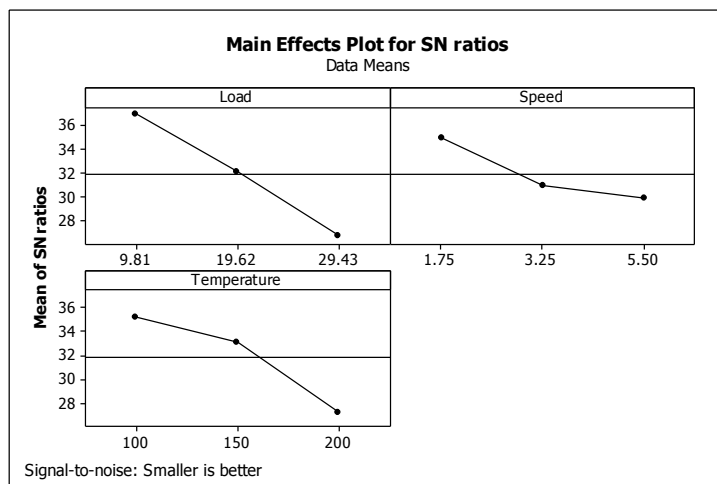


Figure 6.2 Main effects plot for S/N ratios-wear rate

Table 6.6 Optimum operating conditions for wear rate

Load, L (N)	Speed, S (m/s)	Temperature [°C]
9.81	1.75	100

Input control parameter worth with highest SNR bestows most advantageous wear rate. From analysis of test results, it is instituted that the factors combination signified in table 6.6 gave least wear rate.

6.3.2 Analysis of Variance for Wear Rate

ANOVA was exploited to analyse effect of control factors on wear rate. Analysis was done for $\alpha=0.05$.

Table 6.7 Analysis of variance for wear rate

Source	DOF	Seq. SS	Adj. SS	Adj. MS	F-test	P-value	P (%)
Load	2	154.434	154.434	77.217	22.69	0.042	50.28
Speed	2	42.511	42.511	21.256	6.25	0.138	13.83
Temperature	2	103.414	103.414	51.707	15.20	0.062	33.67
Error	2	6.805	6.805	3.403			2.22
Total	8	307.163					100

ANOVA for wear rate is shown in table 6.7. It illustrates that load (50.28%) has supreme contribution on wear rate trailed by temperature (33.67%) and speed (13.83%).

6.3.3 Regression Analysis

A regression model was developed based on the investigational outcome to render a correlation between significant factors. LRM developed for wear rate is;

$$\text{Wear rate (m}^3/\text{m)} = (-0.0373 + 0.00144 * L + 0.00204 * S + 0.000218 * T) 10^{-12} \text{-----Eqn. 6.1}$$

It is observed from equation 6.1 that coefficients related to load, speed and temperature is positive. This clearly shows that as load and temperature increase the wear rate also increases. Also as speed is incremented wear rate enhances unlike at RT. All selected factors are directly proportional to wear rate.

6.3.4 Confirmation Test

LRM was validated by conducting confirmation tests. Factors chosen for confirmation test must be dissimilar from earlier parameters utilized for analysis. Factors used in the confirmation tests are indicated in table 6.8.

Table 6.8 Parameters for confirmation test

Test no.	Load L, (N)	Sliding speed S, (m/s)	Temperature T, (°C)
1	14.715	1.5	80
2	24.525	3	120
3	34.335	4.5	160

Table 6.9 shows experimental results for the verification tests carried out. Wear rate in m^3/m is calculated as earlier.

Table 6.9 Experimental confirmation test results

Test no.	Load L, (N)	Sliding speed S, (m/s)	Temperature T, (°C)	Initial weight, W_i (g)	Final weight, W_f (g)	Weight loss, W_o (g)	Wear rate (m^3/m) $\times 10^{-12}$
1	14.715	1.5	80	15.4762	15.4754	0.0008	0.0045
2	24.525	3	120	15.6257	15.6201	0.0056	0.0315
3	34.335	4.5	160	15.7216	15.7109	0.0107	0.0603

Wear rate was also computed from LRM given by eqn. 6.1. Confirmation test outcomes and that obtained from equation are depicted in table 6.10.

Table 6.10 Confirmation wear test results and their comparison with regression model

Test no.	Experimental wear rate (m^3/m) $\times 10^{-12}$	Regression model – predicted wear rate (m^3/m) $\times 10^{-12}$	Error (%)
1	0.0045	0.0044	2.22
2	0.0315	0.0303	3.81
3	0.0603	0.0562	6.80

Error between outcomes of investigation and values achieved from regression equation is less than 7%. Hence obtained LRM from trial data is an effectual and realistic way to predict rate of wear for ADI2.

6.4 Influence of Parameters on COF

Trial results of frictional load and computed COF along with SNR is indicated in table 6.11.

Table 6.11 Experimental results of coefficient of friction

Expt. No.	Load, L [N]	Sliding Speed, S [m/s]	Temperature, T [°C]	Frictional load [N]	COF	S/N ratio [dB]
1	9.81	1.75	100	2.8	0.2854	10.89
2	9.81	3.25	150	2.6	0.2650	11.54
3	9.81	5.50	200	2.4	0.2446	12.23
4	19.62	1.75	150	6.7	0.3415	9.33
5	19.62	3.25	200	6.3	0.3211	9.87
6	19.62	5.50	100	6.2	0.3160	10.01
7	29.43	1.75	200	13.6	0.4621	6.71
8	29.43	3.25	100	14.2	0.4825	6.33
9	29.43	5.50	150	14.0	0.4757	6.45

6.4.1 S/N Ratio Analysis

Influence of key control factors on COF were obtained using SNR. Parameter for highest value of delta has greatest influence on COF. It was established that load has vital brunt on COF followed by speed and temperature.

Table 6.12 Response table for S/N ratio-COF

Level	Load [N]	Sliding Speed [m/s]	Temperature [°C]
1	11.552	8.976	9.076
2	9.735	9.244	9.107
3	6.496	9.563	9.601
Delta	5.056	0.587	0.525
Rank	1	2	3

MEP for mean COF is indicated in figure 6.3. From plot, it is conjectured that COF augments with increase in applied load. It dwindles with temperature and speed. As temperature rises, material befalls softer resulting in poorer friction. With

enhancement in speed, contact time among pin and disc shrinks, hence decreased COF. MEP for SNR is revealed in fig. 6.4. Figure 6.5 depicts disparity of frictional force with time and attained its steady state after 100 seconds.

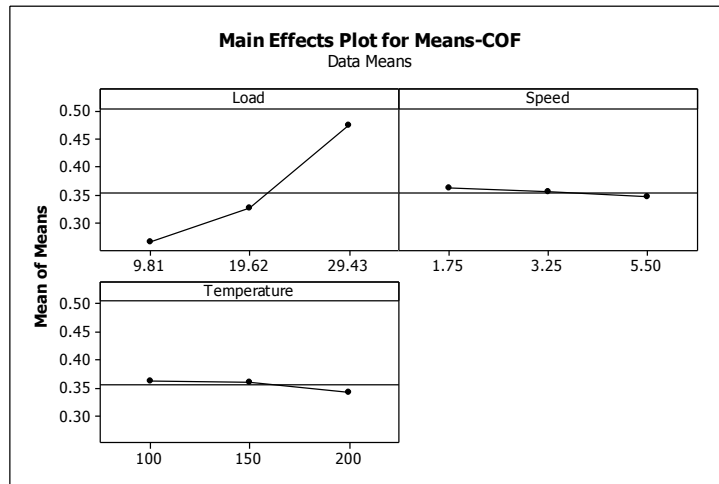


Figure 6.3 Main effects plot for means-COF

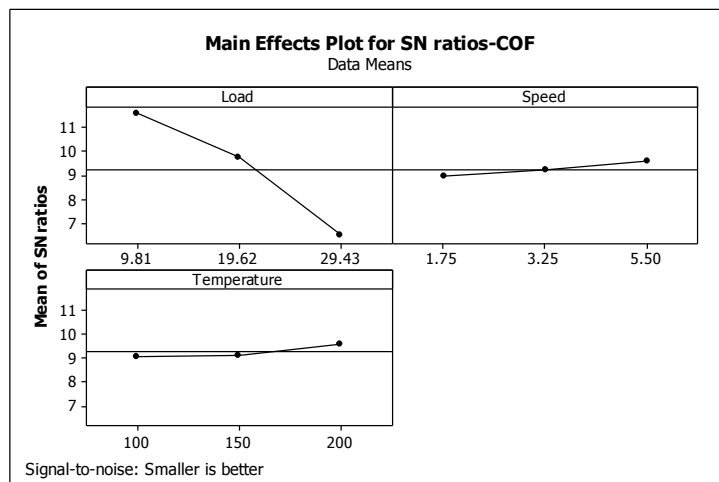


Figure 6.4 Main effects plot for S/N ratios-COF

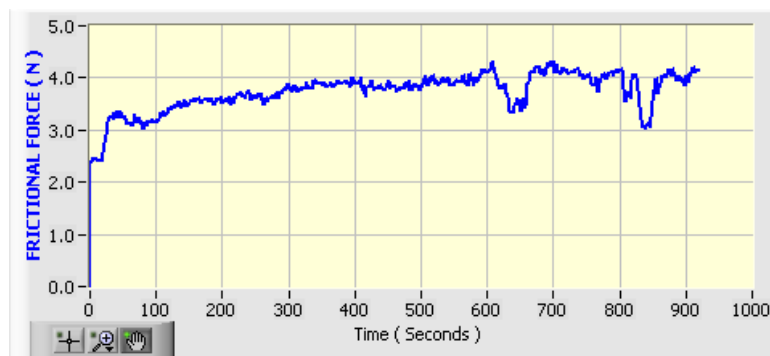


Figure 6.5 Variation of frictional force with time

6.4.2 Analysis of Variance for COF

ANOVA was exploited to analyse the consequence of parameters on COF. Analysis was executed for a significance of $\alpha=0.05$.

Table 6.13 Analysis of variance for COF

Source	DOF	Seq. SS	Adj. SS	Adj. MS	F-test	P-value	P (%)
Load	2	39.3568	39.3568	19.6784	213.24	0.005	96.98
Speed	2	0.5186	0.5186	0.2593	2.81	0.262	1.28
Temperature	2	0.5212	0.5212	0.2606	2.82	0.262	1.27
Error	2	0.1846	0.1846	0.0923			0.45
Total	8	40.5812					100

ANOVA for COF is shown in table 6.7. Last column explains that load (96.98%) has highest control on COF. Temperature and speed are less significant.

6.4.3 Regression Analysis

An LRM was obtained based on trials. This establishes a correlation between parameters under study. The LRM developed for COF is;

$$COF = 0.191 + 0.0106 * L - 0.00469 * S - 0.000187 * T \text{-----Eqn. 6.2}$$

From eqn. 6.2, it is viewed that coefficient associated with load is positive. This illustrates that COF is proportional to load. Speed and temperature have negative coefficients indicating inverse relation with COF.

6.4.4 Confirmation Test

Confirmation trials were performed to corroborate developed LRM. The factors chosen for test are indicated in table 6.8. Table 6.14 depicts investigational outcome. Eqn. 6.2 was used to work out COF. Computed and experimental COF are given in table 6.15.

Table 6.14 Confirmation test results

Test no.	Load L, (N)	Sliding speed S, (m/s)	Temperature T, (°C)	Frictional load	COF
1	14.715	1.5	80	4.7	0.3194
2	24.525	3	120	10.0	0.4077
3	34.335	4.5	160	19.1	0.5563

Table 6.15 Confirmation COF test results and their comparison with regression model

Test no.	Experimental COF	Regression model COF	Error (%)
1	0.3194	0.3313	3.59
2	0.4077	0.4271	4.54
3	0.5563	0.5229	6.00

Maximum error among two values is 6%. Hence LRM obtained from the trial information is viable and an effective approach to envisage COF of ADI2 at ET.

Chapter 7

RESULTS AND DISCUSSION – IV

WEAR BEHAVIOR OF ADI1 AND ADI2

Here a contrast of wear behavior of DI, ADI1 and ADI2 is presented by conducting dry sliding wear tests for an applied load of 29.43N, speed of 3m/s and sliding distances varying from 1000m to 5000m at RT. Table 7.1 depicts the experimental wear test results.

7.1 Effect of Sliding Distance on Wear Rate

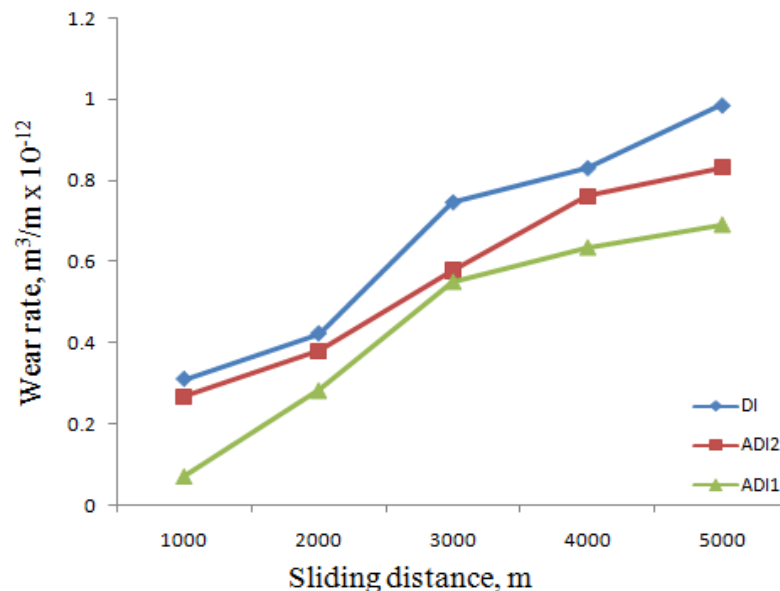


Figure 7.1 Experimental wear rates as a function of sliding distance

In figure 7.1 investigational steady state wear rates of DI, ADI1 and ADI2 are shown against sliding distance. In concord with [20] wear rates are noticed to increase with speed. It is gazed that ADI1 is more wear impervious to ADI2. At a sliding distance of 3000m both ADIs showed nearly a similar wear rate. The gap between two wear rates is greatest at 1000m and 5000m. ADI2 demonstrated linear wear rate from sliding distance 2000m to 4000m. ADI 345 illustrated practically linear wear rate from 1000m to 3000m and 3000m to 5000m.

7.2 Effect of Sliding Distance on COF

In figure 7.2, steady state COF is accounted against sliding distance. Steady state was arrived at after about 60 seconds. COF is noticed to boost for DI with sliding distance up to 4000m and descends for 5000m. COF for ADI2 is more at 1000m, drops at 2000m and then rise subsequently. There is continuous drop and augment of COF for ADI1. Figure 4 shows COF as a function of time. It indicated little variation after about 60 seconds at which point of time observations were made.

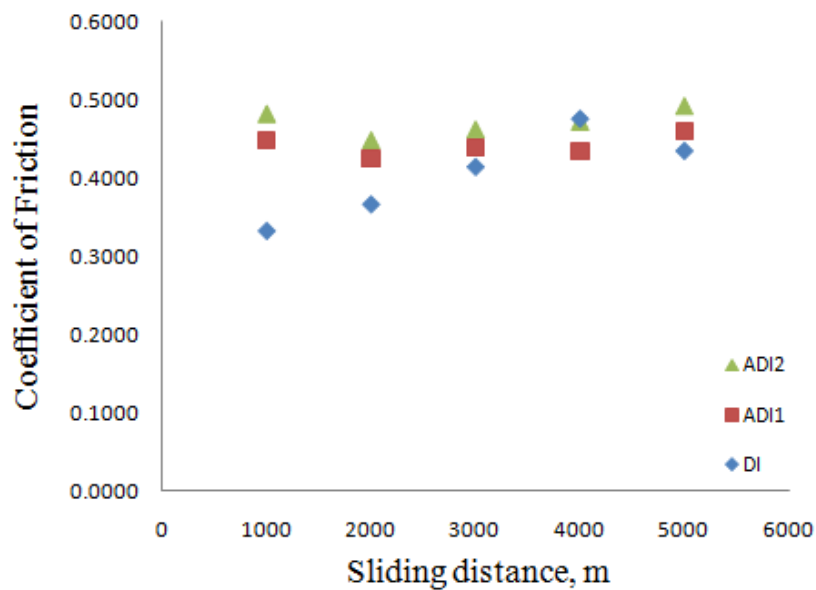


Figure 7.2 Coefficient of friction as a function of sliding distance

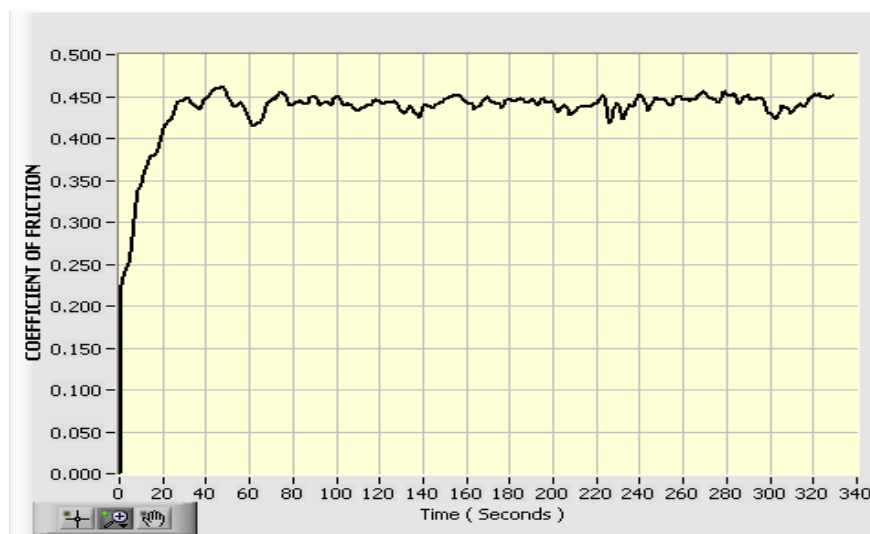


Figure 7.3 Coefficient of friction as a function of time

7.3 Effect of Wear Rate and Specific Wear Rate

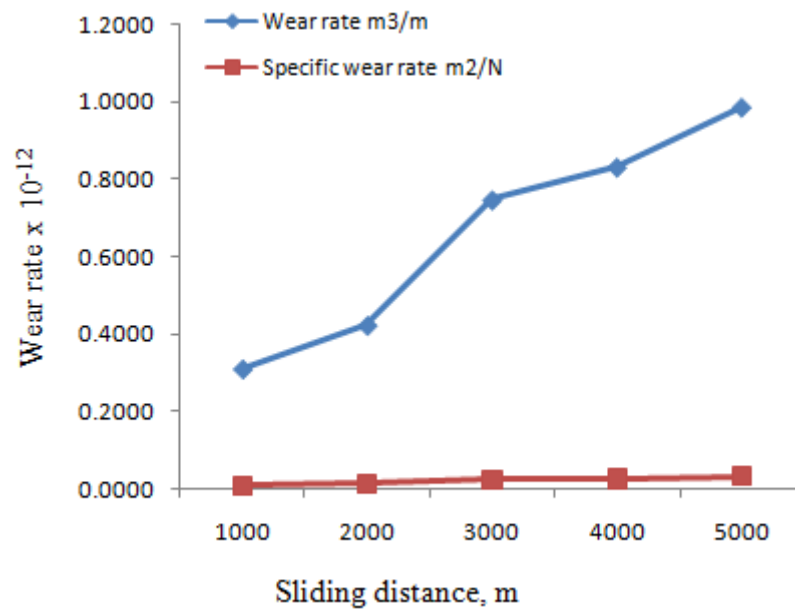


Figure 7.4 Wear rate and specific wear rate of DI

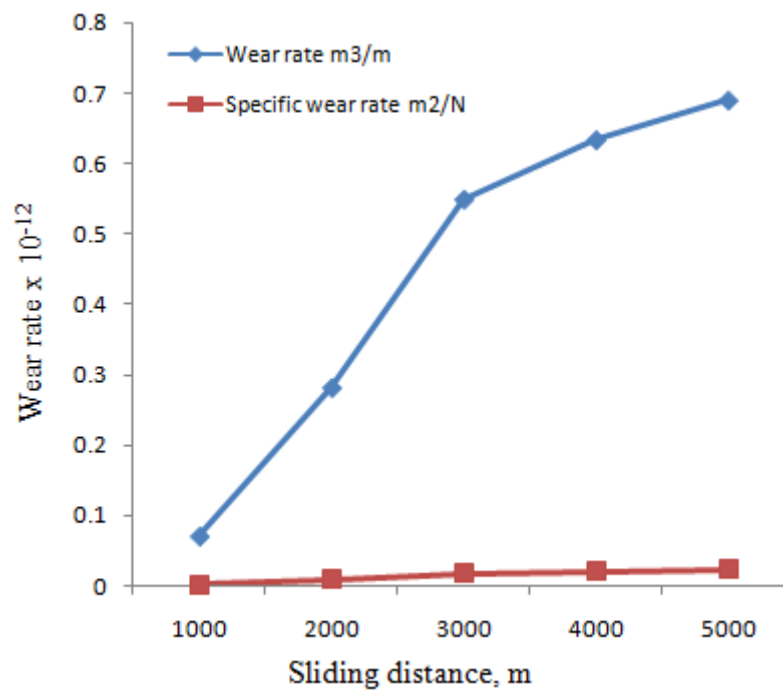


Figure 7.5 Wear rate and specific wear rate of ADI1

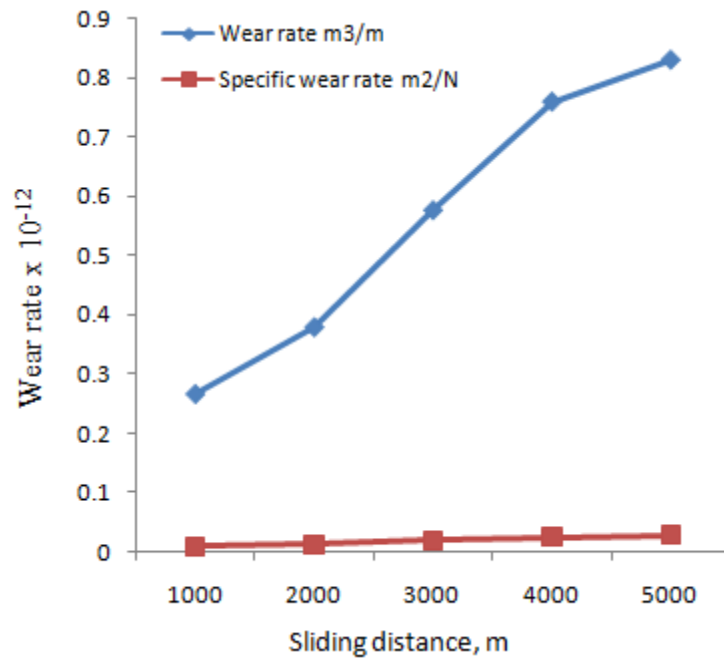


Figure 7.6 Wear rate and specific wear rate of ADI2

Figures 7.4, 7.5 and 7.6 designate the relation with sliding distance between wear rate (m^3/m) and specific wear rate (m^2/N). The gap between two is least at a sliding distance of 1000m and maximum for 5000. The specific wear rate of DI varied from 0.01053×10^{-12} to $0.03350 \times 10^{-12} \text{ m}^2/\text{N}$, ADI1 from 0.00239×10^{-12} to $0.2345 \times 10^{-12} \text{ m}^2/\text{N}$ and ADI2 from 0.00909×10^{-12} to $0.02823 \times 10^{-12} \text{ m}^2/\text{N}$.

Specific wear rate is practically linear for three materials chosen for investigation.

Table 7.1 Experimental results

Expt . No.	Material	Load , L, (N)	Speed, S, (m/s)	Speed, N (rpm)	Sliding Distance, D (m)	Time (mins.)	Initial weight, W _i (g)	Final weight, W _f (g)	Weight loss, W _o (g)	Wear rate (m ³ /m) x10 ⁻¹²	Frictional Load, (N)	Coefficient of Friction, μ	Specific wear rate m ³ /Nm x10 ⁻¹²
	(1)	(2)	(3)	(4)	(6)	(7)	(8)	(9)	(10)	(11)	(12)	(13)	(14)
1	DI	29.43	3	478	1000	5.55	16.7945	16.7923	0.0022	0.3099	9.8	0.3330	0.01053
2	DI	29.43	3	478	2000	11.11	16.7945	16.7915	0.003	0.4225	10.8	0.3760	0.01435
3	DI	29.43	3	478	3000	16.67	16.7945	16.7892	0.0053	0.7465	12.2	0.4145	0.02536
4	DI	29.43	3	478	4000	22.22	16.7945	16.7886	0.0059	0.831	14	0.4757	0.02823
5	DI	29.43	3	478	5000	27.78	16.7945	16.788	0.0065	0.9859	12.8	0.4349	0.03350
6	ADI2	29.43	3	478	1000	5.55	14.8674	14.8655	0.0019	0.2676	14.2	0.4825	0.00909
7	ADI2	29.43	3	478	2000	11.11	14.8674	14.8647	0.0027	0.3803	13.2	0.4485	0.01292
8	ADI2	29.43	3	478	3000	16.67	14.8674	14.8633	0.0041	0.5775	13.6	0.4621	0.01962
9	ADI2	29.43	3	478	4000	22.22	14.8674	14.8620	0.0054	0.7605	13.9	0.4723	0.02584
10	ADI2	29.43	3	478	5000	27.78	14.8674	14.8615	0.0059	0.8309	14.5	0.4927	0.02823
11	ADI1	29.43	3	478	1000	5.55	16.1406	16.1401	0.0005	0.0704	13.15	0.4468	0.00239
12	ADI1	29.43	3	478	2000	11.11	16.1406	16.1386	0.002	0.2817	12.5	0.4247	0.00957
13	ADI1	29.43	3	478	3000	16.67	16.1406	16.1367	0.0039	0.5493	12.9	0.4383	0.01866
14	ADI1	29.43	3	478	4000	22.22	16.1406	16.1361	0.0045	0.6338	12.75	0.4332	0.02154
15	ADI1	29.43	3	478	5000	27.78	16.1406	16.1357	0.0049	0.6901	13.5	0.4587	0.02345

Chapter 8

RESULTS AND DISCUSSION – V

PREDICTION OF WEAR BY USING ARTIFICIAL NEURAL NETWORKS

MATLAB 2011b variant was used for design, simulation and execution of networks with feed forward back propagation (FFBP) algorithm. FFBP algorithm was utilized as linear rule and mean square gaffe as execution work. In each parameter demonstrate, preparation and testing were standardized (0, 1) because of usage of hyperbolic tangent sigmoid function in the model and system.

8.1 Prediction for ADI1

The data used for the prediction is from the previous experimental results of ADI1 and is indicated in table 8.1.

Table 8.1 Experimental results of ADI1

Expt. No.	Load L (N)	Speed S (m/s)	Sliding distance D (m)	Weight loss in gms.	COF	Normalised weight loss	Normalised COF
1	19.62	1.047	1257	0.0009	0.4485	0.2083	0.6250
2	19.62	2.095	2514	0.0011	0.5556	0.2917	0.9064
3	19.62	3.142	3770	0.0004	0.3772	0.0000	0.4376
4	29.43	1.047	2514	0.0028	0.4179	1.0000	0.5445
5	29.43	2.095	3770	0.0016	0.4135	0.5000	0.5803
6	29.43	3.142	1257	0.0005	0.2107	0.0417	0.0000
7	39.24	1.047	3770	0.0017	0.4918	0.5417	0.7388
8	39.24	2.095	1257	0.0006	0.4791	0.0833	0.7054
9	39.24	3.142	2514	0.002	0.5912	0.6667	1.0000

8.1.1 Modelling for Prediction of Weight Loss

The present work incorporates ANN model with three neurons in the input layer (load, speed and sliding distance), one output neuron (weight loss) and single hidden layer with 10 neurons to predict the loss of weight by wear for a range of values of input parameters. The choice on number of neurons in shrouded layer is finished by experimentation approach. It is based on the mean square error criterion. It was noticed that the network with single hidden layer having ten neurons fits well in the proposed neural network model and is a 3-10-1 architecture (fig. 8.1). Hidden neurons made use of nonlinear tangent sigmoid activation function and output neuron used activation function. Sigmoid function is the outstanding basic actuation work in ANN as it consolidates in light of the estimation of information almost direct conduct, curvilinear conduct and about steady conduct [272, 273].

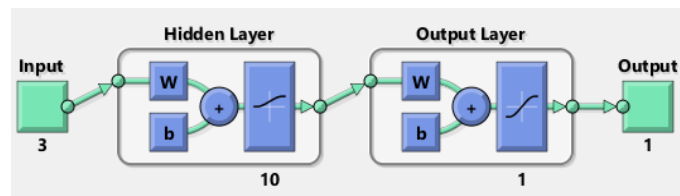


Figure 8.1 ANN model for ADI1

Here 17 networks were formed by using the above procedure. Network one with 10 neurons gave the best outcomes. Figure 8.2 depicts the performance plot and figure 8.3 the regression plot for the analysis. The normalised yield data is indicated in figure 8.4 from the output of the network performance results. The results were transformed into the weight loss back from these normalised yield data and are specified in table 8.2. From figure 8.2 best validation performance is 0.029106 at epoch 1. Plot regression (target, outputs) plots the linear regression of target relative to output. From figure 8.3 $R=0.97724$.

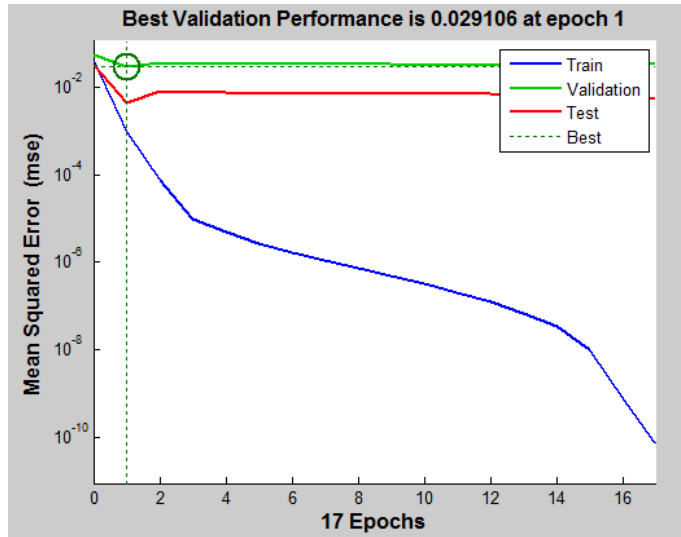


Figure 8.2 Performance plot for weight loss

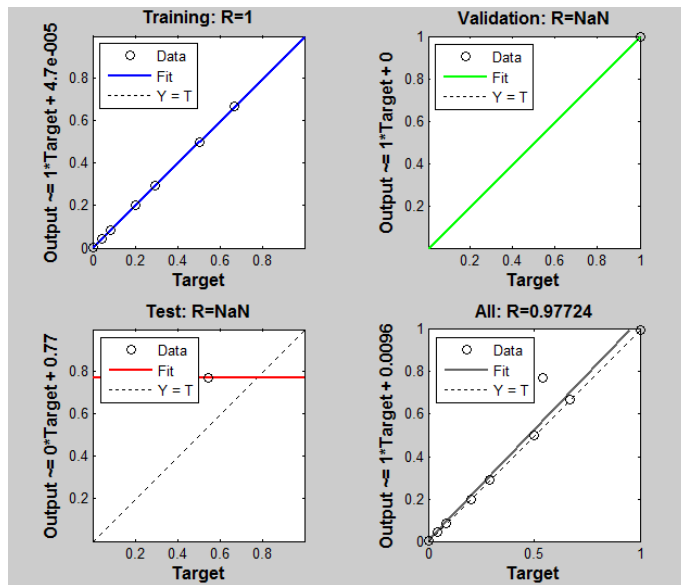


Figure 8.3 Regression plot for weight loss

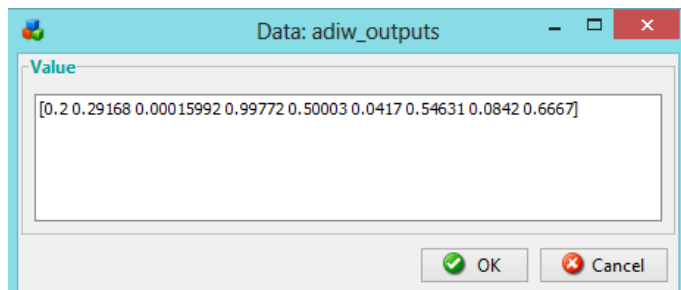


Figure 8.4 Normalised output results of weight loss from ANN

8.1.2 Modelling for Prediction of COF

Here 19 networks were produced by using the same procedure. Network one with 10 neurons gave the finest results. Figure 8.5 indicates the performance plot and figure 8.6 the regression plot for the analysis. The normalised output information is indicated in figure 8.7 from the output of the network performance results. The results were translated into COF back from the normalised output and same is indicated in table 8.2. From figure 8.6 best validation performance is 0.00056373 at epoch 1.

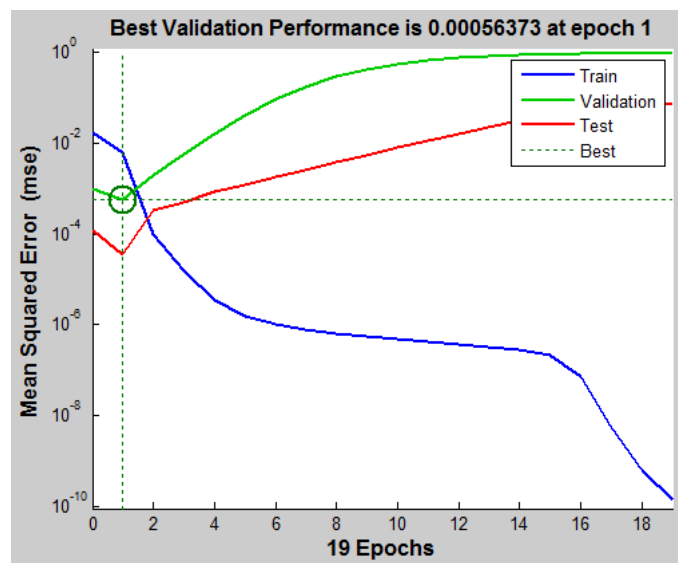


Figure 8.5 Performance plot for COF

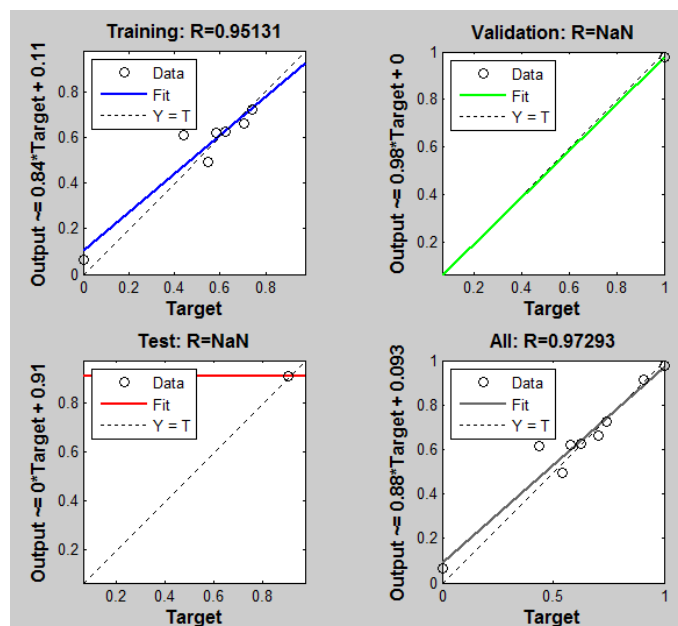


Figure 8.6 Regression plot for COF

Plot regression (target, outputs) plots the linear regression of target relative to output. From figure 4 $R=0.97293$.

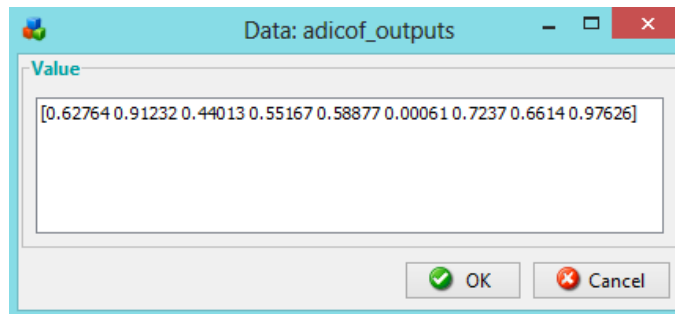


Figure 8.7 Normalised output results of COF from ANN

8.1.3 Comparison of Results

The experimental values of weight loss and COF are compared with values predicted by ANN and are indicated in table 8.2 below.

Table 8.2 Comparison of experimental and ANN values

Expt. No.	Experimental weight loss	Weight loss predicted by ANN	Experimental COF	COF predicted by ANN
1	0.0009	0.00088	0.4485	0.44952
2	0.0011	0.0011	0.5556	0.55784
3	0.0004	0.0004	0.3772	0.37817
4	0.0028	0.00279	0.4179	0.42061
5	0.0016	0.0016	0.4135	0.43473
6	0.0005	0.0005	0.2107	0.21093
7	0.0017	0.00171	0.4918	0.48584
8	0.0006	0.0006	0.4791	0.46236
9	0.002	0.002	0.5912	0.58217

A comparison of the experimental value with predicted value by ANN is represented by figures 8.8 and 8.9 for weight loss and coefficient of friction. It is detected that two results obtained are in good concord indicating ANN as the best tool in the prediction of performance results.

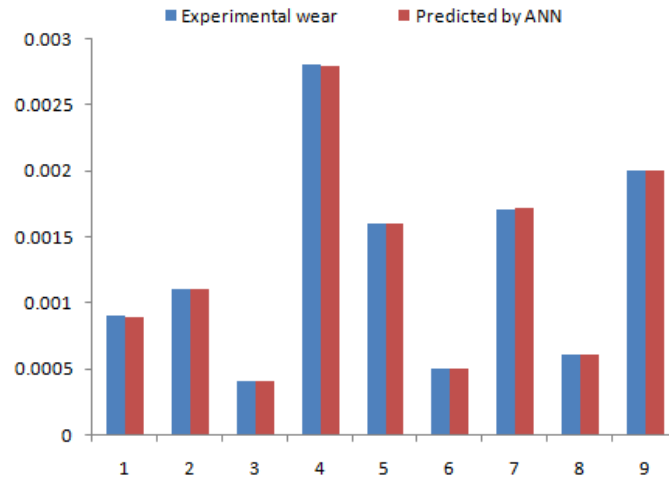


Figure 8.8 Comparison of experimental weight loss with the predicted loss

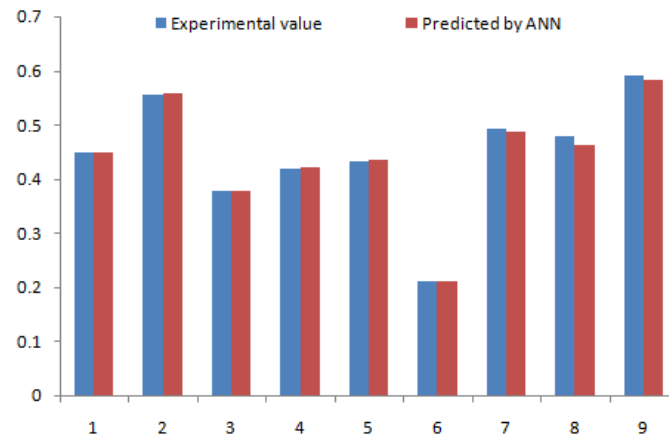


Figure 8.9 Comparison of experimental COF with predicted COF

The maximum percentage error is 2.2% for the weight loss and 3.49% for the coefficient of friction between investigational and predicted value. Reasonable agreement results were attained between the observed and predicted values.

8.2 Prediction for ADI2

The data used for the prediction is from the previous experimental results of ADI2 and is indicated in table 8.3.

Table 8.3 Experimental results of ADI2

Expt. no.	Load L (N)	Speed S (m/s)	Sliding distance, D (m)	Weight loss in gms.	COF	Normalised weight loss	Normalised COF
1	9.81	1.75	100	0.0011	0.4179	0.0000	0.7225
2	9.81	3.25	150	0.0024	0.4664	0.1529	0.9308
3	9.81	5.5	200	0.0063	0.4825	0.6118	1.0000
4	19.62	1.75	150	0.0031	0.3415	0.2353	0.3943
5	19.62	3.25	200	0.0076	0.4638	0.7647	0.9197
6	19.62	5.5	100	0.0037	0.3160	0.3059	0.2848
7	29.43	1.75	200	0.0096	0.2497	1.0000	0.0000
8	29.43	3.25	100	0.0071	0.2829	0.7059	0.1426
9	29.43	5.5	150	0.0081	0.2684	0.8235	0.0803

8.2.1 Modelling for Prediction of Weight Loss

Here ANN with three neurons in the info layer (load, speed and temperature), single shrouded layer with 10 neurons and one yield neuron (weight loss) has been developed to anticipate the loss of weight by wear for different estimations of information parameters. It was discovered that the system with single shrouded layer having ten neurons fits well in the proposed system and is a 3-10-1 architecture (fig. 8.10).

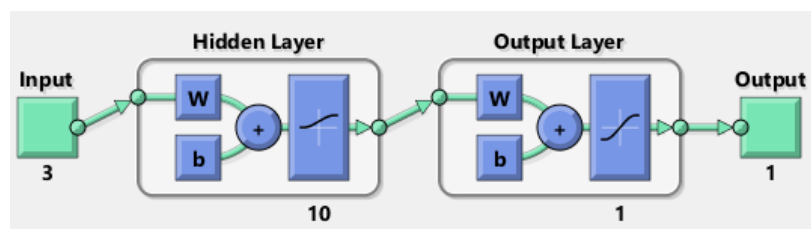


Figure 8.10 ANN model for ADI2 (weight loss)

Here 25 networks were produced by using the above procedure. Network six with 10 neurons gave the most excellent results. Figure 8.11 depicts the performance plot and figure 8.12 the regression plot for the analysis. The normalised output data from the output of the network performance results is indicated in figure 8.13. Table 8.4 indicates the translated normalized output into weight loss. From figure 8.11 best validation performance is 0.015899 at epoch 6. “Plot regression (target, outputs) plots the linear regression of target relative to output”. From figure 8.12 $R=0.97936$.

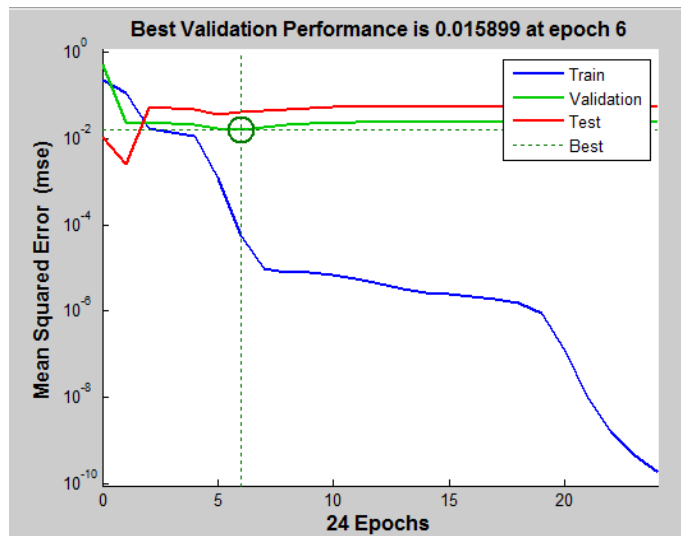


Figure 8.11 Performance plot for weight loss

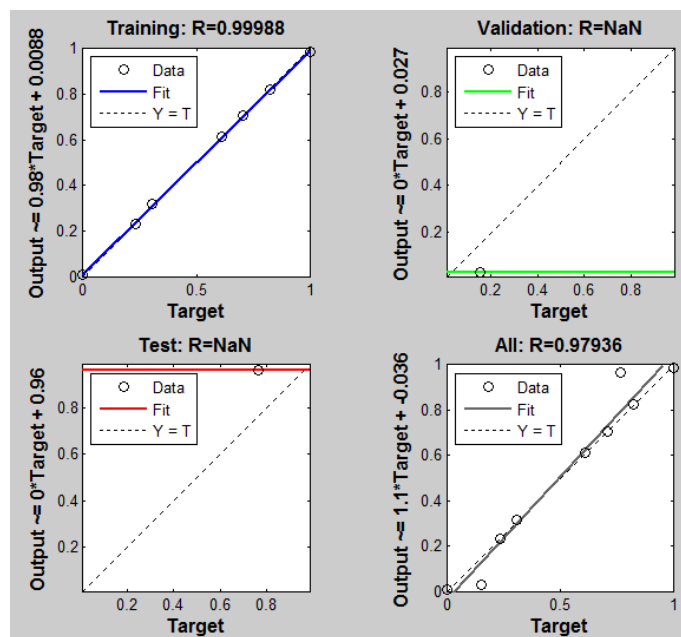


Figure 8.12 Regression plot for weight loss

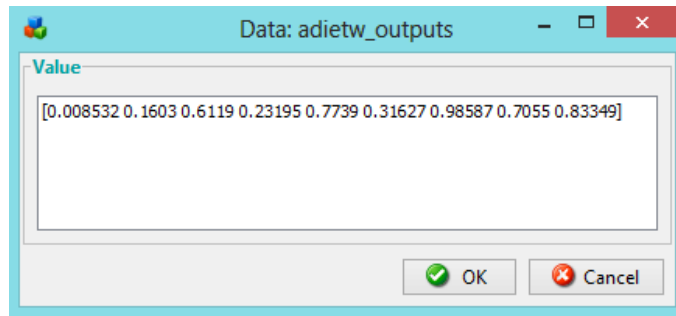


Figure 8.13 Normalised output results of weight loss from ANN

8.2.2 Modelling for Prediction of COF

It was instituted that network with single veiled layer with twelve neurons suits well in the proposed neural network model as shown in figure 8.14 and is a 3-12-1 architecture.

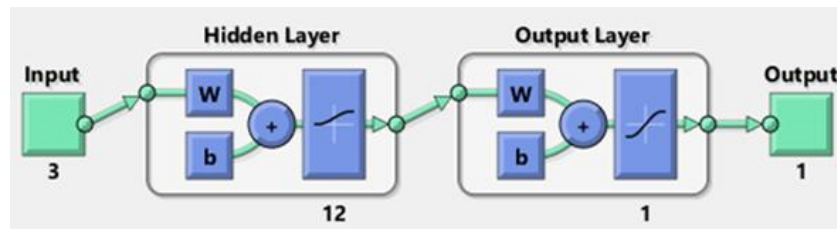


Figure 8.14 ANN model for ADI2 (COF)

Here 19 networks were made by utilizing the above strategy. Network fifteen with 12 neurons gave the best outcomes. Figure 8.15 portrays the performance plot and figure 8.16 the regression plot. Figure 8.17 shows the normalised output data from the output of the network performance outcomes. The outcomes were transformed into COF back from this normalised yield and are indicated in table 8.4. From figure 8.15 best validation performance is 0.001715 at epoch 15. “Plot regression (target, outputs) plots the linear regression of target relative to output”. From figure 8.16 $R=0.98002$.

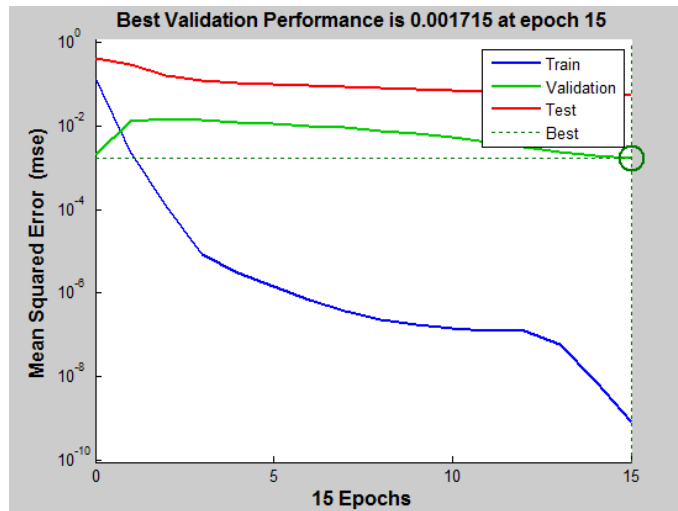


Figure 8.15 Performance plot for COF

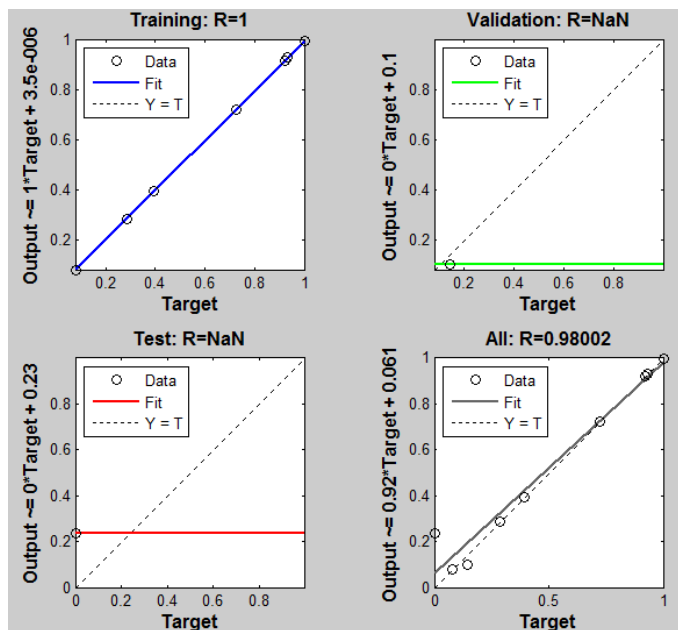


Figure 8.16 Regression plot for COF

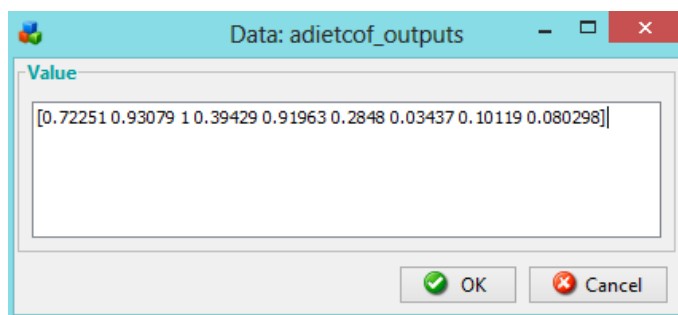


Figure 8.17 Normalised COF output results from ANN

8.2.3 Comparison of Results

ANN predicted values are represented in table 8.4. A comparison of these values is represented by figures 8.18 and 8.19 for weight loss and coefficient of friction.

Table 8.4 Comparison of experimental and ANN values

Expt. No.	Experimental weight loss	Weight loss predicted by ANN	Experimental COF	COF predicted by ANN
1	0.0011	0.00117	0.4179	0.4179
2	0.0024	0.00246	0.4664	0.4664
3	0.0063	0.00630	0.4825	0.4825
4	0.0031	0.00307	0.3415	0.3415
5	0.0076	0.00768	0.4638	0.4638
6	0.0037	0.00379	0.3160	0.3160
7	0.0096	0.00948	0.2497	0.2577
8	0.0071	0.00709	0.2829	0.2733
9	0.0081	0.00819	0.2684	0.2684

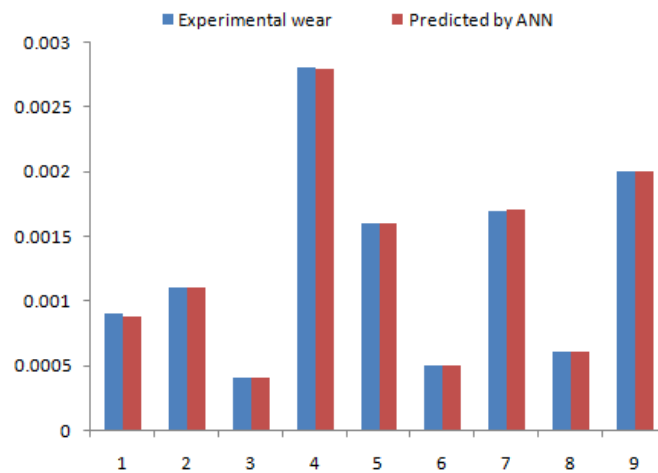


Figure 8.18 Comparison of experimental weight loss with the predicted loss

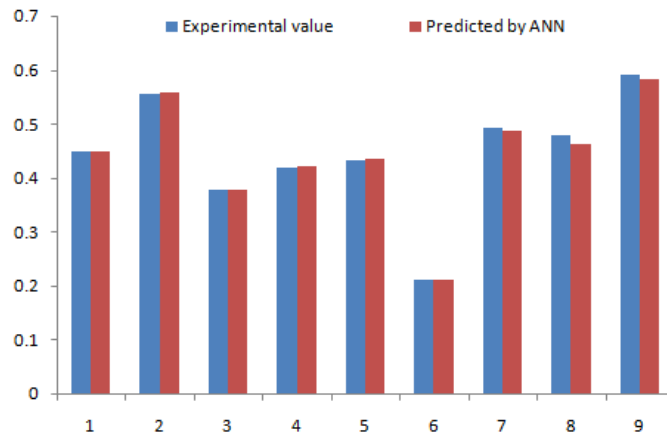


Figure 8.19 Comparison of experimental COF with predicted COF

The maximum percentage error is 5.98% for the weight loss and 3.4% for the coefficient of friction between the predicted and experiment value. It can be concluded based on the error, that ANN is the preminent contrivance for predicting the response in any given system.

Chapter 9

CONCLUSIONS AND RECOMMENDATION FOR FURTHER RESEARCH

9.1 Conclusions

The study on the dry sliding wear behavior of Austempered Ductile Iron both at room temperature and elevated temperature directed to following conclusions.

1. Two types of ADIs (ADI1 and ADI2), one solutionised for 90 minutes at 870°C, austempered at 345°C for 150 minutes and another solutionised for 120 minutes, austempered at 380°C for 180 minutes have been successfully produced.
2. The study on the wear behavior of ADI1 and DI revealed that austempering of DI increased wear resistance by nearly 85%. Taguchi method was successfully employed to attain optimum operating conditions. The operating conditions for minimum wear rate are $S=3.142\text{m/s}$, $L=19.62\text{N}$, $D=3770\text{m}$ and for minimum COF are $S=2.095\text{m/s}$, $L=29.43\text{N}$, $D=3770\text{m}$. ANOVA results show that wear rate of ADI1 is highly influenced by sliding distance (51.92%), followed by load (29.88%) and last speed (15.70%). Linear regression equations were developed to find wear rate and COF. Confirmation tests validated the developed regression models.
3. The wear rate of ADI2 declined with sliding speed due to reduction in the COF value with speed. However, wear rate increases with speed at ET operating conditions. For all speeds wear rate at ET is more than RT working conditions for the given load and time. The wear rate drastically increased for 6m/s speed from 4m/s at ET. It is subjected to severe wear at ET conditions. This makes ADI2 not suitable for ET applications.
4. The wear rate increases with load both at RT and ET due to the increase in frictional force. Its value is more at ET than RT at all loads for the chosen speed and time. The weight loss has suddenly became high at $L=49.05\text{N}$ from

L=39.24N. Since ADI2 is subjected to severe wear, it is not appropriate for ET applications.

5. The surface hardness increased slightly in a linear way at RT with speed. However, hardness decreased with speed at ET resulting in higher weight loss. The same trend is observed for varying loads. Surface and estimated flash temperatures increase with load and speed both at RT and ET. The rate of increase of heat flux is more with load than speed. The hardenability profile has a negative slope for RT and positive for ET for all speeds and loads.
6. The ADI is subjected to oxidational wear which enhances with temperature resulting in higher wear rates. The burnt spots observed at few locations on the worn out surfaces were subjected to severe plastic deformation and slivered off from the surface by adhesion. This was observed at higher speeds and loads. Work hardening effects were reduced with speed and load at ET. This prevented the possible conversion of retained austenite into martensite making the surface soft accelerating the weight loss.
7. Taguchi approach was lucratively adopted to study wear behavior of ADI2 choosing temperature as one of the control factors. The optimum operating conditions are L=9.81N, S=1.75m/s, T=100°C. The ANOVA results evidenced that, load is the most momentous factor (50.28%) followed by temperature (33.67%) and speed (13.83%). A regression model was generated and validated by confirmation tests. Temperature and load together accelerated wear rate.
8. The wear study conducted on ADI1, ADI2 and DI far varying sliding distances from 1000m to 5000m at a load of 29.43N and speed of 3m/s indicates that ADI1 is more wear resistant to ADI2. The hardness reduced with the austempering temperature. The average percentage increase in wear resistance is 28%.
9. The wear characteristics of ADI1 and ADI2 were evaluated by back propagation neural network. The well trained NN model predicted wear rate of ADI1 and in comparison with experimental values has maximum error of 2.2%. ADI2 has a maximum error of 5.89%. Hence ANN can well be used as a prophecy technique in materials characterisation and tribology.

9.2 Recommendation for Further Research

The present research work puts down extensive possibility for future investigators to explore several other facets of ADI. Some proposals for future research include:

1. In this study response of ADI2 at ET is studied. This can be further extended to study response of ADI1 at ET.
2. A comparative study can be performed on the different grades of ADI at ET working conditions.
3. Study on the alloying of ADI to make it suitable for ET applications.
4. Cost analysis and comparative study with forged steels can be performed with possible potential of replacement of existing forged steels in different applications.

REFERENCES

- [1] Eugene F. Finkin, An explanation of the wear of metals, *Wear*, 47 (1978), pp 107-117.
- [2] P. L. Hurricks, Some metallurgical factors controlling the adhesive and abrasive wear resistance of steels-a review, *Wear*, 26 (1973), pp 285-301.
- [3] Welsh N. C., *Phil. Trans. Royal Soc. London*, A257-31 (1965), 51.
- [4] Wayne S. F. and Rice S. L., *Wear*, 85 (1983), 93.
- [5] Lim S. C. and Asby M. F., *Acta. Metall.*, 35 (1987), 1.
- [6] Lim S. C., Asby M. F. and Brunton J. H., *Acta. Metall.*, 35 (1987), 1343.
- [7] Sawa M. and Rigney D. A., *Wear*, 119 (1987), 369.
- [8] Prasad B. K. and Prasad S. V., *Wear*, 151 (1991), 1.
- [9] Wang Y., Pan L. and Lei T. C., *Wear*, 143 (1991), 57.
- [10] Garnham J. E. and Beynon J. H., *Wear*, 157 (1992), 81.
- [11] Venkateshan S. and Rigney D. A., *Wear*, 153 (1992), 163.
- [12] Gupta V. K. and Pandey O. P., *Indian. J. Engg. Mater. Sci.*, 7 (2000), 354.
- [13] Tyagi R., Nath S. K. and Ray S., *Metall. Mater. Trans.*, A32 (2001), 359.
- [14] Tyagi R., Nath S. K. and Ray S., *Metall. Mater. Trans.*, A33 (2002), 3479.
- [15] Tyagi R., Nath S. K. and Ray S., *Wear*, 255 (2003), 327.
- [16] Tyagi R., Nath S. K. and Ray S., *Mater. Sci. Tech.*, 20 (2004), 645.
- [17] Mohan S., Prakash V. and Pathak J. P., *Wear*, 252 (2002), 16.
- [18] Deng S., Sun L. and Li Z., *Lubrication Engg.*, 4 (2005), 84.
- [19] Kaul R., Ganesh P., Tiwari P., Nandekar R. V. and Nath A. K., *J. Mater. Proc. Tech.*, 167 (2005), 83.
- [20] Amamoto Y. and Goto H., *Tribology International*, 39 (2006), 756.
- [21] Ceschinia L., Palombarinia G., Sambogna G., Firraob D., Scavinob G. and Ubertallib G., *Tribology International*, 39 (2006), 748.
- [22] R. G. Tikotkar, V. R. Kabadi, S. M. Ganeshari, Effect of wear rate and specific wear rate on hadfield steel, *International Journal on Mechanical & Automobile Engineering*, Volume 1, No. 1, 2008 Jan. 2009.
- [23] P. L. Hurricks, Some metallurgical factors controlling the adhesive and abrasive wear resistance of steels-a review, *Wear*, 26 (1973) 285-301.
- [24] Smith, William F., Hashemi, Javad (2006), *Foundations of materials science and engineering* (4th ed.), McGraw-Hill, ISBN 0-07-295358-6.

- [25] A. A. Zavaras, H. D. Broady, US government research announcement index, PB-126647/xab, National Centre for Manufacturing Science, 1990.
- [26] M. A. Islam, A.S.M.A. Haseeb, A.S.W. Kurny, *Wear* 188 (1995) 61– 65.
- [27] J. M. Prado, A. Pujol, J. Culler, J. Tartera, *Mater. Sci. Technol.* 11 (1995) 294–298.
- [28] ASM Handbook, Properties and selection: irons, steels and high performance alloys, vol. 1, ASM International, Materials Park, Ohio, 1990.
- [29] K. L. Hayrynen, ADI: another avenue for ductile iron foundries, *Mod. Casting* 8 (1995) 35–38.
- [30] N. S. Tiedje, Solidification, processing and properties of ductile cast iron, *Mater. Sci. Technol.* 26 (2010) 505–514.
- [31] Dorazil E., Barta B., Munsterova E., Stransky L., Huvar A. (1982) *AFS Int. Cast Metal* 7:52
- [32] Janowak J. F., Gundlach R. B. (1983) *AFS Trans.* 91:377.
- [33] Rouns T. N., Rundman K. B., Moore D. M. (1984) *AFS Trans.* 92:815.
- [34] Darwish N., Elliot R. (1993) *Mater Sci Technol* 9:882.
- [35] Moore D. J., Rouns TN, Rundman K. B. (1985) *AFS Trans.* 93:705.
- [36] Moore D. J., Rouns TN, Rundman K. B. (1987) *AFS Trans.* 95:765.
- [37] Shea M. M., Ryntz E. F. (1986) *AFS Trans.* 94:683.
- [38] Rundman K. B., Moore D. J., Hayrynen K. L., Dubensky WJ, Rouns T. N. (1988) *J. Heat treat* 5(2):79.
- [39] Bayati H., Elliot R., *Mater science technology*, (1995), 11:285
- [40] Rao P. P., *J. Engg. Mater Sci.*, (1995), 2:24
- [41] Bahmani M., Elliot R., Varahram N., *J. Mater Sci.*, (1997) 32:4783. doi:10.1023/A:1018687115732
- [42] Refaey A., Fatahalla N., *J Mater Sci.*, (2003), 38:351. doi:10.1023/A:1021177902596.
- [43] R. D. Forrest, The challenge and opportunity presented to the S.C. iron industry by the development of austempered ductile iron. *Proc. Conf. on S.G. Irons - the next 40 years*, Warwick, 1987, British Cast Iron Research Association, 24 - 1, 1987.
- [44] S. Shepperson and C. Allen, The abrasive wear behavior of austempered spheroidal cast irons, *Wear*, 121 (1988) 271 - 287.

- [45] Hua-Qin S, Qigui W, Mi Y, Xinli G, Some problems in the application of austempered ductile iron in China. In: Proc World Conf on ADI, Bloomingdale, IL, 1991, p. 388–407.
- [46] Defoirdt F. Research, development and industrial applications of ADI at ferromatrix foundries. In: Proc 3rd Int Conf on Austempered Ductile Iron, AFS, Bloomingdale, Chicago, USA, 1991, p.113–28.
- [47] Okazaki K, Asai H, Tokoyushi M, Hiroaki K, Sakahara S., Application of ADI to automotive parts. In: Proc 3rd Int. Conf. on Austempered Ductile Iron, AFS, Bloomingdale, Chicago, USA, 1991, p. 288–99.
- [48] Hatate M., Shiota T., Takahashi N., Shimizu K., Influences of graphite shapes on wear characteristics of austempered cast iron, *Wear* 2001; 251:885–9.
- [49] Zhou W.S., Zhou Q.D., Meng. S. K., Abrasion resistance of austempered ductile iron. *Cast Met* 1993;6:69–76.
- [50] Janowak J., Morton P. A., A guide to mechanical properties possible by austempering 1.5%Ni, 0.3%Mo ductile iron, *Trans. Am. Foundrymen's Soc.* 1984;92:489–98.
- [51] Blackmore P., Harding R., The effect of metallurgical variables on the properties of austempered ductile irons, *J. Heat Treating* 1984; 3(4):310–25.
- [52] Voigt R. C., Austempered ductile iron-processing and properties, *Cast Metals* 1989;2(2):71–93.
- [53] Robinson L., Tuffnell W., High cycle fatigue properties of austempered ductile iron, *Proceedings of the 1st International Conference on Austempered Ductile Irons*, Chicago Illinois. 1984. p. 39–43.
- [54] Shiokawa T., The influence of alloying elements and heat treatment condition on the microstructure and mechanical properties of austempered ductile iron. In: *Proceedings of the 3rd International Conference on ADI*, Chicago: Bloomingdale; 1991. p. 375–87.
- [55] Grech M., Bowen P., Young M., Effect of austempering temperature on the fracture toughness and tensile properties of ADI alloyed with Cu and Ni, *Proceedings of the 1st International Conference on Austempered Ductile Irons*. Chicago Illinois, 1984. p. 338–74.
- [56] Harding R. A., Opening up the market for ADI, *The Foundryman*, June 1993, 197–208.

- [57] Harding R. A., Control of the retained austenite content of ADI, In: Proceedings of the 3rd International Conference on ADI. Chicago: Bloomingdale; 1991. p. 22.
- [58] Mayr P., Vettters H., Walla J., Investigation on the stress induced martensite formation. In: Proceedings of the 2nd International Conference on ADI, Ann Arbor: University of Michigan; 1986. p. 171–8.
- [59] Vuorinen J., Strain hardening mechanisms and characteristics of austempered ductile iron, In: Proceedings of the 2nd International Conference on ADI, Ann Arbor: University of Michigan; 1986. p. 181–8.
- [60] K. L. Hayrynen, Carbide austempered ductile iron (CADI) – The New Wear Material, Transactions of AFS, V 111, paper No. 03- 088p, 845-850, 2003.
- [61] S. A. Patil, Development and wear analysis of carbide austempered ductile iron (CADI), IFJ, Vol. 58, No 8, Aug 2012.
- [62] Y. Tanaka and H. Kage, Development of austempered spheroidal graphite cast iron, Mat. Trans, JIM, vol.33, No.6, 1992.
- [63] W. Dubensky and K. B. Rundman, An electron microscope study of carbide formation in austempered ductile iron” AFS transactions vol. 93, pp 389 - 394 (1985)
- [64] T. N. Rouns and K. B. Rundman, Constitution of austempered ductile iron and the kinetics of austempering, AFS Transactions vol. 95, pp 851 - 874 (1987).
- [65] K. L. Hayrynen, The production of ADI, 2002 World Conference on ADI, pp 1– 13.
- [66] J. R. Parolini, D. J. Moore, and K. B. Rundman, On the kinetics of austempered gray iron, AFS Transactions, vol. 110 pp (2003).
- [67] Fordyce E. P., The unlubricated sliding wear behavior of austempered ductile irons, M.Sc. Engineering Thesis, Department of Materials Engineering, University of Cape Town, South Africa, 1988.
- [68] Tada M., Kurikuma T., Makimura Y., Mizuno S., Sekiguchi T., Ishikawa H., Development of high damping austempered grey cast iron, In: Proc. 3rd Int. Conf. on Austempered Ductile Iron, AFS, Bloomingdale, Chicago, USA, 1991, p. 300–7.

- [69] Riposan I., Chisamera M., Austempered compact graphite cast iron. In: Proc. 3rd Int. Conf. on Austempered Ductile Iron, AFS, Bloomingdale, Chicago, USA, 1991, p. 437–55.
- [70] Nili Ahmadabadi M., Nategh S., Davami P., Wear behavior of austempered ductile iron, *Cast Met.* 1992;4:188–93.
- [71] Sugishita J., Fujiyoshi S., The effect of cast iron graphites on friction and wear performance II: variables influencing graphite film formation, *Wear* 1981;68:7–20.
- [72] Shepperson S., Allen C., The abrasive wear behavior of austempered spheroidal cast iron, *Wear* 1988; 121: 271–87.
- [73] C. Chen, J. J. Vuorinen, M. Johanson, The stability of austenite in ADI: 2nd International ADI and Simulation Conference, Helsinki University of Technology, Finland, May 28–30, 1997.
- [74] K. L. Hayrynen, D. J. Moore, K. B. Rundman, *AFS Trans.* 98 (1992) 93–104.
- [75] A. Owhadi, J. Hedjazi, P. Davami, *Mater. Sci. Technology*, 14 (1998) 245–250.
- [76] Davenport E. S., Bain E. C., Transformation of austenite at constant sub-critical temperatures, *Trans. Am. Inst. Mining Metallurgy Engg., Iron and Steel Division* 1930:117–54.
- [77] J. K. Telford, A brief introduction to design of experiments, *Johns Hopkins Apl. Technical Digest*, 27 (2007), pp. 224-232.
- [78] M. Anderson, *Design of experiments, The Industrial Physicist*, (1997), pp. 24-26.
- [79] S. P. Kondapalli, S. R. Chalamalasetti, N. R. Damera, Application of Taguchi based design of experiments to fusion arc weld processes: a review, *International Journal of Technology & Management*, 2 (2013), pp. 1-8.
- [80] H. Guo, A. Mettas, *Design of experiments and data analysis, Annual Reliability and Maintainability Symposium*, (2010).
- [81] Roy, K. R., *A Primer on the Taguchi method*, Van Nostrand Reinhold, New York, NY, 1990.
- [82] Ross, P. J., *Taguchi technique for quality engineering*, McGraw-Hill, New York, NY, 1993.

- [83] Taguchi, G., Konishi, S., Taguchi methods orthogonal arrays and linear graphs: tools for quality engineering, American Supplier Institute, Dearborn, 1987.
- [84] Taguchi, G., Taguchi on robust technology development: bringing quality engineering upstream, ASME press, New York, N.Y., 1993.
- [85] US patent 2485760, Keith Millis, Cast ferrous alloy, issued 1949-10-25.
- [86] Higgins. R. A., Engineering metallurgy-applied physical metallurgy. London, Edward Arnold, Sixth edition 1993.
- [87] W. F. Smith, Principals of materials science and engineering, cast irons, Mc-Graw-Hill, Inc. Third Edition, 551-560.
- [88] I. C. Hughes; *BCIRA*, International Centre for Cast Metals Technology, Great Britain, 647-666.
- [89] S. I. Karsay; Ductile iron production, Quebec Iron and Titanium Corporation, Canada, (1985) 9,71,88,103-104,109,111 and 182.
- [90] I. Kay, Modern castings, (2004) 46.
- [91] S. Gowri, Understanding austempered ductile iron process, production, properties and applications – part ii, Indian Foundry Journal, Vol. 59 No. 2, February 2013.
- [92] S. Gowri and K. Hayrynen, Understanding austempered ductile iron process, production, properties and applications – part iii, Indian Foundry Journal Vol. 59, No. 3, March 2013.
- [93] Keough, J. R. and Hayrynen, K. L., Automotive applications of austempered ductile (adi): a critical review, Paper No. 2000- 01-0764, Society of Automotive Engineers, www.sae.org.
- [94] Keough, J. R., Dorn, T., Hayrynen, K. L., Popovski, V., Sumner, S. and Rimmer, A., Agricultural applications of austempered iron, metal casting design & purchasing, Sept./Oct. 2009, p. 28-31.
- [95] Lefevre, J. and Hayrynen, K., Austempered materials for power train applications, Proceedings of the 26th ASM Heat Treating Society Conference, ASM International, Oct. 2011.
- [96] Kojo Kato, Koshi Adachi, Modern tribology handbook, CRC Press LLC, 2001.
- [97] K. L. Hayrynen, D. J. Moore, and K. B. Rundman, Tensile and fatigue properties of relatively pure adi, Trans. AFS, 1992, 100, p 93–104.

- [98] T. N. Rouns, K. B. Rundman, and D. J. Moore, On the structure and mechanical properties of adi, *Trans. AFS*, 1984, 92, p 815–840.
- [99] T. S. Shih, C. S. Chang, and L. Z. Huang, Mechanical properties and microstructures of austempered ductile iron, *Trans. AFS*, 1991, 107, p 793–808.
- [100] R. B. Gundlach and J. F. Janowak, Austempered ductile iron combines strength with toughness and ductility, *Met. Prog.*, 1985, 128, p 19–26.
- [101] N. Darwish and R. Elliot, Austempering of low manganese ductile iron, part 3, variation of mechanical properties with heat-treatment conditions, *Mater. Sci. Technol.*, 1993, 9, p 882–889.
- [102] D. J. Moore, T. N. Rouns, and K. B. Rundman, The relationship between microstructure and tensile properties in austempered ductile iron, *Trans. AFS*, 1987, 95, p 765–774.
- [103] D. J. Moore, T. N. Rouns, and K. B. Rundman, Structure and mechanical properties of austempered ductile iron, *Trans. AFS*, 1985, 93, p 705– 718.
- [104] U. Batra, S. Ray, and S. R. Prabhakar, Austempering and austempered ductile iron microstructure in copper alloyed ductile iron, *J. Mater. Engg. Perform.*, 2003, 112, p 426–429.
- [105] R. Harding, Prospects for the exploitation of ADI, 2nd International conference on austempered ductile iron, March 17–19, 1986 (ASME Gear Research Institute, ANN Arbor, MI), p 39–54.
- [106] B. Kovacs, Austempered ductile iron fact and fiction, *Mod. Cast.*, March 1990, p 38–41.
- [107] Y. S. Lerner and G. R. Kingsbury, Wear resistance properties of austempered ductile iron, *J. Mater. Eng. Perform.*, 1998, 7(1), p 48–52.
- [108] M. A. Islam, A.S.M.A. Haseeb, and A. S. W. Kurmy, Study of wear of as-cast and heat-treated spheroidal cast iron under dry sliding conditions, *Wear*, 1995, 188, p 61–65.
- [109] M. N. Ahmadabadi, H. M. Ghasemi, and M. Osia, Effects of successive austempering on tribological behavior of ductile cast iron, *Wear*, 1999, 231, p 293–300.
- [110] J. Vuorinen, Strain hardening mechanisms and characteristics of austempered ductile iron, *Proceedings of the 2nd International Conference on Austempered Ductile Iron* (University of Michigan, Ann Arbor, MI, USA), 1986, p 181-188.

- [111] R. B. Gundlach, J. F. Janowak, Proceedings of 2nd International Conference on Austempered Ductile Iron, ASME (Gear Research Institute, Ann Arbor, MI, USA), 1986, p23.
- [112] J. M. Velez, D. K. Tanaka, A. Sinatora, and A.P. Tschiptschin, Evaluation of abrasive wear of ductile cast iron in a single pass pendulum device, *Wear*, 2001, 251, p 1315–1319.
- [113] S. Mohan, V. Parkash, and J. P. Pathak, Wear characteristics of hsla steel, *Wear*, 2002, 252, p 16–25.
- [114] S. Daber, K. S. Ravishankar, and P. P. Rao, Influence of austenitising temperature on the formation of strain induced martensite in austempered ductile iron, *J. Mater. Sci.*, 2008, 43(14), p 4929-4937.
- [115] S. Daber and P. P. Rao, Formation of strain-induced martensite in austempered ductile iron, *J. Mater. Sci.*, 2008, 43(1), p 357–367.
- [116] R. C. Voigt, C. R. Loper, Austempered ductile iron-process control and quality assurance, *Journal of Heat Treating* 3 (1984)291–309.
- [117] J. Race, L. Stott, Practical experience in the austempering of ductile iron, *Heat Treatment of Metals*4(1991)105–109.
- [118] J. Zimba, M. Samandi, D. Yu, T. Chandra, E. Navara, D. J. Simbi, Un-lubricated sliding wear performance of unalloyed austempered ductile iron under high contact stresses, *Materials and Design* 25 (2004) 431–438.
- [119] G. Straffelini, M. Pellizzari, L. Maines, Effect of sliding speed and contact pressure on the oxidative wear of austempered ductile iron, *Wear*, 270(2011) 714–719.
- [120] T. Nasir, D. O. Northwood, J. Han, Q. Zou, G. Barber, X. Sun, P. Seaton, Heat treatment-microstructure-mechanical/tribological property relationships in austempered ductile iron, in: *Surface Effects and Contacts Mechanics X*, 2011.
- [121] B. Bosnjak, B. Verlinden, B. Radulovic, Dry sliding wear of low alloyed austempered ductile iron, *Materials Science and Technology* 19(7)(2003) 650–656.
- [122] S. C. Lim, M. F. Ashby, Wear-mechanism maps, *Acta Metallurgica* 35 (1987) 1–24.
- [123] Y. H. Tan, S. I. Yu, J. L. Doong, J. R. Wang, Abrasive wear property of bainitic nodular cast iron in laser processing, *Journal of Materials Science* 25(1990) 4133–4139.

- [124] G. X. Lu, H. Zhang, The structure and sliding-contact wear resistance of a laser-hardened austempered ductile iron, *Wear* 138(1990)1–12.
- [125] L. Xue, M. U. Islam, G. McGregor, Dotmatrix hardening of steels using a fibre optic coupled pulsed Nd:YA Glaser, *Materials and Manufacturing Processes* 14 (1999)53–651999.
- [126] V. Schulze, *Proceedings of the 8th International Conference on Shot Peening*, Garmisch-Partenkirchen, Wiley, Germany, 2002.
- [127] H. Ohba, S., Matsuyama, T. Yamamoto, Effect of shot peening treatment on rolling contact fatigue properties of austempered ductile iron, *Tribology Transactions* 45 (2012) 576–582.
- [128] J. W. Ho, C. Noyan, J. B. Cohen, V. D. Khanna, Z. Eliezer, Residual stresses and sliding wear, *Wear* 84(1983)183–202.
- [129] N. M. Vaxevanidis, D. E. Manolakos, A. Koutsomichalis, G. Petropoulos, A. Panagotas, I. Sideris, A. Mourlas, S. S. Antoniou, The effect of shotpeening on surface integrity and tribological behavior of tool steels in AITC-AIT, Parma, Italy, 2006.
- [130] A. Zammit, M. Mhaede, M. Grech, S. Abela, L. Wagner, Influence of shot peening on the fatigue life of Cu–Ni austempered ductile iron, *Materials Science and Engineering A* 545, pp.78–85.
- [131] V. Schulze, *Modern mechanical surface treatment*, WILEY-VCH, 2006.
- [132] Y. Ochi, K. Masaki, T. Matsumura, T. Sekino, Effect of shot-peening treatment on high cycle fatigue property of ductile cast iron, *International Journal of Fatigue* 23(2001)441–448.
- [133] A. Ebenau, D. Lohe, O. Vohringer, E. Macherauch, Influence of shot peening on the microstructure and the bending fatigue strength of bainitic-austenitic nodular cast iron, in: *ICSP-4*, 1990, pp.389–398.
- [134] M. H. Mhaede, K. M. Ibrahim, M. Wollmann, L. Wagner, Enhancing fatigue performance of ductile iron by austempering and mechanical surface treatments, in: *Arabcast 2008*, 2008.
- [135] A. Owahdi, J. Hedjazi, P. Davami, Wear behavior of 1.5Mn austempered ductile iron, *Mater. Sci. Technol.* 14 (1998) 245–250.
- [136] Y. Sahin, O. Durak, Abrasive wear behavior of austempered ductile iron, *Materials and Design* 28 (2007) 1844–1850.

- [137] G. X. Lu, H. Zhang, Sliding wear characteristics of austempered ductile iron with and without laser hardening, *Wear*, 138 (1990) 1–12.
- [138] M. J. Perez, M. M. Cisneros, H F. Lopez, Wear resistance of Cu–Ni–Mo austempered ductile iron, *Wear*, 260 (2006) 879–885.
- [139] Y. Sahin, M. Erdogan, V. Kilicli, Wear behavior of austempered ductile irons with dual matrix structures, *Materials Science and Engineering A* 444 (2007) 31–38.
- [140] K.H. Zum Gahr, *Microstructure and wear of materials*, Elsevier, Amsterdam, 1987.
- [141] J. Sugisghita, S. Fujiyoshi, The effect of cast graphite on friction and wear performance III: the lubricating effect of graphite under rolling-sliding conditions, *Wear* 77 (1982) 181–193.
- [142] N. Darwish, R. Elliott, Austempering of low manganese ductile iron, part I processing window, *Mater. Sci. Technol.* 9 (1993) 572–585.
- [143] S. Daber, P. P. Rao, Formation of stress-induced martensite in austempered ductile iron, *J. Mater. Sci.* 43 (2008) 357–367.
- [144] A. Owahdi, J. Hedjazi, P. Davami, Wear behavior of 1.5Mn asutempered ductile iron, *Mater. Sci. Technol.* 14 (1998) 245–250.
- [145] G. X. Lu, H. Zhang, Sliding wear characteristics of austempered ductile iron with and without laser hardening, *Wear* 138 (1990) 1–12.
- [146] A.S.M.A. Haseeb, Md. Aminul Islam, Md. Mohar Ali Bepari, Tribological behavior of quenched and tempered, and austempered ductile iron at the same hardness level, *Wear* 244 (2000) 15–19.
- [147] M. J. Perez, M. M. Cisneros, H. F. Lopez, Wear resistance of Cu–Ni–Mo austempered ductile iron, *Wear*, 260 (2006) 879–885.
- [148] U. R. Kumari, P. P. Rao, Study of wear behavior of austempered ductile iron, *J. Mater. Sci.* 44 (2009) 1082–1093.
- [149] T. F. J. Quinn, J. L. Sullivan, D. M. Rowson, Origins an development of oxidational wear at low ambient temperatures, *Wear* 94 (1984) 175–191.
- [150] F. H. Stott, The role of oxidation in the wear of metals, *Tribology Int.* 31 (1998) 61–71.
- [151] G. Straffelini, D. Trabucco, A. Molinari, Oxidative wear of heat-treated steels, *Wear*, 250 (2001) 485–491.

- [152] G. W. Stachowiak, A.W. Batchelor, *Engineering Tribology*, Tribology series 24, Elsevier, Amsterdam, 1993.
- [153] H. So, The mechanism of oxidational wear, *Wear*, 184 (1995) 161–167.
- [154] S. C. Lim, M. F. Ashby, Wear mechanism maps, *Acta Mater.* 35 (1987) 1–24.
- [155] S. Wilson, A. T. Alpas, Wear mechanism maps for metal matrix composites, *Wear* 212 (1997) 41–49.
- [156] C. Allen, E. P. Fordyce, The dry sliding wear behavior of an austempered spheroidal cast iron, *Wear*, 135 (1990) 265–278.
- [157] A. R. Riahi, A. T. Alpas, Wear map for grey cast iron, *Wear* 255 (2003) 401–409.
- [158] Masud L., Martinez R., Simison S., Boeri R. (2003) *J Mater Sci.* 38:2971. doi: 10.1023/A:1024425727963.
- [159] Li D., Zhou Z., Sun D., (2004) *J Mater Sci* 39:7119. doi:10.1023/B:JMISC.0000047563.46550.e6.
- [160] Lin C., Yang C., Wang J., (2003) *J Mater Sci.* 38:1667. doi:10.1023/A:1023211323116.
- [161] Gundalach R. B., Janowak J. F., (1985) *Metal Prog.* 128(2):19.
- [162] Gundalach R. B., Janowak J. F. (1984) Amax Materials Research Center Report No. X G 184-02.
- [163] Harding R. A., Gillbert G. N. J., (1986) *British Foundryman*, IBF, Conference paper, BFS 79, p 489.
- [164] Schmidt I., (1984) *Z. Metallkd* 75:747.
- [165] Shah S. M., Verhoeven J. D. (1986) *Wear*, 113:267.
- [166] Schmidt I., Schuchert A. (1987) *Z. Metallkd* 78:871.
- [167] Bartosiewicz L., Krause A.R., Alberts F.A., Singh I., Putatunda S.K., (1993) *Mater Charact.* 30:221.
- [168] Shanmugam P., Rao P. P., Udupa K. R., Venkataraman N., (1994) *J Mater Sci.* 29:4933. doi:10.1007/BF00356546.
- [169] Bahmani M., Elliot R., Varahram N., (1997) *J Mater Sci.* 32:5383. doi:10.1023/A:1018631314765.
- [170] Lin C., Chang C., (2002) *J Mater Sci.* 37:709. doi:10.1023/A:1013827511859.
- [171] Jayamathy M., Vasanth R., (2003) *SAE Trans.* 112 (3): 2066.

- [172] Yasutoune A., Ryohei I., Yoji M., Masahito G., (2004) JSME Symposium on Motion and Power Transmissions, p 138.
- [173] Brezina R., Filipek J., Senberger J., (2008) Res Agr Eng 50:75.
- [174] Rimmer A., (2006) Foundry Trade J 180:58.
- [175] Prado J. M., Pujol A., Cullel J., Tartera J., (1995) Mater Sci. Technol. 11:294.
- [176] Owhadi A., Hedjazi J., Davami P., (1998) Mater Sci. Technol. 14:245.
- [177] Ahmadabadi M. N., Nategh S., Davami P., (1992) J Cast Metals 4:188.
- [178] Shepperson S., Allen C., (1988) Wear 121:271.
- [179] Vuorinen J., (1986) In: Proceedings of 2nd International conference on austempered ductile iron, Ann Arbor, MI, USA, p 179.
- [180] Gundalach RB, Janowak JF (1986) In: Proceedings of 2nd international conference on austempered ductile iron, Ann Arbor, MI, USA, p 23.
- [181] Gundalach R. B., Janowak J. F., (1987) Wear 11:171.
- [182] Zum-Gahr K. H. (1979) Metal Prog. 116(4):46
- [183] Velez J. M., (2001) Wear, 251:1315.
- [184] Mohan S., Prakash V., Pathak J. P., (2002) Wear, 252:16
- [185] Zhou WS, Zhou QD, Meng SK (1993) Wear 162–164:696
- [186] Daber S., Rao P.P. (2008) J. Mater Sci. 43:357. doi:10.1007/s10853- 007-2258-6
- [187] Daber S., Ravishankar K. S, Rao P. P. (2008) J. Mater Sci. 43:4929. doi: 10.1007/s10853-008-2717-8.
- [188] Boutorabi S. M. A., Young J. M., Kondic V., (1993) Wear, 175:19.
- [189] Ahmadabadi M. N., Ghasemi H. M., Osia M., (1999) Wear, 231:293.
- [190] M. Grech, J. M. Young, AFS Trans. 98 (1990) 341–352.
- [191] D. J. Moore, T. N. Rouns, K. B. Rundman, AFS Trans. 103 (1985) 705–712.
- [192] Trudel, M. Gagne, Can. Metall. Q. 36 (1997) 289–298.
- [193] S. Yazdani, R. Elliot, Mater. Sci. Technol. 15 (1999) 531–540.
- [194] W. Zhao, G. Wang, J. Mater. Proc. Technol. 95 (1999) 27–29.
- [195] M. Bahmani, R. Elliot, N. Varahram, J. Mater. Sci. 32 (1997) 4783–4791.
- [196] J. Mallia, M. Grech, R. E. Smallman, Mater. Sci. Technol. 14 (1998) 452–460.
- [197] S. K. Putatunda, Mater. Man Proc. 16 (2001) 245–263.
- [198] H. Bayati, R. Elliot, G. W. Lorimer, Mater. Sci. Technol. 11 (1995) 776–786.

- [199] ASM Metals Handbook, Heat Treating, vol. 4, Metals Park, Ohio, 1991, p. 683.
- [200] H. Sin, N. Saka, N. P. Suh, *Wear*, 55 (1979) 163–190.
- [201] S. Jacobson, P. Wallen, S. Hogmark, *Wear*, 123 (1988) 207–223.
- [202] Hughes I.C.H, *Austempered Ductile Irons - Their Properties & Significance, Materials & Design, Vol-6, No-3, 1985, 124-126.*
- [203] Z. Gahr, *Tribology Int.* 31 (10) (1998) 587–596.
- [204] N. Rebaso, R. Dommarco, J. Sikora, *Wear*, 253 (2002) 855–861.
- [205] M .A. Moore, R. M. Douthwaite, *Metall. Trans.*, 7A (1976) 1833– 1837.
- [206] Zhou W. S., Zhou QD, Meng S. K., Lubricated sliding and rolling wear of austempered ductile iron, *Wear* 1993;162–164:696–702.
- [207] Johansson M., *Austenitic–bainitic ductile iron, AFS Trans.*, 1977; 85:117–22.
- [208] Ball A., Allen C., Prothoreo B., The abrasive–corrosive wear of stainless steels. *Wear* 1981; 74:287–305.
- [209] Zimba J., Transformation kinetics during the austempering of ductile iron and practical implications, D.Phil. Thesis, Department of Metallurgical Engineering, University of Zimbabwe, 2002.
- [210] W. C. Weng, F. Yang, A. Z. Elsherbeni, *Electromagnetics and antenna optimization using Taguchi's method, Morgan & Claypool Publisher Series, USA (2007).*
- [211] A. Arunkumar, T. Prabakaran, Optimization of cutting parameters in machining of polyphenylene sulphide composites, *International Journal of Innovative Research in Science, Engineering and Technology*, 3 (2014), pp. 1082-1086.
- [212] M. P. Jenarathanan, R. Jeyapaul, Optimisation of machining parameters on milling of gfrp composites by desirability function analysis using Taguchi method, *International Journal of Engineering, Science and Technology*, 5 (2013), pp. 23-26.
- [213] K. Palanikumar, L. Karunamoorthy, R. Karthikeyan, B. Latha, Optimization of machining parameters in turning gfrp composites using a carbide (k10) tool based on the Taguchi method with fuzzy logics, *Metals and Materials International*, 12 (2006), pp. 483-491.

- [214] G. D. Babu, K. S. Babu, B. U. M. Gowda, Optimization of machining parameters in drilling hemp fibre reinforced composites to maximize tensile strength using design experiments, *Indian Journal of Engineering & Material Sciences*, 20 (2013), pp. 385-390.
- [215] S. A. Hussain, V. Pandurangadu, K. P. Kumar, Optimization of surface roughness in turning of gfrp composites using genetic algorithm, *International Journal of Engineering, Science and Technology*, 6 (2014), pp. 49-57.
- [216] P. Maheswaran, C. J. T. Renald, Investigation on wear behavior of al6061-al2o3-graphite hybrid metal matrixb composites using artificial neural network, *International Journal of Current Engineering and Technology*, DOI:dx.Doi.Org/10.14741/Ijcet/Spl.2.2014.66.
- [217] S. Sathiyamurthy, A. S. A. Thaheer, S. Jayabal, Prediction and optimization of mechanical properties of particles filled coir-polyester using ANN and RSM algorithms, *Indian Journal of Fiber & Textile Research*, 38 (2013), pp. 81-86.
- [218] Y. Xu, T. You, Minimizing Thermal residual stresses in ceramic matrix composites by using iterative map reduce guided particle swarm optimization algorithm, *Composite Structures*, 99 (2013) , pp. 388–396.
- [219] A. Kacal, M. Gulesin, Determination of optimal cutting conditions in finish turning of austempered ductile iron using Taguchi design method, *Journal of Scientific & Industrial Research*, Vol. 70, April 2011, pp 278-283.
- [220] H. B. Bhaskar, Abdul Sharief, Dry sliding wear behavior of Aluminium / $\text{Be}_3\text{Al}_2(\text{SiO}_3)_6$ composite using Taguchi method, *Journal of Minerals and Materials Characterization and Engineering*, 2012,11,679-684.
- [221] Rama Rao S. and Padmanabhan G., Application of Taguchi methods and ANOVA in optimization of process parameters for metal removal rate in electrochemical machining of Al/5%SiC composites, *International Journal of Engineering Research and Applications (IJERA)*, Vol. 2, Issue 3, May-Jun 2012, pp. 192-197.
- [222] Radhakrishnan Ganesh, Kesavan Chandrasekaran, Mohammed Ameen, Raja Pavan Kumar, Optimization of the process parameters for dry-sliding wear of an Al 2219-sicp composite using the Taguchi-based grey relational analysis, *Materials and Technology*, 48 (3), 2014, 361–366.

- [223] Vinod Kumar, Surender Sharma, Anup Verma, Optimization of tribological performance of Al6061T6/15% SiC/15% Al₂O₃/10% graphite HMMC using Taguchi method and grey relational analysis, International Journal of Engineering Trends and Technology (IJETT) – ISSN: 2231-5381, Volume 8 Number 4- Feb 2014.
- [224] V. C. Uvaraja, N. Natarajan, Optimization on friction and wear process parameters using Taguchi technique, International Journal of Engineering and Technology ISSN: 2049-3444 Volume 2 No. 4, April 2012.
- [225] T. R. Hemanth Kumar, R. P. Swamy, T. K. Chandrashekar, An experimental investigation on wear test parameters of metal matrix composites using Taguchi technique, Indian Journal of Engineering and Material sciences, Volume 20, August 2013, pp. 329-333.
- [226] S. Basavarajappa, K.V. Arun, J. Paulo Davim, Effect of filler materials on dry sliding wear behavior of polymer matrix composites – a Taguchi approach, Journal of Minerals & Materials Characterization & Engineering, Vol. 8, No.5, pp 379-391, 2009.
- [227] Hemanth Kumar.T. R. Swamy.R. P. and Chandrashekar T. K., Taguchi technique for the simultaneous optimization of tribological parameters in metal matrix composite, Journal of Minerals & Materials Characterization & Engineering, Vol. 10, No.12, 2011, pp.1179-1188.
- [228] M. Senthil kumar, S. Natarajan, Analysis of tribological factors on dry sliding wear behavior of thermally sprayed carbide and ceramic coatings by Taguchi method, International Journal of Engineering Science and Technology, ISSN : 0975-5462 Vol. 3 No. 4 April 2011.
- [229] Bala Murugan Gopalsamy, Biswanath Mondal, Sukamal Ghosh, Taguchi method and ANOVA: An approach for process parameters optimization of hard machining while machining hardened steel, Journal of Scientific & Industrial research, pp 686-695, Vol. 68, August 2009.
- [230] Bharat Admile, G. Kulkarni, S. A. Sonawane, Application of Taguchi method for optimization of process parameters for wear loss of Im25/flyash composite, International Journal of Innovations in Engineering and Technology, ISSN: 2319 – 1058, Volume 4 Issue 4 December 2014.

- [231] N. Radhika, A. Vaishnavi, G. K. Chandran, Optimisation of dry sliding wear process parameters for aluminium hybrid metal matrix composites, *Tribology in Industry*, 188-194, Vol. 36, No. 2, 2014.
- [232] Panchakshari H. V., Girish D. P., Krishna M., Investigation on effect of cryogenic parameters on wear behavior of aluminium-AL₂O₃ MMCs using Taguchi method, *International Journal of Soft Computing and Engineering*, ISSN: 2231-2307, Volume-2, Issue-3, July 2012.
- [233] S. Rajesh, S. Rajakarunakaran, R. Sudhakara Pandian, Modeling and optimization of sliding specific wear and coefficient of friction of aluminum based red mud metal matrix composite using Taguchi method and Response surface methodology, *Materials Physics and Mechanics* 15, 2012, 150-166.
- [234] Dinesh Kumar Kasdekar, Vishal Parashar, Jasveer singh, M. K. Gour, Taguchi method and ANOVA: an approach for selection of process parameters of EDM of EN-353 steel, *International Journal of Emerging Technology and Advanced Engineering*, ISSN 2250-2459, Volume 4, Issue 6, June 2014.
- [235] Oji, J.O., Kareem, B., Idusuyi, N., Akinluwade, K. J., Isadare, D. A., Taiwo, A. T., Adetunji, A. R., Optimization of process parameters for the ultimate tensile strength of aluminium alloy sand castings using Taguchi method, *Scholars Journal of Engineering and Technology*, ISSN 2347-9523, 2(3B):383-387, 2014.
- [236] Vijayanand Dharanikota, Optimization of tribological properties of al-6082/sic metal matrix composite by Grey-Taguchi's method, *International Journal of Scientific & Engineering Research*, ISSN 2229-5518, Volume 5, Issue 12, December-2014.
- [237] Ganpat B. Jambukar, Dr. Y. R. Kharde, Dry sliding wear behavior of AL-Si-Ti alloys using Taguchi method, ISSN 2319-7064, *International Journal of Science and Research*, Volume 3, Issue 11, November 2014.
- [238] A. Taskesen, K. Kutukde, Analysis and optimization of drilling parameters for tool wear and hole dimensional accuracy in B₄C reinforced Al-alloy, *Science Direct, Trans. Nonferrous Met. Soc. China* 23(2013) 2524–2536.
- [239] S. Srinivasa Moorthy and K. Manonmani, Research on sliding wear behavior of tio₂ filled glass fiber reinforced polymer composite, *Research Journal of*

- Applied Sciences, Engineering and Technology, ISSN: 2040-7459, 7(16): 3356-3361, 2014.
- [240] Ashok Kr. Mishra, Rakesh Sheokand, Gopal Pr. Yadav, Dr. B. C. Sharma, Dr. R. K. Srivastava, Optimization of tribological parameters in al6061/sic metal matrix composite, International Journal of Innovative Technology and Creative Engineering, ISSN 2045-8711, Vol.2 no.11 November 2012.
- [241] Vinod Kumar, Phool Kumar, Surender Sharma, Wear characterization of aluminium/SiC/Al₂O₃ hybrid metal matrix composite using Taguchi technique, International Journal of Innovative Research & Development, ISSN 2278 – 0211, Vol 3 Issue 1, January, 2014.
- [242] K. N. P. Prasad, M. Ramachandra, Evaluation of factors affecting sliding wear behavior of Al-flyash metal matrix composites by using design of experiments, International Journal of Modern Engineering Research, ISSN: 2249-6645, Vol. 3, Issue. 5, pp-2591-2599, Sep - Oct. 2013.
- [243] Madeva Nagaral, Shivananda B K, Shambhuling V S, V Auradi, Wear behavior of SiC reinforced Al6061 alloy metal matrix composites by using Taguchi's techniques, International Journal of Research in Engineering and Technology, ISSN: 2321-7308, Volume: 03 Special Issue: 03, May-2014.
- [244] Rachit Marwaha, Rahul Dev Gupta, Vivek Jain, Krishnan Kant Sharma, Experimental investigation & analysis of wear parameters on Al/SiC/Cr – metal matrix hybrid composite by Taguchi method, Global Journal of Researches in Engineering, Mechanical and Mechanics Engineering, ISSN 0975-5861, Volume 13, Issue 9, Version 1.0, 2013.
- [245] Abhay D Kulkarni, Dr. Geeta Lathkar, Analysis of used oil on the basis of wear volume using Taguchi method, IOSR Journal of Engineering, ISSN 2278-8719, PP 34-40, Vol. 04, Issue 04, April. 2014.
- [245] P .G. Kochure, K. N. Nandurkar, Taguchi method and ANOVA: An approach for selection of process parameters of induction hardening of EN8 D steel, International Journal of Advance Research in Science, Engineering and Technology, Vol.01, Issue 02, (2012) pp. 22 -27.
- [246] S. M. Darshan, B. Suresha, B. N. Ravi Kumar, Optimization of dry sliding wear behavior of Zirconium filled Bismaleimide Nanocomposites, International Journal of Mechanical Engineering and Technology, ISSN 0976 – 6340, Volume 5, Issue 9, September 2014, pp. 62-70.

- [247] Ferit Ficici, Murat Kapsiz and Mesut Durat, Applications of Taguchi design method to study wear behavior of boronized AISI 1040 steel, *International Journal of the Physical Sciences*, ISSN 1992 – 1950, Vol. 6(2), 18 January, 2011, 237-243.
- [248] Aslan Coban, Ahmet Demirer, Ferit Ficici, Optimization of wear parameters of Polyamide-6 composite materials filled with wollastonite particles, *Periodicals of Engineering and Natural Sciences*, ISSN 2303-4521, Vol. 2, No. 1, 2014.
- [149] Z. Zhang, K. Friedrich, K. Velten, *Wear*, 252 (2002) 668–675.
- [250] Z. Zhang, M. Barkoula, K. Karger-Kocsis, K. Friedrich, *Wear*, 255 (2003) 708–713.
- [251] A. P. Vassilopoulos, E. F. Georgopoulos, V. Dionysopoulos, *International Journal of Fatigue* 29 (2007) 20–29.
- [252] J. A. Lee, D. P. Almond, B. Harris, *Composites: Part A* 30 (1999) 1159–1169.
- [253] C. Sinanoglu, *Industrial Lubrication and Tribology*, 58 (2) (2006) 95–109.
- [254] N. Altinkok, R. Koker, *Journal of Materials Science* 40 (2005) 1767–1770.
- [255] A. A. Mukherjee, S. S. Schqmquder, M. Ruhle, *Acta Metal* 43 (11) (1995) 4083–4091.
- [256] K. Sudharshan Rao, Y. S. Varadarajan and N. Rajendra, Artificial neural network approach for the prediction of abrasive wear behavior of carbon fabric reinforced epoxy composite, *Indian Journal of Engineering and Material Sciences*, Vol. 21, pp. 16-22, February 2014.
- [257] H. K. Durmus, E. Ozkaya, C. Meric, *Materials and Design* 27 (2006) 156–159.
- [258] K. Velten, R. Reinicke, K. Friederich, *Tribology International* 33 (2000) 731–736.
- [259] H. Cetinel, H. Ozturk, E. Celik, B. Karlik, *Wear*, 261 (2006) 1064–1068.
- [260] D. A. Rigney, Comments on the sliding wear of metals, *Tribology International* Vol.30, Number-5, 1997, pp.361-367.
- [261] M. F. Ashby, J. Abulawi, H. S. Kong, *On surface temperatures at dry sliding surfaces*, Cambridge University Press, Cambridge, 1990.
- [262] M. F. Asbhy, *Materials selection in mechanical design*, Pergamon Press, Oxford, 1993.
- [263] O. Kubashewski, B.E. Hopkins, *Oxidation of metals and alloys*, 2nd ed., Butterworths, London, 1962.

- [264] N. P. Petrov, Friction in machines and the effect of the lubricant, *Inzh. Ah*, (1983) 71-140; 2 (1893) 227-279, 3 (1893) 377-436, 4 (1893), pp 535-564.
- [265] Ashok Sharma and T. V. Rajan, Scanning electron microscopic studies of wear-out leaded Al-silicon alloy surfaces, *Wear*,174(1994), pp217-228.
- [266] K. Sudharshan Rao, Y. S. Varadarajan, N. Rajendra, Artificial neural network for the prediction of abrasive wear behavior of carbon fabric reinforced epoxy composite, *Indian Journal of Engineering and Material Sciences*, Vol. 21, February 2014, pp. 16-22.
- [267] E.P. Fordyce, C. Allen, The dry sliding wear behavior of an austempered spheroidal cast iron, *Wear* 135 (1990) 265–278.
- [268] J. Hemanth, Wear characteristics of austempered chilled ductile iron, *Mater. Des.* 21 (2000) 139–148.
- [269] Ducom characterization systems user manual of TR-20-LE wear testing machine, 3rd Edition, 2012.
- [270] P. R. Gangasani, Friction and wear characterization of ductile Iron in dry sliding condition, *Proceedings of Keith Millis Symposium on Ductile Cast Iron*, Hilton Head Island, SC, October 2003, p 9–24.
- [271] Nofal Al-Araji, Hussein Sarhan, Effect of temperature on sliding wear mechanism underlubricated conditions, *International Journal of Engineering*, Vol. 5, 2011.
- [272] J.R. Rogier, M.W. Geatz, *Data Mining: A Tutorial-based primer*, Addison-Wesely, 2003.
- [273] Michal Negnevitsky, *Artificial Intelligence*, second ed., Addison-Wesley, 2005.

APPENDICES

A1. List of Publications from the Present Research Work

Papers Published in International Journals

1. Rajendra M. Galagali, Dr. R. G. Tikotkar, “Tribological Behaviour of Si-Cu-Mo-Ni Austempered Ductile Iron”, World Academy of Science, Engineering and Technology, International Journal of Materials and Metallurgical Engineering, Vol. 11, No. 5, 2017.
2. Rajendra M. Galagali, Dr. R. G. Tikotkar, “Parameters Optimization in the Experimental Wear Study on ADI at Elevated Temperature”, International Journal of Emerging Technology and Advanced Engineering (IJETAE)-ISSN 2250-2459, Volume 7, Issue 6, June 2017.
3. Rajendra M. Galagali, Dr. R. G. Tikotkar, “Investigations on Wear Behaviour of ADI using Artificial Neural Network”, Journal of Product Design, Quality Engineering & Technology, Volume 2, Issue 2, 538, Page 1-13 @ Mantech Publications 2017.
4. Rajendra M. Galagali, Dr. R. G. Tikotkar, “Experimental investigations on wear process parameters optimization of Austempered Ductile Iron using Taguchi technique”, International Journal of Innovative Research in Science, Engineering and Technology (IJIRSET) – eISSN: 2319-8753, pISSN:2347-6710, Volume4, Issue 4, April 2015.
5. Rajendra M. Galagali, Dr. R. G. Tikotkar, “Friction studies on Austempered Ductile Iron: A Taguchi Approach”, International Journal of Engineering Technology, Management and Applied Sciences (IJETMAS) – ISSN: 2349-4476, Volume 3, Issue 4, April 2015.

Paper Published in International Conference

6. Rajendra M. Galagali, Dr. R. G. Tikotkar, —Artificial Neural Network approach for the prediction of elevated temperature wear behaviour of ADI”, Proceedings of the 4th International Conference on Research Trends in Engineering, Applied Science and Management (ICRTE SM-2017), Organized by conference info in association with Academic Science at IETE, Hyderabad, on 24th June, 2017 published in IJETSR, ISSN: 2394-3386, June 2017.

Papers to be Communicated to International Journals

1. Rajendra M. Galagali, Dr. R. G. Tikotkar, “Effect of sliding speed and temperature on the dry sliding wear behaviour of Austempered Ductile Iron”, Preferably to Elsevier.
2. Rajendra M. Galagali, Dr. R. G. Tikotkar, “Investigations on the Effect of Applied load and Temperature on the Dry Sliding Wear behaviour of Austempered Ductile Iron”, Preferably to Springer.

A2. Brief Bio-data of the Author

The author, **Rajendra M. Galagali**, born on 24-09-1977 graduated in Mechanical Engineering from Karnataka University, Darwad in the year 1999. He did his postgraduate study in Product Design and Manufacturing from Visvesvaraya Technological University, Belagavi, in the year 2004. Before joining for the Ph.D. programme at Visvesvaraya Technological University, Belagavi, he had served at various organisations;

1. Worked as Lecturer in Maratha Mandal Engineering College, Belagavi from 1999 to 2002.
2. Worked as Lecturer in Sir M. Visvesvaraya Institute of Technology, Bengaluru from 2004 to 2007.
3. Worked as SAP Functional Consultant in Cusat Technologies Pvt. Ltd., Bengaluru in 2007.
4. Worked as SAP Functional Consultant in Bristlecone India Pvt. Ltd., Bengaluru from 2007 to 2009.
5. Worked as Senior Lecturer in S. G. Balekundri Institute of Technology, Belagavi from 2009 to 2011.

He is presently working as Assistant Professor in the Department of Mechanical Engineering at Jain College of Engineering, Belagavi from 2011.

He has authored four research papers in International Journals and one research paper in International Conference and one in National Conference. Since 2012, he has been engaged in his Doctoral Research in the area of Tribology at V.T.U., Belagavi.